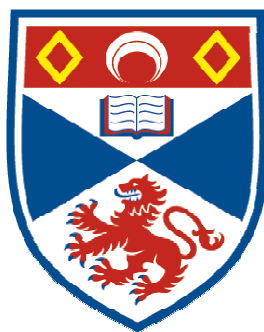# Polymer Electrolytes – Synthesis and Characterisation

University of
St Andrews

600
YEARS

School of Chemistry

# Krzysztof Jerzy Marański

*This thesis is submitted for the degree of*
*Doctor of Philosophy at the University of St Andrews*

Supervisor: Prof. Peter G. Bruce

February 2013

**1. Candidate's declarations:**

I, Krzysztof Jerzy Marański, hereby certify that this thesis, which is approximately 25800 words in length, has been written by me, that it is the record of work carried out by me and that it has not been submitted in any previous application for a higher degree.

I was admitted as a research student in February 2008 and as a candidate for the degree of Doctor of Philosophy in February 2009; the higher study for which this is a record was carried out in the University of St Andrews between 2008 and 2012.

Date ……................... signature of candidate …..…........................................

**2. Supervisor's declaration:**

I hereby certify that the candidate has fulfilled the conditions of the Resolution and Regulations appropriate for the degree of Doctor of Philosophy in the University of St Andrews and that the candidate is qualified to submit this thesis in application for that degree.

Date ……................... signature of supervisor …..…........................................

**3. Permission for electronic publication:**

In submitting this thesis to the University of St Andrews I understand that I am giving permission for it to be made available for use in accordance with the regulations of the University Library for the time being in force, subject to any copyright vested in the work not being affected thereby. I also understand that the title and the abstract will be published, and that a copy of the work may be made and supplied to any bona fide library or research worker, that my thesis will be electronically accessible for personal or research use unless exempt by award of an embargo as requested below, and that the library has the right to migrate my thesis into new electronic forms as required to ensure continued access to the thesis. I have obtained any third-party copyright permissions that may be required in order to allow such access and migration, or have requested the appropriate embargo below.

The following is an agreed request by candidate and supervisor regarding the electronic publication of this thesis:

Embargo on both all of printed copies and electronic copy for the same fixed period of 2 years on the following ground(s):

publication would preclude future publication;

Date ………................. signature of candidate ….…….......................................

signature of supervisor ….…….......................................

## Acknowledgements

Firstly, I would like to thank Professor Peter G. Bruce for giving me the opportunity to join his research group and for his excellent guidance throughout the course of my PhD.

I would particularly like to express my appreciation to Dr Yuri Andreev, Dr Chuhong Zhang and Dr David Ainsworth for all the helpful discussions and suggestions along the way, and for answering all my questions.

Thanks are also due to Dr Catherine Botting, Dr Sally Shirran, Dr Matthew Fuszard, Mr Alexander Houston and Mrs Caroline Horsburgh for their help with the mass spectrometry and Dr Tomas Lebl and Mrs Melanja Smith for their assistance with solution NMR spectroscopy. I would also like to acknowledge Prof. Alexandra Slavin for single crystal structure determination and Mrs Sylvia Williamson for all her help with the thermal characterisation of my samples.

I would also like to thank all the members of the Bruce group, both past and present, who I encountered during my studies.

Finally, I would like to express my gratitude to my family for all their love, support and understanding which sustained me during my PhD.

Thanks must go to EPSRC for funding this project.

*Dedicated to the ones I love*

*"Logic will get you from A to B.*

*Imagination will take you everywhere."*

Albert Einstein

1879 - 1955

**ABSTRACT**

Crystalline polymer/salt complexes can conduct, in contrast to the view held for 30 years. The $\alpha$-phase of the crystalline poly(ethylene oxide)$_6$:LiPF$_6$ is composed of tunnels formed from pairs of $(CH_2\text{-}CH_2\text{-}O)_x$ chains, within which the Li$^+$ ions reside and along which the latter migrate.[1] When a polydispersed polymer is used, the tunnels are composed of 2 strands, each built from a string of PEO chains of varying length. It has been suggested that the number and the arrangement of the chain ends within the tunnels affects the ionic conductivity.[2] Using polymers with uniform chain length is important if we are to understand the conduction mechanism since monodispersity results in the chain ends occurring at regular distances along the tunnels and imposes a coincidence of the chain ends between the two strands.[2] Since each Li$^+$ is coordinated by 6 ether oxygens (3 oxygens from each of the two polymeric strands forming a tunnel), monodispersed PEOs with the number of ether oxygen being a multiple of 3 ($N_O = 3n$) can form either "all-ideal" or "all-broken" coordination environments at the end of each tunnel, while for both $N_O = 3n\text{-}1$ and $N_O = 3n+1$ complexes, both "ideal" and "broken" coordinations must occur throughout the structure.

A synthetic procedure has been developed and a series of 6 consecutive (increment of EO unit) monodispersed molecular weight PEOs have been synthesised. The synthesis involves one end protection of a high purity glycol, functionalisation of the other end, ether coupling reaction (*Williamson's* type ether synthesis[3]), deprotection and reiteration of ether coupling. The parameters of the process and purification methods have been strictly controlled to ensure unprecedented level of monodispersity for all synthesised samples.

Thus obtained high purity polymers have been used to study the influence of the individual chain length on the structure and conductivity of the crystalline complexes with LiPF$_6$. The results support the previously suggested model of the chain-ends arrangement in the crystalline complexes prepared with monodispersed PEO[2] over a range of consecutive chain lengths. The synthesised complexes constitute a series of test samples for establishing detailed mechanism of ionic conductivity. Such series of monodispersed crystalline complexes have been studied and characterised here (PXRD, DSC, AC impedance) for the first time.

# References

1. G. S. MacGlashan, Y. G. Andreev, P. G. Bruce, *Structure of the polymer electrolyte poly(ethylene oxide)$_6$:LiAsF$_6$.* Nature, 1999, **398**(6730): p. 792-794.

2. E. Staunton, Y. G. Andreev, P. G. Bruce, *Factors influencing the conductivity of crystalline polymer electrolytes.* Faraday Discussions, 2007, **134**: p. 143-156.

3. A. Williamson, *Theory of Aetherification.* Philosophical Magazine, 1850, **37**: p. 350-356.

# Contents

## 1. INTRODUCTION – POLYMER ELECTROLYTES

As natural gas and oil supplies dwindle, and also for ecological reasons, we need to increase the number of renewable energy sources. However, most of them (e.g. wind, tidal, solar power) are dependent on the time of day and weather conditions, which means that they cannot supply energy 24 hours a day and 365 days per year – they are only available intermittently. This is why we need to store energy. Many forms of energy storage are known. When considering the storage of electricity, rechargeable batteries offer certain potential advantages such as high efficiency and modular design. This makes them suitable for use in electric vehicles for load levelling and for portable electronics although, of course, the detailed characteristics and hence design will differ from one application to another.[1]

Despite the impressive growth in sales of batteries worldwide, the science underlying battery technology is often criticised for its slow advancement. This applies to all battery types: nickel-cadmium, nickel-metal hydride, Li-ion etc. Certainly, when compared with the computer industry, energy storage struggles to keep pace with the rate of demand.

The key part of every battery is an electrochemical cell which consists of electronically conducting positive and negative electrodes separated by an ionically conducting electrolyte, which enables ion transfer between the two electrodes. Among the various technologies, Li-based cells provide the highest energy density (Fig. 1). This explains why they receive most attention at both fundamental and applied levels.
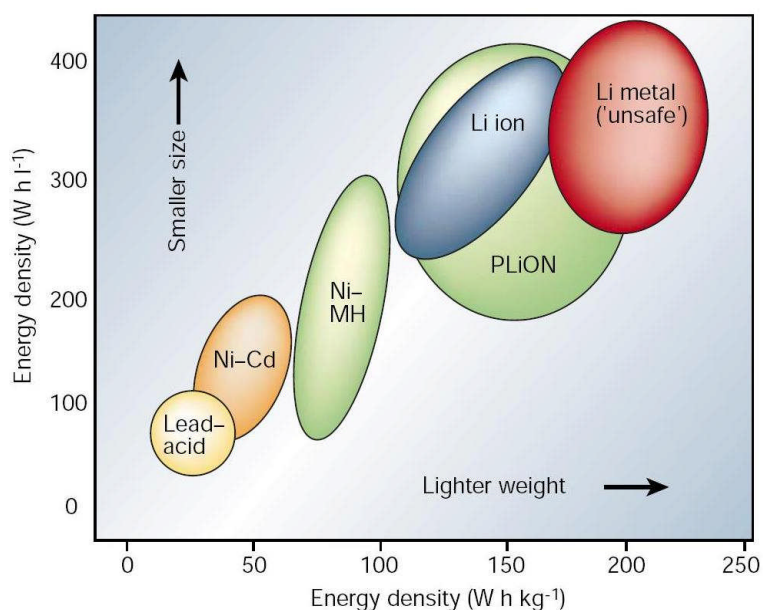


Fig. 1 Comparison of the different battery technologies in terms of volumetric and gravimetric energy density.[2]

The widely commercialised rechargeable Li-ion battery is known as a *rocking-chair battery* (Fig. 2). It contains a liquid electrolyte (a lithium salt dissolved in an organic solvent). The conductivity of the electrolyte has to be sufficient to ensure the voltage drop across the electrolyte is minimal ($V_{electrolyte} = i \times R_{electrolyte}$).
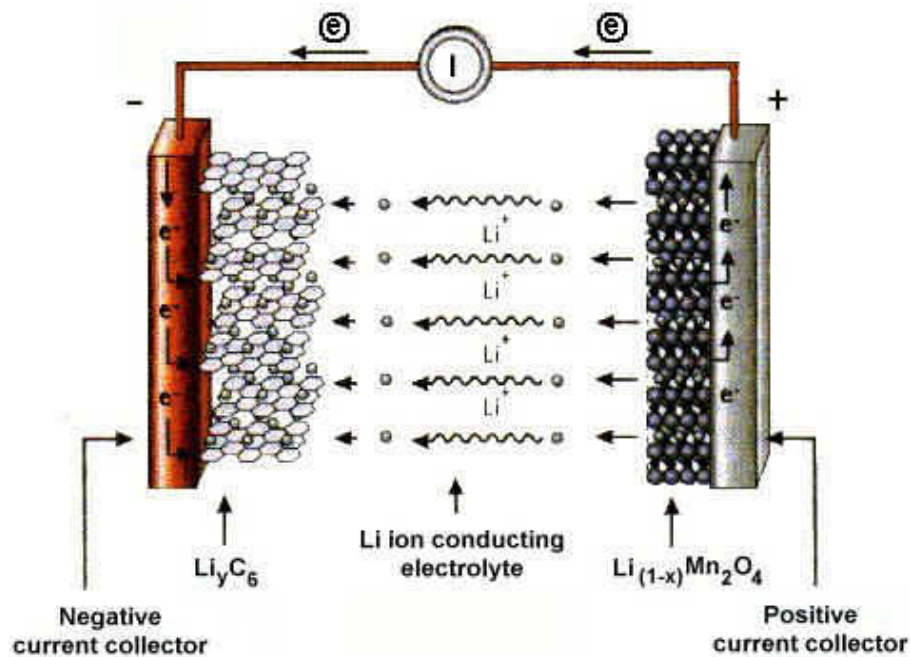


Fig. 2 The *rocking-chair* cell. The discharge process is shown. On charging the direction of ions and electrons movement is reversed.

The main drawbacks of all liquid electrolytes are their toxicity and flammability. A number of fire accidents or even explosions have been reported to date.[3] For this reason and also to ease construction of cells, significant research efforts are focused on development of solid state electrolytes.[2] In general, lithium-ion conducting solid electrolytes used for all-solid-state rechargeable lithium batteries must possess the following properties:

- high lithium-ion conductivity (at least $10^{-3}$ S·cm$^{-1}$ at r.t.[4,5]) with negligible electronic conductivity at operating temperature. However, it would be acceptable to use a solid electrolyte with ionic conductivity of the order of $10^{-4}$ S·cm$^{-1}$ at r.t. providing that it can be fabricated into a very thin film with large surface area.[6]

- wide potential window at both positive and negative electrode sides – sufficient stability versus both electrodes,

- mechanical and dimensional stability – sufficient to clearly separate the electrodes from each other under the battery operating conditions, while providing good contact with electrodes,[7]

- environmentally benign, non-hygroscopic, low cost, and easy processing.

Solid inorganic superionic conductors at first glance meet many of the above requirements. They have been known since 1970s and can be divided into 2 groups:[8]

1. high temperature ionic conductors, e.g. $Li_4SiO_4$ ($10^{-4}$-$10^{-3}$ S·cm$^{-1}$ at 300°C)[9] or $Li_{14}Zn(GeO_4)_4$ (LISICON) ($10^{-2}$-$10^{-1}$ S·cm$^{-1}$ at 300°C)[10-12],

2. low temperature ionic conductors, e.g. $Li_3N$ ($10^{-3}$ S·cm$^{-1}$ at r.t.)[13,14] or recently reported $Li_{10}GeP_2S_{12}$ ($10^{-2}$ S·cm$^{-1}$ at r.t.)[15].

Although the latter have conductivity comparable with that of liquid electrolytes, their use as electrolytes presents considerable challenge of establishing a good contact with the electrodes. Only one ceramic electrolyte, LiPON, has found application in a commercially available rechargeable battery. It was processed into a thin film by means of radio-frequency (RF) reactive magnetron sputtering and sandwiched between electrodes.[16,17] However, the low ionic conductivity ($10^{-6}$ S·cm$^{-1}$ at r.t.) of this electrolyte limits the utility of such battery.[18]

The possible alternative to ceramics, which would provide the desired mechanical properties, is polymer electrolytes. In 1973, *Wright et al* discovered that certain salts of alkali metals dissolved in high molecular weight poly(ethylene glycol) (PEG) were able to form ionically conducting solid materials.[19] In 1978 *Armand et al* highlighted the potential of these materials as a new class of solid electrolytes for energy storage applications.[20] Segmental motion of the polymer chains above the glass transition temperature ($T_g$) not only enables ionic conductivity of the complexes but makes them mechanically soft – a decisive factor to achieve a good contact with the electrodes.[6,21]

**Polymer electrolyte** – '*a solvent free system where the ionically conducting phase is formed by dissolving salts in a high molecular weight polar polymer matrix*'[22]

## 1.1. Application of Polymer Electrolytes

Although the main application for polymer electrolytes are rechargeable lithium batteries, they can be also used in a number of other applications: smart windows, electrochromic displays and ion detectors.[22]

Currently, polymer electrolytes are used in batteries for mobile phones and laptop computers, but only in the gel form, where they are plasticised with organic solvents such as ethylene carbonate (EC). Their advantage over the completely liquid electrolytes is that the presence of a polymer significantly increases the viscosity of electrolyte reducing the possibility of leakages. Unfortunately thus gained advantage is accompanied by a lower conductivity.[23]

## 1.2. Formation of polymer electrolytes

The dissolution of a salt into a host polymer is governed by the same thermodynamic equation as for all other chemical processes – in order to occur the change in Gibbs free energy ($\Delta G$) must be negative.

$$\Delta G = \Delta H - T\Delta S$$

The factors influencing the enthalpy term ($\Delta H$) are related to the energy required to break up starting materials and the energy gained when a complex is formed. Lattice energy of the salt introduces a positive enthalpy change while the solvation of the cation causes a negative enthalpy change.

Two competing factors influence the entropy change term ($\Delta S$), which is positive due to break up of the crystal lattice in starting components (growing disorder) and negative due to coordination of cations by the polymer chains (growing order).

This explains why a polymer which is capable of coordinating a cation must be selected.

### 1.2.1. The Hard/Soft Acid/Base Concept

The solvation enthalpy of a salt is determined by the cation-polymer interaction. This can be understood in terms of the acid-base interaction between the solvent and the solute. This is known as the hard/soft acid/base theory (H.S.A.B.). A hard acid is a small cation with no easily removed or polarised valence electrons, e.g. alkaline earth metal ion like $Mg^{2+}$. A soft acid is a large cation with easily distorted or removed valence electrons e.g. partially filled $d$ orbital $Hg^{2+}$.

Bases can also be hard or soft; a hard base is a non-polarisable ligand with electrostatic forces primarily responsible for bonding, e.g. oxygen in ether. A soft base contains polarisable groups, and the orbital overlap is primarily responsible for bonding, e.g. sulphur in thioether. A strong interaction, and hence large solvation enthalpy, is produced when a hard-hard or soft-soft interaction occurs. For hard cations the best donors are:

$$-O- > -NH- >> -S-$$

For a soft cation, the best donors are in an order which is different but not simply reversed because the interactions between cation and donor are no longer dominated exclusively by electrostatic forces:[24]

$$-NH- > -S- > -O-$$
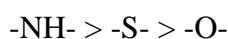
### 1.2.2. Anion Solvation

Anions in solution are stabilised by hydrogen bonds but even in the absence of the latter they can still enter solutions. In solvents less polar than water, such as polyethers and acetonitrile, the stability of an anion in the solution is dependent on the charge localisation. Large delocalised anions require little solvation. The most suitable anions for aprotic, low-dielectric-constant dipolar polymer electrolytes are given below in descending suitability:

$$AsF_6^- \sim BF_4^- > CF_3SO_3^- \sim ClO_4^- > SCN^- \sim I^- > Cl^- >> F^-$$

Smaller and harder anions can be forced to enter the polymer solution by 2+ and 3+ cations. The larger solvation energies associated with the larger charges make the formation of a complex favourable. This opens the door to a number of different coordination systems. Soft-soft salts such as AgI are totally insoluble in poly(ethylene oxide) (PEO). When preparing a polymer electrolyte the selection of large monovalent anions with delocalised charge is necessary. The low lattice energy of these salts is easily overcome by the enthalpy of solvation and the positive change in entropy. The most studied anions are: $ClO_4^-$, $CF_3SO_3^-$, $(CF_3SO_2)_2N^-$, $BPh_4^-$, $BF_4^-$, $SCN^-$ and $XF_6^-$ (X = P, As and Sb). A number of "non-coordinating" anions have been recently investigated by computational modelling for a variety of applications.[25] Some of these anions are suitable for electrochemical applications,

e.g. tris(pentafluoroethyl)trifluorophosphate, $[F_3P(C_2F_5)_3]^-$. Most of these anions are presently available only in ionic liquids.

### 1.3. Examples of polymer electrolytes hosts

Many types of polar polymers containing atoms like oxygen, nitrogen or sulphur have been studied as hosts for polymer electrolytes because these atoms can coordinate cations.[6,22]

### 1.3.1. Polyethers

Polyethers $[-(CH_2)_mO-]_x$ show remarkable variation in physical properties depending on the number of methylene repeat units. These differences affect the ability to coordinate inorganic salts.[6]

In accordance with the solubility theory (described in 1.2) a polyether, $-(CH_2)_m-O-$, more readily solvates a salt, when $m = 2$. For both $m = 1$ and $m = 3$ the solubility of the salt is reduced. When $m = 1$ strain is introduced into the polymer preventing easy coordination of the cation, even though larger number of oxygen atoms provide more opportunities for coordination. On the other hand, polyethers with $m \geq 3$ prevent coordination by many oxygen atoms because large regions of backbone produce steric hindrances. Thus, $m = 2$, poly(ethylene oxide) (PEO), also called poly(ethylene glycol) (PEG), appears to be the most suitable matrix for polymer electrolytes. PEO is capable of solvating most cations, including alkaline earth and transition metals. In this respect it is very similar to water. However, unlike water, PEO cannot solvate anions. The highest reported conductivities of complexes made with high Mw branched PEO polymer and lithium salts are slightly above $10^{-4}$ S·cm$^{-1}$.[26]

PEO with a finite distribution of molecular weights (hereafter referred to as 'polydispersed') can be synthesised from ethylene oxide via anionic ring opening polymerisation.[27] Synthesis of monodispersed PEO is developed in this thesis.

### 1.3.2. Poly(ethylene imine) (PEI)

Poly(ethylene imine) $[-(CH_2)_2NH-]_x$ can be prepared as a highly branched amorphous polymer by the cationic ring-opening polymerisation of ethylene imine (aziridine). PEI synthesised from 2-oxazoline through the alkaline hydrolysis of poly(N-formylethylenimine) is a highly crystalline, linear polymer with molecular weight of approximately $10^4$ Da.[28] *Shriver et al* prepared a number of PEI:NaSO$_3$CF$_3$ complexes with various compositions. The highest conductivities of $10^{-5}$ S·cm$^{-1}$ were reached at 40°C.[29]

### 1.3.3. Poly(alkylene sulfides)

Poly(alkylene sulfides) $[-(CH_2)_mS-]_x$ are direct analogues of polyethers. Poly(ethylene sulfide) ($m = 2$) and poly(propylene sulfide) ($m = 3$) can be synthesised from 3- and 4-membered cyclic sulfides respectively by either cationic or anionic initiation.[27,30] *Shriver et al* described preparation and properties of poly(alkylene sulfides), $m = 2–6$, by the reaction of a disodium salt of the appropriate dimercaptan with a dibromoalkane. Polymer electrolytes prepared with each of these polymers and silver salts achieved the conductivities of only $10^{-9}$ S·cm$^{-1}$ at room temperature.[31]

### 1.3.4. Rigid Polymers

Many avenues have been explored in order to find a polymer electrolyte with low $T_g$ which would provide high conductivity at room temperature. However, in 1994 *Yamamoto et al* reported a very rigid polymer ($T_g = 315$°C) which when mixed with an inorganic salt exhibited the conductivity of $10^{-5.5}$ S·cm$^{-1}$.[32] In 1999 *Imrie et al* confirmed that ionic transport can occur in certain polymeric glasses below $T_g$.[33]

These developments encouraged *Shriver et al* to search for new rigid polymers which can provide pathways for ion hopping. They investigated 2 rigid polymer systems (Fig. 3): poly(vinylene carbonate) (PVIC) and poly(1,3-dioxolan-2-one-4,5-diyl oxalate) (PVICOX). The polymers displayed both good mechanical properties and high conductivities ($10^{-4}$ S·cm$^{-1}$ for PVICOX system at room temperature).[34]
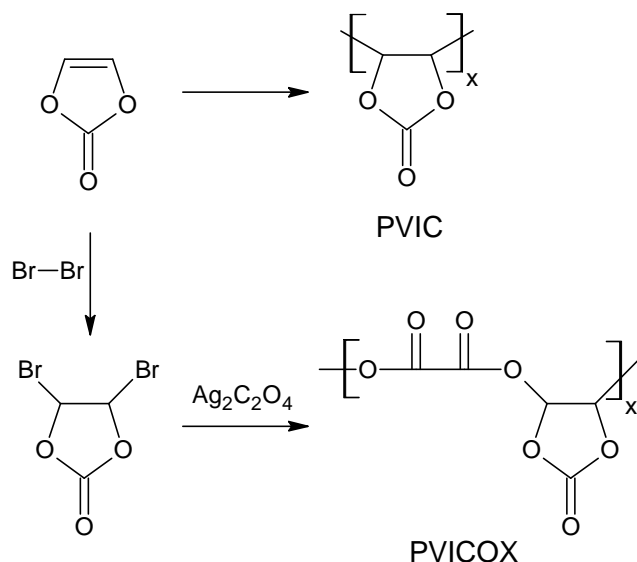
Fig. 3 Structures and synthetic route for PVIC and PVICOX.[34]

However, attempts to reproduce those results were unsuccessful.

## 1.4. Ion transport

The highest reported conductivity of solid polymer electrolytes, $10^{-4}$ S·cm$^{-1}$ at room temperature, is still relatively low when compared to the conductivity of typical liquid electrolytes ($10^{-1}$ S·cm$^{-1}$). That is why significant research efforts are focused on increasing the ionic conductivity in the sold state. The success of these efforts heavily relies on the knowledge of the detailed mechanism of conduction. [2,35,36]

### 1.4.1. Amorphous polymer electrolytes

Since the  discovery of polymer electrolytes in 1973, the established theory was that ionic conduction occurred only in the amorphous phase above $T_g$ of a polymer/salt complex.[19] This view was demonstrated by *C. Berthier et al* in a study of PEO:LiCF$_3$SO$_3$, where the crystalline 3:1 complex and the amorphous phase coexist above $T_g$.[37] Segmental motion of the polymer chains in the amorphous phase enables diffusion of ions by means of constant creation and destruction of free volume.

The temperature dependent conductivity in this case is expressed by the Vogel-Tamman-Fulcher (VTF) equation:

$$\sigma = \sigma_0 T^{-0.5} \exp\left(\frac{-B}{T - T_0}\right),$$

where: $\sigma$ is the conductivity at temperature $T$, $\sigma_0$ is the conductivity at the equilibrium glass transition temperature $T_0$ and $B$ is a constant.

The equation is generally used to describe diffusion of uncharged molecules through disordered materials such as fluids or polymers, but it turned out to also be appropriate for the description of ions movement in amorphous polymer electrolytes.

The theory explaining the conduction mechanism led to the design strategies for new polymer electrolytes in which crystallinity was suppressed and segmental motion maximised.[20,38] Majority of the investigated materials were based on PEO of high molecular weight or other polymers containing -CH$_2$CH$_2$-O- repeat unit because it provides an excellent ligand for cations.[39] The common salts for polymer electrolytes are: LiClO$_4$, LiPF$_6$, LiAsF$_6$, LiCF$_3$SO$_3$, LiN(SO$_2$CF$_3$)$_2$ (LiTFSI), etc.

There are, however, other types of electrolytes which also contain polymers, although they do not exactly obey the definition of polymer electrolyte quoted in chapter 1:

### 1.4.1.1. Polymer-in-salt

Polymer-in-salt materials represent a reverse concept to conventional polymer electrolytes, since a salt is mixed with small quantity of a polymer, e.g. poly(ethylene oxide), poly(propylene oxide) or polyacrylonitrile. Polymer-in-salt electrolytes provide the benefit of improved mechanical flexibility at r.t. compared to glassy electrolyte, while preserving good lithium-ion conductivities (up to $10^{-4}$ S·cm$^{-1}$ at r.t.) and high electrochemical stability.[40,41]

### 1.4.1.2. Gel electrolytes

As indicated earlier, a polymer electrolyte can be plasticised with an organic solvent to form a gel electrolyte. Commonly used liquid plasticisers are: propylene carbonate, ethylene carbonate, dimethyl carbonate.[42,43] In order to provide enough mechanical integrity of gels, the polymer must either be cross-linked or contain crystalline domains.[44] The conductivities of gel systems reach up to $10^{-2}$ S·cm$^{-1}$ at r.t.[45] Although due to higher viscosity gel electrolytes possess better mechanical properties than purely liquid electrolytes, they can still leak solvents meaning that the related safety problems remain.

### 1.4.1.3. Hybrid polymer electrolytes

Hybrid polymer electrolytes comprise of a polymer (matrix), salt and solid filler (e.g. $TiO_2$, $Al_2O_3$, $ZrO_2$, $SiO_2$)[46-49]. The latter is a plasticiser reducing the amount of crystalline phase in the complex and hence increasing its conductivity (up to slightly over $10^{-5}$ $S \cdot cm^{-1}$ at r.t.)

Gels with ceramic fillers have also been studied [P(VdF-HFP)+ceramic filler+liquid electrolyte][45]. They reach up to $10^{-2}$ $S \cdot cm^{-1}$ at r.t. while improving the mechanical properties. However, they still possess the disadvantages of gels.

### 1.4.2. Crystalline polymer electrolytes

The view that conductivity in polymer electrolytes was confined to the amorphous phase above the glass transition temperature was challenged by *Bruce et al.*[50] The group discovered crystalline polymer electrolytes formed by poly(ethylene oxide) and $LiXF_6$ (X = P, As, Sb) with 6 ethylene oxide groups per 1 molecule of the inorganic salt (abbreviated as $PEO_6:LiXF_6$) (Fig. 4).[50-52] These complexes are ionically conducting and the conductivity is dominated by $Li^+$ ions transport (cation transport number $t_+ = 1$).[53,54]

The crystalline phase will be hereafter referred to as $\alpha$, because other crystalline less conductive phases also exist.[55] The complexes are isostructural and consist of rows of $Li^+$ ions encapsulated within columns formed by pairs of nonhelical PEO chains. The $Li^+$ ion is coordinated by 5 ether oxygen atoms from both chains, three ether oxygens from one and two from the other (the 6$^{th}$ ether oxygen in the coordination site is located at a slightly larger distance). Each coordinating ether oxygen coordinates only one $Li^+$ ion. The anions reside between the columns and do not coordinate the cations, hence cannot impede the diffusion of the latter along the tunnels.
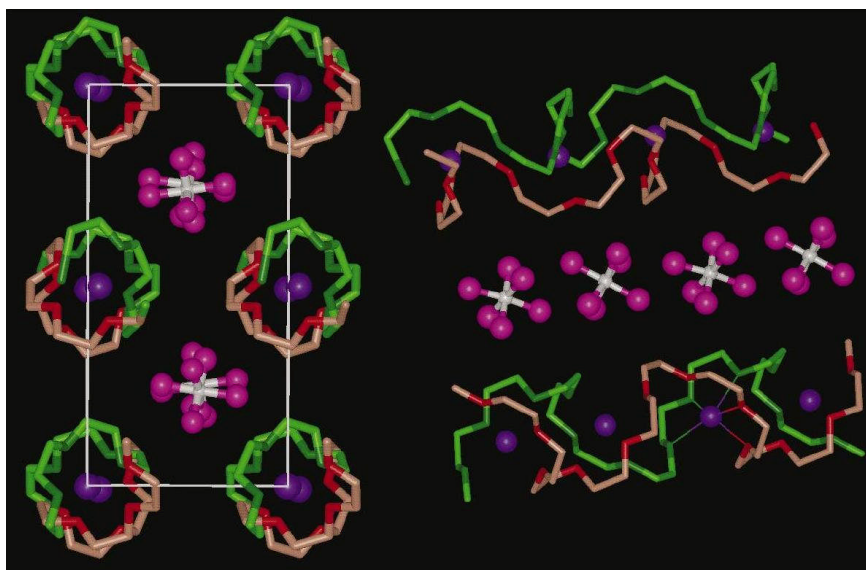
Fig. 4 The structure of the polymer electrolyte $PEO_6$:$LiAsF_6$. Left, view of the structure along the chain axis showing rows of $Li^+$ ions perpendicular to the page. Right, view of the structure showing the relative position of the chains and their conformation (hydrogens not shown). Blue spheres, lithium; white spheres, arsenic; pink spheres, fluorine; light green, carbon in chain 1; dark green, oxygen in chain 1; light red, carbon in chain 2; dark red, oxygen in chain 2. Thin lines indicate coordination around the $Li^+$ cation. The structure was solved from powder diffraction data using a newly developed simulated annealing method.

When compared to amorphous electrolytes, the structure of crystalline complexes implies that free volume does not need to be created in order to enable the movement of ions, because the site to which an ion migrates is already present and aligned in the structure and ion hopping could take place as soon as sufficient activation energy is available for the ion to hop. The schematic $Li^+$ diffusion pathway along the polymer tunnels is shown in Fig. 5.
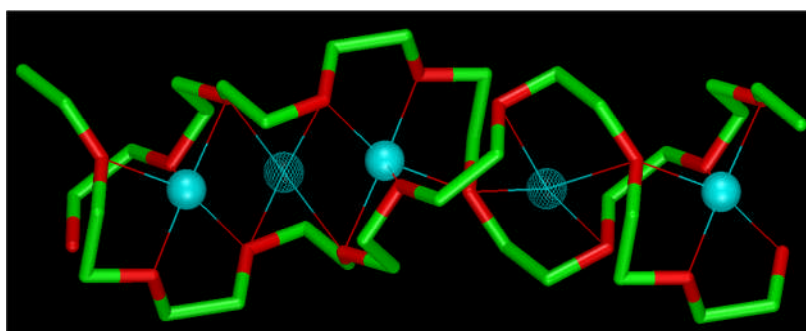


Fig. 5 Schematic diffusion pathway of the $Li^+$ cations in $PEO_6$:$LiPF_6$. Thin lines indicate coordination around the $Li^+$ cation; solid blue spheres, lithium in the crystallographic five-coordinate site (note that the fifth thin line is very short in this view); meshed blue spheres, lithium in the intermediate four-coordinate site; green, carbon; red, oxygen.

In order for a Li$^+$ ion to migrate from one stable five-coordinate site to another, it has to pass through an intermediate site formed by four ether oxygens defining a rectangle. Such a pathway for ion transport is an approximation, since it is based on a static model derived from the crystal structure, whereas in reality there is undoubtedly some flexing of the polymer chains.[56] Molecular dynamics simulations also support the passage through the intermediate site.[57] It has been suggested that aligning or organising the polymer chains should enhance the ionic conductivity.[5,58-63] A series of complexes made with the same lithium salt and PEOs of different average molecular weight (750 Da, 900 Da, 1000 Da, 1500 Da, 2000 Da, all -CH$_3$-terminated)[56,64] was reported. All those complexes form exactly the same crystalline α phase, but the crystallite size increases with decreasing Mw of PEO. AC impedance measurement results confirmed that the larger the crystallites, the higher the conductivity of a complex (Fig. 6). However, it has to be noted that complexes made with PEO of lower Mws also have larger number of chain ends than complexes made with larger Mws. Chain ends are effectively defects in the crystal structure, thus, by analogy with ceramic ionic conductors, higher conductivities could then be attributed to larger number of defects.[56]
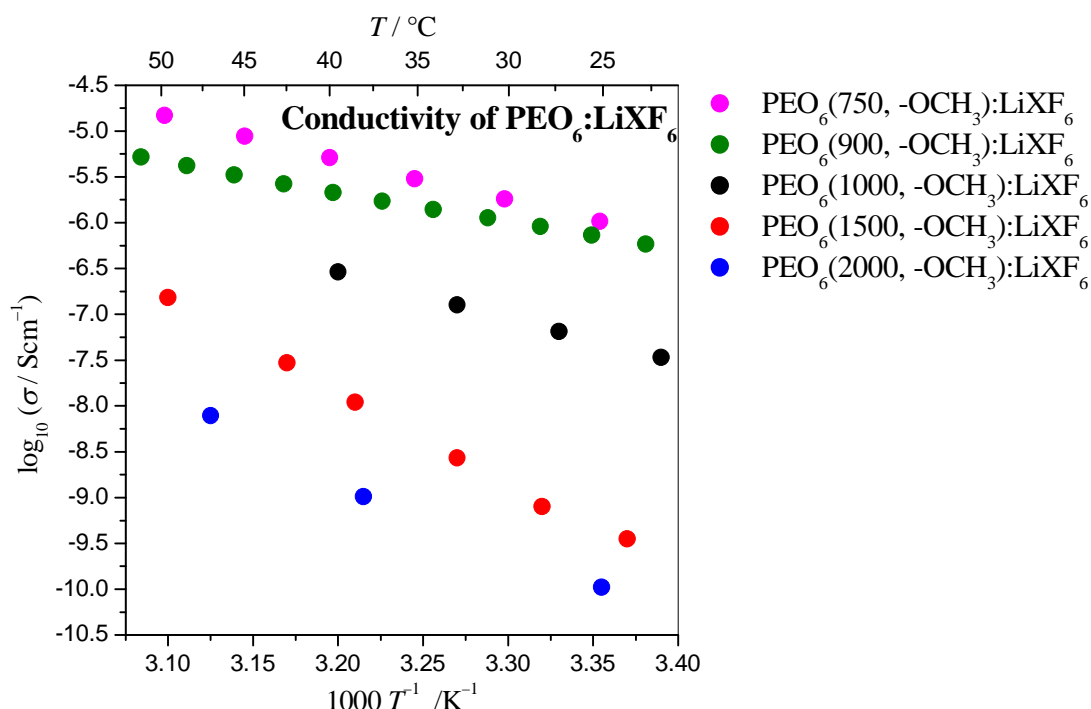


Fig. 6 Ionic conductivities for crystalline PEO$_6$:LiXF$_6$ complexes of different Mws of PEO.

Further increase of the chain-end density in crystalline $PEO_6:LiXF_6$ was achieved by doping the complexes made of 1000 Da PEO with tetraglyme (G4). A series of different compositions was studied in order to obtain single $\alpha$ phase. Only the complex in which 75% of oxygen atoms come from PEO and the remaining 25% from tetraglyme $(PEO_{0.75}G4_{0.25})_6:LiPF_6$ forms pure $\alpha$ phase. The conductivity of such complex is ~1.5 order of magnitude higher compared to the undoped electrolyte.[65]

The influence of other defects in the crystalline polymer electrolytes on their ionic conductivity was studied using different types of anionic doping of complexes prepared with PEO of <Mw> = 1000 Da. An increase in conductivity of 1.5 orders of magnitude was detected when a small amount (up to 5 mol %) of $AsF_6^-$ anions in the crystalline $PEO_6:LiAsF_6$, was replaced by $(SO_2CF_3)_2N^-$ (TFSI) anions. The two anions are isovalent, but TFSI is larger, irregular in shape and with more delocalised charges than $AsF_6^-$. All that causes a disruption of the potential around the $Li^+$ ions and results in enhancement of the ionic conductivity.[36]

Even doping with an isovalent anion of the same shape, but only slightly different size – $AsF_6^-$ (ionic radius = 1.67 Å) and $SbF_6^-$ (ionic radius = 1.81 Å) – results in increase of conductivity of 1 order of magnitude. Interestingly, disruption caused by replacing 10% of one $XF_6^-$ anion with another exhibits the highest conductivity amongst all the different proportions studied (0-100%). Such phenomenon was attributed to the fact that doping with small amounts leads to strain and hence local disruption of the potential around the $Li^+$ ions in the 6:1 crystal structure, resulting in the observed higher conductivities. Once more than 1 out of 10 of the anions has been substituted, further doping does not lead to an increase in conductivity.[66] Similar effect was previously observed in ceramic materials $AgBr_{1-y}I_y$.[67]

In case of isovalent doping no extra $Li^+$ ions or vacancies are introduced into the structure. It is generally the case that both interstitial ions and vacancies lead to increase in conductivity.[12,68-70] The level of ionic conductivity was raised by 1.5 orders of magnitude when less than 5 mol % of the $SbF_6^-$ ions in the crystalline conductor $PEO_6:LiSbF_6$ were replaced by $SiF_6^{2-}$. Such aliovalent doping introduces additional, mobile, $Li^+$ ions into the structure because electroneutrality has to be maintained.[70]

Another way of introducing disruptions to the crystalline polymer complexes is replacing the $-OCH_3$ chain termini in the polymer material by $-OC_2H_5$. The structure of complexes made with $-OC_2H_5$-terminated PEO remains that of the $\alpha$ phase, only with a slight change of lattice parameters compared to the complex with $-OCH_3$ terminated PEO.

However, the introduction of bulkier polymer chain-ends raises the conductivity of the crystalline complex by 1 order of magnitude.[53,64]

Despite all the knowledge gained from various experiments carried out in order to increase the conductivity of crystalline polymer electrolytes, the detailed mechanism of conduction remains unknown. The so far obtained experimental evidence suggests that disruptions caused by the presence of the chain ends within the structure influences the conductivity significantly and for this reason more efforts are required in investigating the phenomena at the chain junctions.

The influence of molecular weight dispersity (distribution of chain lengths) on the conductivity has also recently been studied by comparison of crystalline complexes prepared with monodispersed dimethoxy end-capped PEO Mw = 1015 Da and with polydispersed dimethoxy end-capped PEO <Mw> = 1000 Da (Fig. 7).
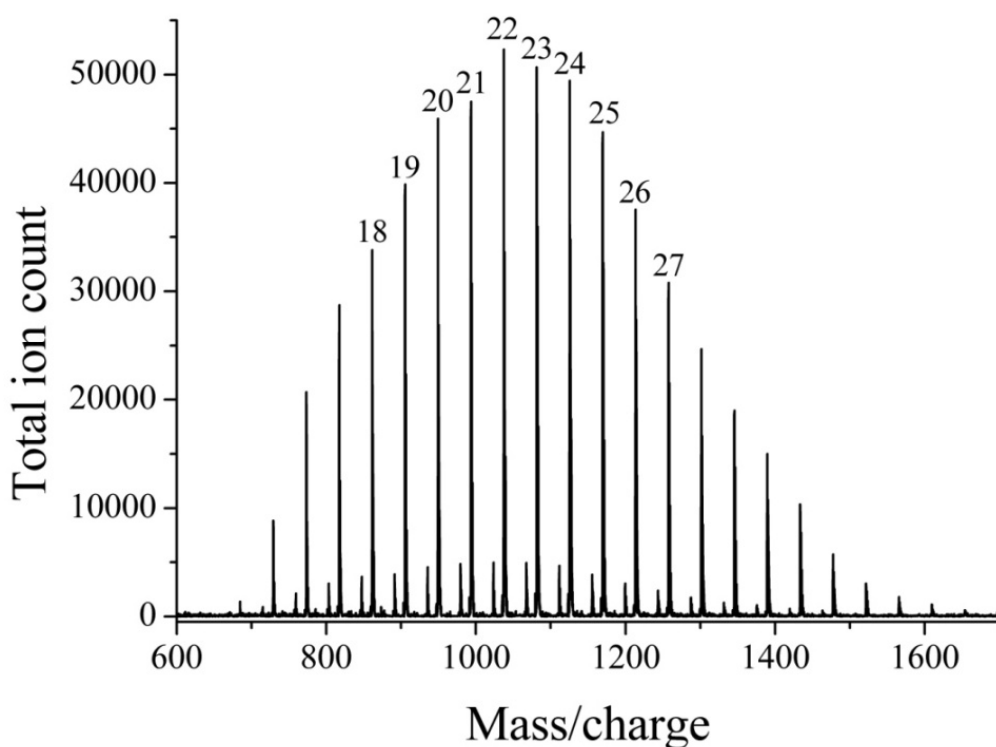


Fig. 7 MALDI-MS of polydispersed methoxy end-capped PEO <Mw> = 1000 Da.

In the polydispersed material the PEO tunnels, within which the $Li^+$ ions reside, are composed of 2 strands each built from PEO chains of varying length. The crystallite size determined by peak shape analysis of the PXRD data (Fig. 8) is in excess of 2000 Å.
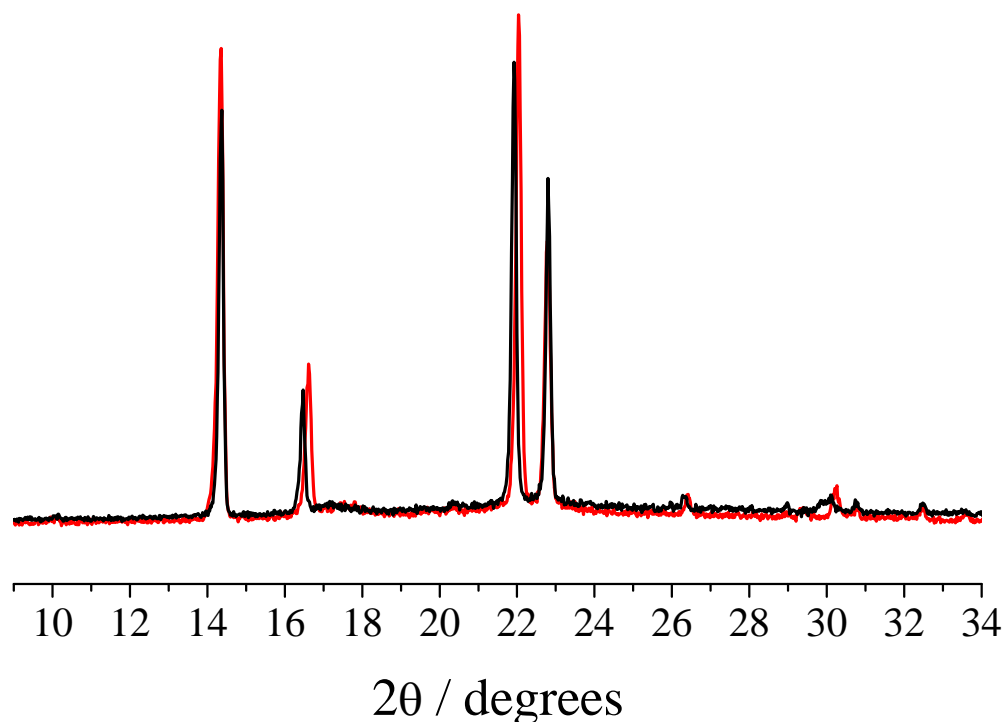
Fig. 8 Powder X-ray diffraction patterns of $PEO_6$:$LiPF_6$ prepared from monodispersed Mw = 1015 Da PEO (red) and polydispersed <Mw> = 1000 Da PEO (black).[53]

Considering that average length of the polymeric chains in the complex is approximately 40 Å, there are many chain ends within each tunnel and they are distributed randomly due to the polydispersity (Fig. 9). Such irregularity is an additional variable in the study of chain-ends effects, thus it should be beneficial to study monodispersed materials instead.
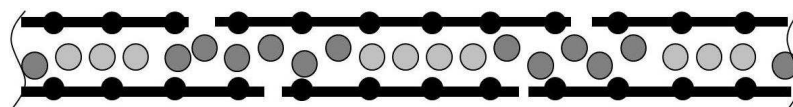


Fig. 9 Arrangement of polydispersed PEO chains in the crystalline complex. The PEO chains are represented by the solid lines and are of different length, resulting in the random occurrence of chain ends. $Li^+$ ions are represented by circles, with the disordered $Li^+$ ions, near chain ends, being represented by darker shading. Anions are not shown.

Monodispersity would, at the least, result in the chain ends occurring at regular distances along the tunnels and most likely exhibit coincidence of the chain ends between the two strands of a tunnel (Fig. 10a). However, complete registry of the chain ends between neighbouring tunnels is unlikely, because of the much weaker interactions between the

tunnels (Fig. 10b). Furthermore, such complete registry is inconsistent with molecular dynamics simulations[71] and the powder X-ray diffraction data, since it is unlikely that blocks equivalent in dimension to the chain length (42 Å) would exhibit sufficient translational symmetry to give long range order but are more likely to be canted as shown in Fig. 10c. Such a short coherence length of only ~40 Å is not consistent with the widths of the peaks in the powder X-ray diffraction pattern (Fig. 8). Taking all these facts into account, the most likely model for a monodispersed, material would be that shown in Fig. 10d. The difference between the mono- and polydispersed materials lies in the number of chain ends per unit length. In the polydispersed material there are more chain ends per unit length, since the chain ends are not coincident between strands, and this in turn leads to a higher conductivity (1 order of magnitude) compared with the monodispersed counterpart. [1,53]
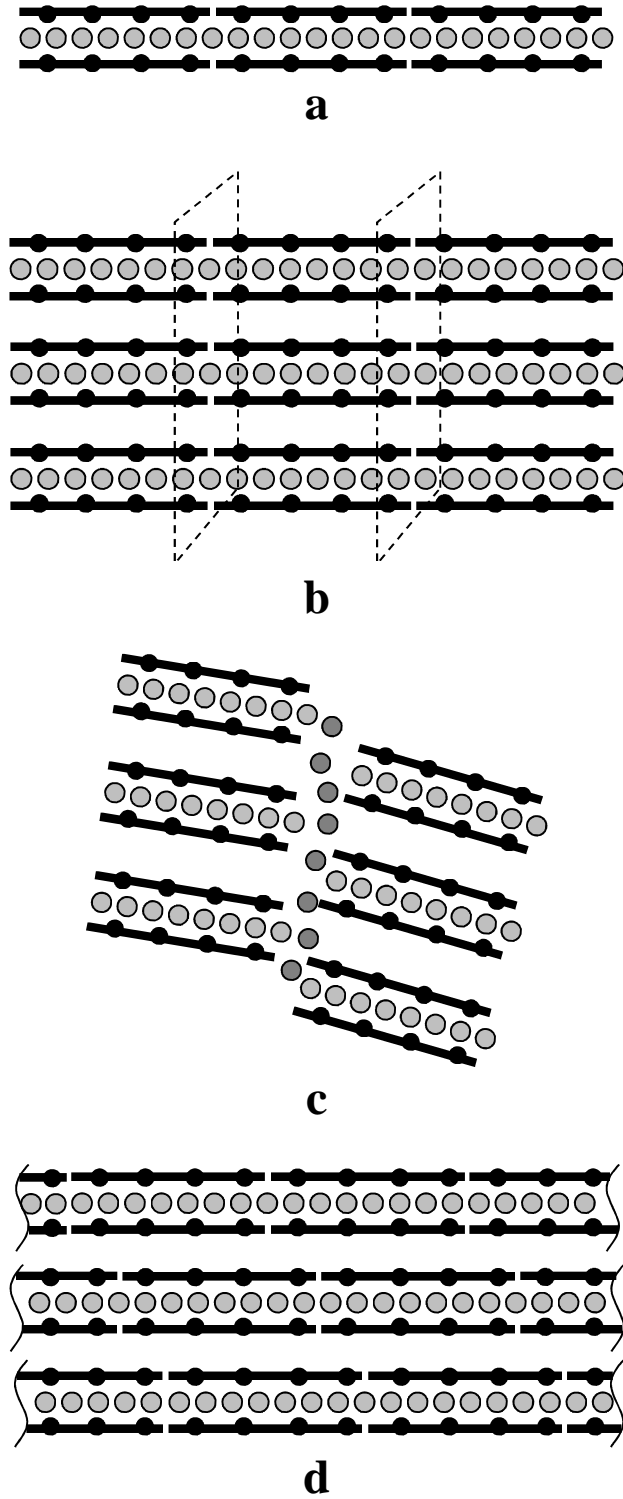
Fig. 10 Schematic representation of part of the monodispersed PEO$_6$:LiXF$_6$ crystal structure. The PEO chains are represented by the solid lines of the same length, resulting in the regular occurrence of chain ends. Li$^+$ ions are represented by circles. Anions are not shown. (a) A single tunnel formed from monodispersed PEO and showing the coincidence of chain ends in each of the two strands of the tunnel. (b) Model based on monodispersed PEO in which the chain ends coincide within and between tunnels such that the ends are located in a plane perpendicular to the tunnel axis. (c) Model based on monodispersed PEO in which the tunnels are canted and displaced. (d) Model based on monodispersed PEO in which the chain-ends coincide within a tunnel but not between tunnels.

17

The model shown in Fig. 10d was extensively studied by *Thomas et al* by means of molecular dynamics simulations and called *Nematic*. The authors distinguish two types of chain-end coordination around the $Li^+$ ions (Fig. 11).
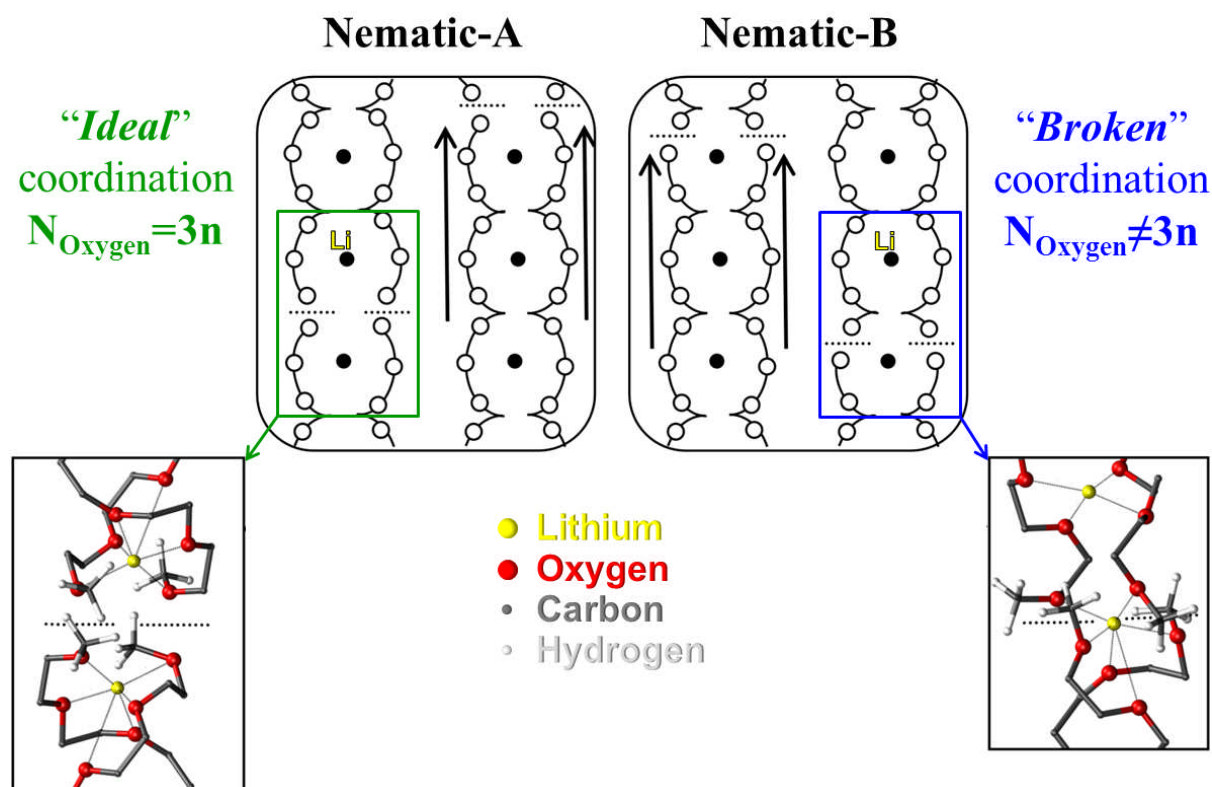


Fig. 11 Results of the molecular dynamics simulations of the chain-ends in monodispersed complexes.[72]

*Nematic-A* is an "ideal" coordination, in which chain termination does not disrupt either of the polymer chains involved in the 6-fold coordination sphere of a $Li^+$ ion. Each coordination site contains exactly 1 lithium ion and 6 oxygen atoms – 3 from each of PEO chains. So the ideal model is only possible if the number of oxygen atoms ($N_{Oxygen}$) in each polymer chain is a multiple of 3. Otherwise, only *Nematic-B* "broken" coordination model can be considered. In the "broken" model the polymer chain-ends are disrupted and such disruptions may influence the conductivity.[72] In order to verify these models, a series of monodispersed PEO with consecutive numbers of EO repeating units is required.

It is important to emphasise at this point that all the crystalline complexes discussed in chapter 1.4.2 preserve exactly the same crystalline α phase represented by PXRD pattern shown in Fig. 8. Moreover, the temperature dependence of conductivity for all those complexes follows Arrhenius rather than VTF equation, supporting the ion hopping mechanism.

# References

1. P. G. Bruce, *Energy storage beyond the horizon: Rechargeable lithium batteries.* Solid State Ionics, 2008, **179**(21-26): p. 752-760.

2. J. M. Tarascon, M. Armand, *Issues and challenges facing rechargeable lithium batteries.* Nature, 2001, **414**(6861): p. 359-367.

3. M. Armand, J. M. Tarascon, *Building better batteries.* Nature, 2008, **451**(7179): p. 652-657.

4. H. S. Choe, B. G. Carroll, D. M. Pasquariello, K. M. Abraham, *Characterization of some polyacrylonitrile-based electrolytes.* Chemistry of Materials, 1997, **9**(1): p. 369-379.

5. P. V. Wright, Y. Zheng, D. Bhatt, T. Richardson, G. Ungar, *Supramolecular order in new polymer electrolytes.* Polymer International, 1998, **47**(1): p. 34-42.

6. F. M. Gray, *Solid polymer electrolytes: fundamentals and technological applications*, VCH, New York, NY, **1991**.

7. P. Arora, Z. Zhang, *Battery Separators.* Chemical Reviews, 2004, **104**(10): p. 4419-4462.

8. S. Stramare, V. Thangadurai, W. Weppner, *Lithium lanthanum titanates: A review.* Chemistry of Materials, 2003, **15**(21): p. 3974-3990.

9. A. R. West, *Ionic conductivity of oxides based on $Li_4SiO_4$.* Journal of Applied Electrochemistry, 1973, **3**(4): p. 327-335.

10. H. Y. P. Hong, *Crystal structure and ionic conductivity of $Li_{14}Zn(GeO_4)_4$ and other new $Li^+$ superionic conductors.* Materials Research Bulletin, 1978, **13**(2): p. 117-124.

11. U. V. Alpen, M. F. Bell, W. Wichelhaus, K. Y. Cheung, G. J. Dudley, *Ionic conductivity of $Li_{14}Zn(GeO_4)_4$ (LISICON).* Electrochimica Acta, 1978, **23**(12): p. 1395-1397.

12. P. G. Bruce, A. R. West, *Ionic conductivity of LISICON solid solutions, $Li_{2+2x}Zn_{1-x}GeO_4$.* Journal of Solid State Chemistry, 1982, **44**(3): p. 354-365.

13. U. V. Alpen, A. Rabenau, G. H. Talat, *Ionic conductivity in $Li_3N$ single crystals.* Applied Physics Letters, 1977, **30**(12): p. 621-623.

14. B. A. Boukamp, R. A. Huggins, *Lithium ion conductivity in lithium nitride.* Physics Letters A, 1976, **58**(4): p. 231-233.

15. N. Kamaya, K. Homma, Y. Yamakawa, M. Hirayama, R. Kanno, M. Yonemura, T. Kamiyama, Y. Kato, S. Hama, K. Kawamoto, A. Mitsui, *A lithium superionic conductor.* Nat Mater, 2011, **10**(9): p. 682-686.

16. N. J. Dudney, *Solid-state thin-film rechargeable batteries.* Materials Science and Engineering B-Solid State Materials for Advanced Technology, 2005, **116**(3): p. 245-249.

17. S. H. Jee, M. J. Lee, H. S. Ahn, D. J. Kim, J. W. Choi, S. J. Yoon, S. C. Nam, S. H. Kim, Y. S. Yoon, *Characteristics of a new type of solid-state electrolyte with a LiPON interlayer for Li-ion thin film batteries.* Solid State Ionics, 2010, **181**(19-20): p. 902-906.

18. X. H. Yu, J. B. Bates, G. E. Jellison, F. X. Hart, *A stable thin-film lithium electrolyte: Lithium phosphorus oxynitride.* Journal of the Electrochemical Society, 1997, **144**(2): p. 524-532.

19. D. E. Fenton, J. M. Parker, P. V. Wright, *Complexes of alkali-metal ions with poly(ethylene oxide).* Polymer, 1973, **14**(11): p. 589-589.

20. M. B. Armand, J. M. Chabango, M. J. Duclot, *Poly-ethers as solid electrolytes,* in *Fast ion transport in solids: electrodes, and electrolytes* (Eds.: P. Vashishta, J. N. Mundy, G. K. Shenoy), North Holland, Amsterdam, **1979**, pp. 131-136.

21. M. A. Ratner, D. F. Shriver, *Ion transport in solvent-free polymers.* Chemical Reviews, 1988, **88**(1): p. 109-124.

22. F. M. Gray, *Polymer Electrolytes*, RSC Materials Monographs, The Royal Society of Chemistry, Cambridge, **1997**.

23. P. G. Bruce, *Energy materials.* Solid State Sciences, 2005, **7**(12): p. 1456-1463.

24. J. R. Lotz, B. P. Block, W. C. Fernelius, *A Thermodynamic Study of some Coordination Compounds of Metal Ions with Amines Containing Oxygen.* The Journal of Physical Chemistry, 1959, **63**(4): p. 541-544.

25. I. Krossing, I. Raabe, *Noncoordinating Anions - Fact or Fiction? A Survey of Likely Candidates.* Angewandte Chemie International Edition, 2004, **43**(16): p. 2066-2090.

26. M. Watanabe, T. Endo, A. Nishimoto, K. Miura, M. Yanagida, *High ionic conductivity and electrode interface properties of polymer electrolytes based on high molecular weight branched polyether.* Journal of Power Sources, 1999, **81**: p. 786-789.

27. G. G. Odian, *Principles of polymerization*, 4th ed., Wiley-Interscience, Hoboken, N.J., **2004**.

28. Y. Chatani, H. Tadokoro, T. Saegusa, H. Ikeda, *Structural studies of poly(ethylenimine). 1. Structures of 2 hydrates of poly(ethylenimine) - sesquihydrate and dihydrate.* Macromolecules, 1981, **14**(2): p. 315-321.

29. C. S. Harris, M. A. Ratner, D. F. Shriver, *Ionic-conductivity in branched polyethylenimine sodium trifluoromethanesulfonate complexes - comparisons to analogous complexes made with linear polyethylenimine.* Macromolecules, 1987, **20**(8): p. 1778-1781.

30. R. H. Gobran, R. Larsen, *Poly(ethylene sulfide). I. Unique seed polymerization technique-growth of "immortal" polymer.* Journal of Polymer Science Part C-Polymer Symposium, 1970, **31**(1): p. 77-86.

31. S. Clancy, D. F. Shriver, L. A. Ochrymowycz, *Preparation and characterization of polymeric solid electrolytes from poly(alkylene sulfides) and silver salts.* Macromolecules, 1986, **19**(3): p. 606-611.

32. T. Yamamoto, M. Inami, T. Kanbara, *Preparation and properties of polymer solid electrolytes using poly(vinyl alcohol) and thermally resistive poly[arylene(1,3-imidazolidine-2,4,5-trione-1,3-diyl)] as matrix polymers.* Chemistry of Materials, 1994, **6**(1): p. 44-50.

33. C. T. Imrie, M. D. Ingram, G. S. McHattie, *Ion transport in glassy polymer electrolytes.* Journal of Physical Chemistry B, 1999, **103**(20): p. 4132-4138.

34. X. Y. Wei, D. F. Shriver, *Highly conductive polymer electrolytes containing rigid polymers.* Chemistry of Materials, 1998, **10**(9): p. 2307-2308.

35. J. R. MacCallum, C. A. Vincent, *Polymer electrolyte reviews vol. 1*, Elsevier, London, **1987**.

36. A. M. Christie, S. J. Lilley, E. Staunton, Y. G. Andreev, P. G. Bruce, *Increasing the conductivity of crystalline polymer electrolytes.* Nature, 2005, **433**(7021): p. 50-53.

37. C. Berthier, W. Gorecki, M. Minier, M. B. Armand, J. M. Chabagno, P. Rigaud, *Microscopic investigation of ionic-conductivity in alkali-metal salts poly(ethylene oxide) adducts.* Solid State Ionics, 1983, **11**(1): p. 91-95.

38. P. M. Blonsky, D. F. Shriver, P. Austin, H. R. Allcock, *Polyphosphazene solid electrolytes.* Journal of the American Chemical Society, 1984, **106**(22): p. 6854-6855.

39. D. W. Bruce, R. I. Walton, D. O'Hare, *Energy materials*, Wiley, Chichester, West Sussex, U.K., **2011**.

40. C. A. Angell, C. Liu, E. Sanchez, *Rubbery solid electrolytes with dominant cationic transport and high ambient conductivity.* Nature, 1993, **362**(6416): p. 137-139.

41. M. Forsyth, J. Z. Sun, D. R. MacFarlane, *Novel polymer-in-salt electrolytes based on polyacrylonitrile (PAN) lithium triflate salt mixtures.* Solid State Ionics, 1998, **112**(1-2): p. 161-163.

42. S. Chintapalli, R. Frech, *Effect of plasticizers on high molecular weight PEO-LiCF$_3$SO$_3$ complexes.* Solid State Ionics, 1996, **86-8**: p. 341-346.

43. G. B. Appetecchi, G. Dautzenberg, B. Scrosati, *A new class of advanced polymer electrolytes and their relevance in plastic-like, rechargeable lithium batteries.* Journal of the Electrochemical Society, 1996, **143**(1): p. 6-12.

44. J. M. Tarascon, A. S. Gozdz, C. Schmutz, F. Shokoohi, P. C. Warren, *Performance of Bellcore's plastic rechargeable Li-ion batteries.* Solid State Ionics, 1996, **86-8**: p. 49-54.

45. P. Raghavan, X. H. Zhao, J. K. Kim, J. Manuel, G. S. Chauhan, J. H. Ahn, C. Nah, *Ionic conductivity and electrochemical properties of nanocomposite polymer electrolytes based on electrospun*

*poly(vinylidene fluoride-co-hexafluoropropylene) with nano-sized ceramic fillers.* Electrochimica Acta, 2008, **54**(2): p. 228-234.

46. F. Croce, G. B. Appetecchi, L. Persi, B. Scrosati, *Nanocomposite polymer electrolytes for lithium batteries.* Nature, 1998, **394**(6692): p. 456-458.

47. M. Forsyth, D. R. MacFarlane, A. Best, J. Adebahr, P. Jacobsson, A. J. Hill, *The effect of nano-particle TiO$_2$ fillers on structure and transport in polymer electrolytes.* Solid State Ionics, 2002, **147**(3–4): p. 203-211.

48. B. Kumar, L. G. Scanlon, *Polymer-ceramic composite electrolytes: conductivity and thermal history effects.* Solid State Ionics, 1999, **124**(3-4): p. 239-254.

49. C. Capiglia, P. Mustarelli, E. Quartarone, C. Tomasi, A. Magistris, *Effects of nanoscale SiO$_2$ on the thermal and transport properties of solvent-free, poly(ethylene oxide) (PEO)-based polymer electrolytes.* Solid State Ionics, 1999, **118**(1-2): p. 73-79.

50. G. S. MacGlashan, Y. G. Andreev, P. G. Bruce, *Structure of the polymer electrolyte poly(ethylene oxide)$_6$:LiAsF$_6$.* Nature, 1999, **398**(6730): p. 792-794.

51. Z. Gadjourova, D. M. Marero, K. H. Andersen, Y. G. Andreev, P. G. Bruce, *Structures of the polymer electrolyte complexes PEO$_6$:LiXF$_6$ (X = P, Sb), determined from neutron powder diffraction data.* Chemistry of Materials, 2001, **13**(4): p. 1282-1285.

52. Z. Stoeva, PhD thesis, University of St Andrews **2001**.

53. E. Staunton, Y. G. Andreev, P. G. Bruce, *Factors influencing the conductivity of crystalline polymer electrolytes.* Faraday Discussions, 2007, **134**: p. 143-156.

54. Z. Gadjourova, Y. G. Andreev, D. P. Tunstall, P. G. Bruce, *Ionic conductivity in crystalline polymer electrolytes.* Nature, 2001, **412**(6846): p. 520-523.

55. E. Staunton, Y. G. Andreev, P. G. Bruce, *Structure and conductivity of the crystalline polymer electrolyte beta-PEO$_6$:LiAsF$_6$.* Journal of the American Chemical Society, 2005, **127**(35): p. 12176-12177.

56. Z. Stoeva, I. Martin-Litas, E. Staunton, Y. G. Andreev, P. G. Bruce, *Ionic conductivity in the crystalline polymer electrolytes PEO$_6$:LiXF$_6$, X = P, As, Sb.* Journal of the American Chemical Society, 2003, **125**(15): p. 4619-4626.

57. A. Liivat, D. Brandell, J. O. Thomas, *A molecular dynamics study of ion-conduction mechanisms in crystalline low-Mw LiPF$_6$•PEO$_6$.* Journal of Materials Chemistry, 2007, **17**(37): p. 3938-3946.

58. P. G. Bruce, *Coordination chemistry in the solid state.* Philosophical Transactions of the Royal Society of London Series a-Mathematical Physical and Engineering Sciences, 1996, **354**(1706): p. 415-436.

59. Y. G. Andreev, P. G. Bruce, *Polymer electrolyte structure and its implications.* Electrochimica Acta, 2000, **45**(8-9): p. 1417-1423.

60. R. Kovarsky, D. Golodnitsky, E. Peled, S. Khatun, P. E. Stallworth, S. Greenbaum, A. Greenbaum, *Conductivity enhancement induced by casting of polymer electrolytes under a magnetic field.* Electrochimica Acta, 2011, **57**(0): p. 27-35.

61. S. H. Chung, Y. Wang, S. G. Greenbaum, D. Golodnitsky, E. Peled, *Uniaxial stress effects in poly(ethylene oxide)-LiI polymer electrolyte film A $^7$Li nuclear magnetic resonance study.* Electrochemical and Solid State Letters, 1999, **2**(11): p. 553-555.

62. D. Golodnitsky, E. Peled, *Stretching-induced conductivity enhancement of LiI-(PEO)-polymer electrolyte.* Electrochimica Acta, 2000, **45**(8-9): p. 1431-1436.

63. D. Golodnitsky, E. Livshits, R. Kovarsky, E. Peled, S. H. Chung, S. Suarez, S. G. Greenbaum, *New generation of ordered polymer electrolytes for lithium batteries.* Electrochemical and Solid State Letters, 2004, **7**(11): p. A412-A415.

64. D. A. Ainsworth, PhD thesis, University of St Andrews **2010**.

65. C. Zhang, E. Staunton, Y. G. Andreev, P. G. Bruce, *Doping crystalline polymer electrolytes with glymes.* Journal of Materials Chemistry, 2007, **17**(30): p. 3222-3228.

66. S. J. Lilley, Y. G. Andreev, P. G. Bruce, *Ionic conductivity in crystalline $PEO_6$:$Li(AsF_6)_{1-x}(SbF_6)_x$*. Journal of the American Chemical Society, 2006, **128**(37): p. 12036-12037.

67. K. Shahi, J. B. Wagner, *Fast ion transport in silver halide solid solutions and multlphase systems.* Applied Physics Letters, 1980, **37**(8): p. 757-759.

68. T. Norby, *Fast oxygen ion conductors - from doped to ordered systems.* Journal of Materials Chemistry, 2001, **11**(1): p. 11-18.

69. P. G. Bruce, *Solid state electrochemistry*, Cambridge University Press, Cambridge ; New York, NY, USA, **1995**.

70. C. H. Zhang, E. Staunton, Y. G. Andreev, P. G. Bruce, *Raising the conductivity of crystalline polymer electrolytes by aliovalent doping.* Journal of the American Chemical Society, 2005, **127**(51): p. 18305-18308.

71. D. Brandell, A. Liivat, A. Aabloo, J. O. Thomas, *Molecular dynamics simulation of the crystalline short-chain polymer system $LiPF_6 \bullet PEO_6$ (Mw ~ 1000).* Journal of Materials Chemistry, 2005, **15**(40): p. 4338-4345.

72. A. Liivat, D. Brandell, A. Aabloo, J. O. Thomas, *A molecular dynamics study of short-chain ordering in crystalline $LiPF_6 \bullet PEO_6$.* Polymer, 2007, **48**(21): p. 6448-6456.

## 2. THE AIM OF THE PROJECT

It is very important to explore the area of crystalline polymer electrolytes as they exhibit promising conductivity and impose selectivity on ion transport, whereas amorphous materials above $T_g$, much like conventional liquids, are not selective, and in fact their conductivity is dominated by anion transport.[1]

Clearly, many various routes have been explored in order to improve the ionic conductivity of crystalline polymer electrolytes, but the conductivity of the best systems is still too low for application of these electrolytes in batteries. Further improvements can only be made if the mechanism of conduction is understood. Both the conductivity data obtained when the density of the chain-end occurrences increased and the molecular dynamics simulations hint that thorough study of the phenomena occurring at the chain ends present in the tunnels may help in establishing the conduction mechanism. As discussed in 1.4.2, using monodispersed PEO would limit the number of variables in such study and enable testing different arrangements of coordination sites of lithium ions at the chain ends – "ideal" or "broken" coordination[2]. Only one complex with monodispersed PEO Mw = 1015 Da (22 repeat unit, 23 ether oxygen atoms) has been investigated so far.[1] That single investigation alone is not enough to gain a significant insight into the conductivity mechanism. Further research of monodispersed materials with different chain lengths is necessary. Preferably the Mws of the monodispersed PEOs to be used should be as close as possible to 1000 Da to allow direct comparison with the reported by the *Bruce* group complexes prepared with polydispersed polymers. Also, the series must contain polymers with consecutive number of repeat units (and hence ether oxygen atoms) in order to investigate the near-end coordination of $Li^+$. The target PEOs are listed in the Table 1:

| Number of ether oxygen atoms, ($N_O$) | Mw [Da] | EO repeat units ($n$) |
|:---:|:---:|:---:|
| **20** | 883.067 | 19 |
| **21** | 927.120 | 20 |
| **22** | 971.172 | 21 |
| **23** | 1015.225 | 22 |
| **24** | 1059.277 | 23 |
| **25** | 1103.330 | 24 |

Table 1: List of the target monodispersed PEOs.

Only the 23-ether-oxygens monodispersed PEO is available commercially so the first aim is to synthesise all the polymers followed by preparation and characterisation of complexes.

# References

1. E. Staunton, Y. G. Andreev, P. G. Bruce, *Factors influencing the conductivity of crystalline polymer electrolytes.* Faraday Discussions, 2007, **134**: p. 143-156.

2. A. Liivat, D. Brandell, A. Aabloo, J. O. Thomas, *A molecular dynamics study of short-chain ordering in crystalline LiPF6 center dot PEO6.* Polymer, 2007, **48**(21): p. 6448-6456.

# 3. EXPERIMENTAL TECHNIQUES

Most experimental techniques used in this project are well established and commonly used in our research laboratories. They include preparation of polymer electrolytes, PXRD, DSC, AC Impedance, transport number measurements. Preparative techniques used for the syntheses of polymers will be described separately. The principles of NMR, FTIR and mass spectroscopy techniques will not be described in detail, because they were used only for finger-printing.

## 3.1. Solution NMR

$^1$H NMR spectra were recorded on a Bruker Avance II 400 (400 MHz) spectrometer using deuterochloroform (unless indicated otherwise) as a reference for internal deuterium lock. The chemical shift data for each signal are given as $\delta_H$ in units of parts per million (ppm) relative to tetramethylsilane (TMS) where $\delta_{(TMS)} = 0.00$ ppm. The multiplicity of each signal is indicated by: s (singlet), d (doublet), t (triplet), q (quartet) or m (multiplet). The number of protons (n) for a given resonance signal is indicated by nH. Coupling constants (J) are quoted in Hz and are recorded to the nearest 0.1 Hz. Identical proton coupling constants (J) are averaged in each spectrum and reported to the nearest 0.1 Hz. The coupling constants are determined by analysis using Bruker TopSpin software.

$^{13}$C NMR spectra were recorded on Bruker Avance II 400 (101 MHz) spectrometer using the DEPT (Distortionless Enhancement by Polarisation Transfer) Q (Quaternaries) pulse sequences with broadband proton decoupling and internal deuterium lock. The chemical shift data for each signal are given as $\delta$ in units of parts per million (ppm) relative to tetramethylsilane (TMS) where $\delta_{C\ (TMS)} = 0.00$ ppm.

The DEPT experiment is used for enhancing the sensitivity of carbon observation and for editing of $^{13}$C spectra. The sensitivity gain comes from starting the experiment with proton excitation and subsequently transferring the magnetisation onto carbon (polarisation transfer). This increase in signal intensity stems from the larger population differences associated with protons. The editing feature alters the amplitude and sign of the carbon resonances according to the number of directly attached protons, allowing the identification of carbon multiplicities. Because quaternary carbons do not possess a directly bonded proton, they do not produce responses in DEPT experiments. For that reason the method has been modified and renamed to DEPT Q where "Q" stands for inclusion of Quaternaries. DEPT Q is a variant of the above DEPT experiment in which the signals of non-protonated carbons

(e.g. quaternary centres, hence the "Q") are also included (although with reduced intensities).[1] The $^1$H and $^{13}$C spectra are assigned and reported for each synthesised compound in relevant chapters.

## 3.2. FTIR

FTIR data was collected on Nicolet 6700 (Fisher Thermo Scientific) in either transmission (CsI pellet) or reflexion (ATR) mode in a nitrogen filled glove box.

## 3.3. Mass spectrometry (MALDI-MS, ESI-MS)

Mass spectrometry was measured either by matrix-assisted laser desorption/ionization (MALDI) or electrospray ionization (ESI) mass spectrometry (MS).

### 3.3.1.  MALDI-MS

The sample, dissolved in the appropriate solvent, was applied to the MALDI target along with a matrix and a sodium salt and allowed to dry.  MALDI-MS was acquired using a 4800 MALDI TOF/TOF Analyser (ABSciex, Foster City, CA) equipped with a Nd:YAG 355 nm laser and calibrated using a mixture of peptides. The spot was analysed in positive MS mode over the appropriate mass range, by averaging 1000 laser spots.  The laser intensity was adjusted to give in the region of 2000 counts for the most intense peak in the spectrum.

### 3.3.2.  ESI-MS

The sample was dissolved in either 50:50 acetonitrile:water or methanol at a concentration of 1 ng/µL and delivered to an electrospray ionisation mass spectrometer (LCT, Micromass, Manchester, U.K.) at 20 µL/min via a syringe pump and analysed in positive ionization mode, using a capillary voltage of 3200 V and a cone voltage tuned to the specific sample.  The instrument had been calibrated on a series of sodium formate adducts.

### 3.4. SEC (GPC)

Synthesised polymers were analysed by means of size-exclusion chromatography (SEC) in order to determine their molecular weight distribution and purity – details of deficiencies of this method will be described in 4.2.

#### 3.4.1. Sample preparation

For each sample, a single solution was prepared with a volume of solvent expected to give a concentration of 10.0 mg/ml. The solutions were left for a minimum of 4 hours to dissolve and were then thoroughly mixed before being filtered through a 0.2 μm membrane.

#### 3.4.2. Chromatographic conditions

Instrument:     Malvern/Viscotek Model 301 TDA with associated pump and autosampler,
Columns:        PLgel guard plus 2 × mixed bed-E, 30 cm, 3 μm,
Solvent:        tetrahydrofuran (stabilised with antioxidant),
Injection:      20 μl,
Flow-rate:      1.0 ml/min (nominal),
Temperature:   30°C (nominal),
Detector:       refractive index (with differential pressure and light scattering).
The data has been collected and analysed using Malvern/Viscotek "OminSec" software.

### 3.5. Gradient flash chromatography

When indicated, purification of a reaction product was performed on an automated gradient flash chromatography system Biotage® SP1. The conditions were individually tailored for particular materials and are described in appropriate sections of the synthesis chapter 4. The separated fractions were analysed on thin layer chromatography (TLC), carried out on Merck silica gel 60 glass-supported thin layer chromatography sheets. Visualisation was achieved by thermal development after dipping in solution of potassium permanganate ($KMnO_4$).

### 3.6. X-Ray Diffraction

By measuring the radiation diffracted by the sample and the variation of intensity with direction or the wavelength, it is possible to identify the position of atoms in the structure. It is the electrons of an atom that scatter the X-rays. Thus every atom has a unique scattering power, which allows to establish the position of all individual atoms.

A crystal is a highly ordered repeating assembly of atoms which can be viewed as regularly spaced planes. When X-rays hit the sample, they are diffracted by the atoms according to the Braggs' law:

$$n\lambda = 2d \sin\theta$$

where: $n$ is an integer number, $\lambda$ is the wavelength of the radiation, $d$ is the interplanar spacing and $\theta$ is the incident angle. The law allows us to predict when a given set of planes will diffract with constructive interference (Fig. 12).
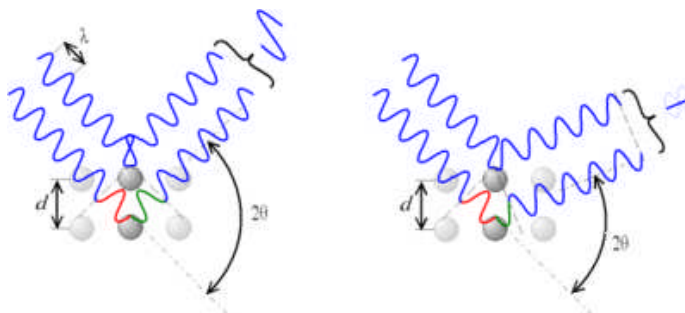


Fig. 12 The interpratation of Braggs' law.

A single crystal gives a diffraction pattern with discrete diffracted spots, each in a definitive direction relative to the orientation of the crystal and the incident beam, according to the Braggs' equation. A stationary single crystal with fixed incident beam gives very few reflections (if any). In order to obtain the complete diffraction pattern it is necessary to perform the data collection in 3D, which includes all possible orientations of the beam/crystal/detector.

In the case of a powder each of the very many randomly oriented micro-crystals comprising the powder produces its own diffraction pattern, all of which are superimposed. Thus, when compared to the single crystal setup, powder pattern is essentially a compression of 3D diffraction into one dimension (scattering angle), which inevitably leads to peak overlap.
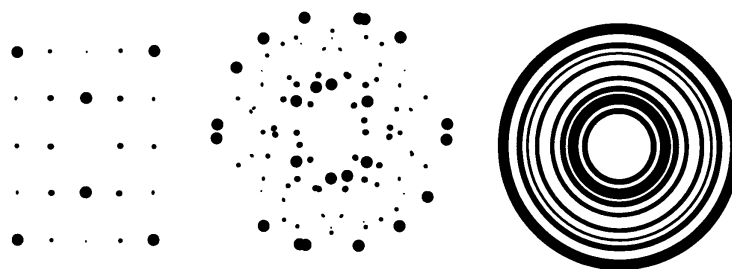
Fig. 13 Diffraction patterns.

Fig. 13 shows an example of different diffraction patterns of the same material. The pattern on the left represents the reflection produced by a single crystal. The diffraction pattern in the middle represents the reflection received when four such crystals are superimposed in random relative orientations. The pattern on the right is what is received when carrying out a powder x-ray diffraction, i.e. the pattern for a very large number of crystals. Each spot on the left diagram is now represented by a circle on the right.[2]

### 3.6.1. Powder X-ray Diffraction (PXRD) – details

Powder X-ray diffraction was carried out using a Stoe STADI/P powder diffractometer with $CuK_{\alpha 1}$ radiation operating in transmission mode and employing a small angle position sensitive detector (PSD). Data were collected with a step width of 0.02° in 2θ. To avoid contact with air the polymer electrolyte samples were sealed in Lindemann (glass) capillaries.

### 3.6.2. Single Crystal – details

Data were collected using a Rigaku MM007 High brilliance RA generator ($MoK_{\alpha}$ radiation, confocal optics) and Saturn70 CCD system. At least a full hemisphere of data was collected using ω scans. Intensities were corrected for Lorentz-polarisation and for absorption. The structures were solved by direct methods. Hydrogen atoms bound to carbon were idealised. Structural refinements were performed with full-matrix least-squares based on $F^2$ by using SHELXTL (Sheldrick, G. M.. SHELXTL. Version 6.14. Bruker AXS Inc., Madison 2004).

## 3.7. Differential Scanning Calorimetry (DSC)

DSC methodology is based upon measuring the change of the difference in the heat flow to the sample under investigation and to a reference sample while they are subjected to a controlled temperature program.[3] Different amounts of heat must be supplied to the sample and the reference, in order to maintain both at the same temperature due to their different heat capacity when the sample undergoes physical transformation (e.g. phase transition) or chemical reaction.
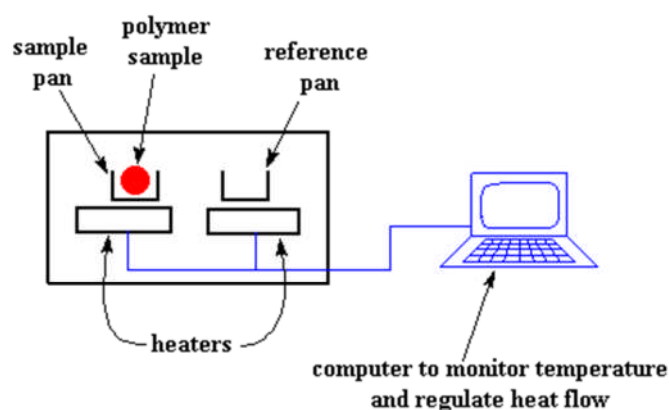


Fig. 14 Schematic representation of a DSC instrument.

A typical DSC instrument is shown in Fig. 14. Both a sample and a reference pan are heated (or cooled) in the way that the temperature difference between them is almost zero.

Consider a polymer sample subjected to heating at a specific rate and analysed by DSC method. To increase the temperature ($T$) of the material, the instrument supplies it with heat ($Q$) over the time ($t$). The heating rate is described as temperature increase per unit time ($\Delta T/t$). If we now divide the heat flow ($Q/t$) by the heating rate we obtain a term called heat capacity ($C_p$), which if further divided by certain amount (mass) of the material gives the specific heat capacity ($C$), which is a characteristic constant value for a material.

$$C = \frac{Q}{m\Delta T} \quad [\text{J·K}^{-1}\text{·kg}^{-1}]$$

As the heat capacity of the analysed polymer is higher than that of air (or an inert gas), we observe the difference in the amount of heat supplied to the polymer sample and the reference pan, what is displayed on the DSC plot (Fig. 15) as a certain value.
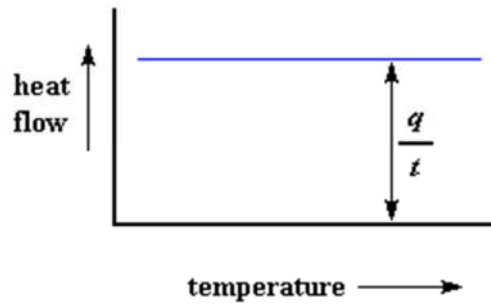
Fig. 15 Heat flow vs. temperature

Polymers may be amorphous, crystalline or semicrystalline depending mainly on their intrinsic properties, but sometimes also on the way they have been treated. This is what makes macromolecular systems very different from molecular ones. Polymers are considered to be completely immobile below certain characteristic temperature known as glass transition temperature ($T_g$). If the examined polymer sample is heated up above the $T_g$, some segmental movements of polymer chains will occur and the polymer will not be 'frozen' anymore. To maintain those movements, more energy must now be supplied to the polymer than in the glassy state, which means that its heat capacity is higher. This change is represented in Fig. 16.
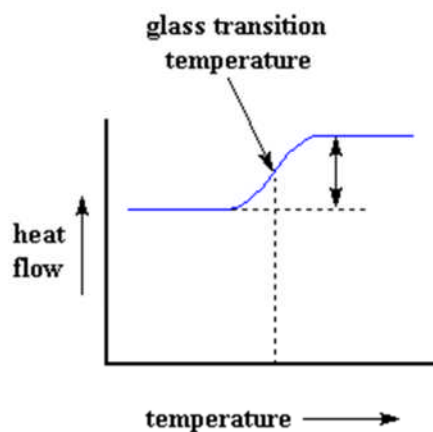


Fig. 16 Glass transition temperature ($T_g$)

Let us assume that our polymer was "frozen" in a predominantly amorphous phase, but possessed the intrinsic capability to create crystalline phase. This means, that it will try to reorganise in the manner to build up some crystallites as the most preferred energetic state. As after crossing $T_g$ the movement of chains were enabled, we should now expect that the polymer will do so. Indeed, during further heating the crystallisation temperature ($T_c$) is

31

reached at which the mobility of chains is strong enough to reorganise the structure. Since the crystalline phase is energetically more favourable, the transition, which leads to this arrangement, will release some energy from the material. This energy is consumed to increase the temperature of the sample, so the heater of the instrument does not have to heat the sample as much as previously to maintain its temperature at the same level as the reference pan. Thus it will be registered in the DSC plot as a dip (Fig. 17).
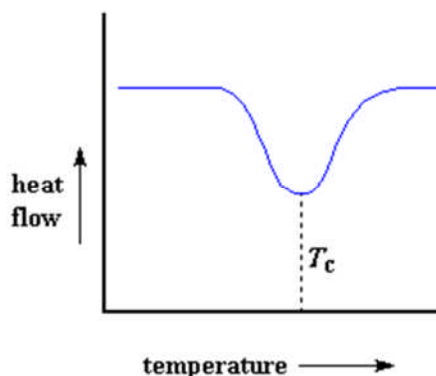


Fig. 17 Crystallisation temperature ($T_c$)

Moreover, the area of the dip can be integrated and if the percentage of crystalline phase in the material and total mass of the sample are known, the calculated area will tell us the specific heat of melting of the crystalline phase of the polymer. Similarly, if the specific heat of melting of the polymer and mass of the sample are known, we can calculate the percentage of crystalline phase in the material.

If the instrument keeps heating the sample, it will finally reach the temperature at which the crystalline phase melts. Since the melting process is endothermic, the sample will require more heat to maintain the same temperature as the reference pan. It will result in a strong peak in the DSC plot and the top of this peak indicates the melting temperature ($T_m$) (Fig. 18).
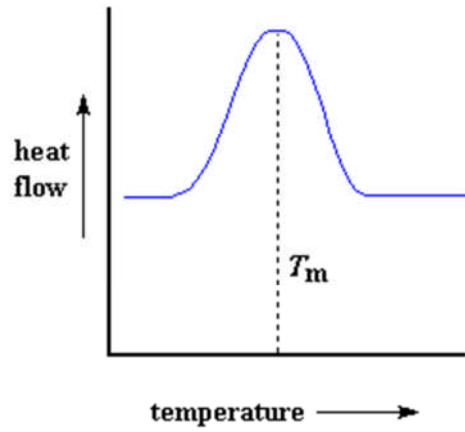
Fig. 18 Melting temperature ($T_m$)

Accordingly, the area of the peak represents the latent heat of melting of the crystalline phase.

### 3.7.1. Differential scanning calorimetry (DSC) – details

The samples (2.0 mg) were placed in aluminium pans which were sealed in an argon filled glove box and differential scanning calorimetry was carried out using a Netzsch DSC 204 Phoenix. All the samples were measured using the same temperature program (Fig. 19).

#### Contents

| Num | Mode | °C | K/min | pts/min | hh:mm | STC | P1 | P2 | PG | LN2 | GN2 | Co |
|---|---|---|---|---|---|---|---|---|---|---|---|---|
| ... | Initial | 20.0 | | | | 1 | 0 | 1 | 1 | 1 | 0 | 0 |
| 1 | Dynamic | -130.0 | 5.00 | 30.00 | 00:30 | 0 | 0 | 1 | 1 | 1 | 0 | 0 |
| 2 | Isothermal | -130.0 | | 10.00 | 00:10 | 0 | 0 | 1 | 1 | 1 | 0 | 0 |
| 3 | Dynamic | 150.0 | 10.00 | 30.00 | 00:28 | 1 | 0 | 1 | 1 | 0 | 1 | 0 |
| 4 | Isothermal | 150.0 | | 10.00 | 00:10 | 1 | 0 | 1 | 1 | 0 | 1 | 0 |
| 5 | Dynamic | -130.0 | 5.00 | 30.00 | 00:56 | 0 | 0 | 1 | 1 | 0 | 1 | 0 |
| 6 | Isothermal | -130.0 | | 10.00 | 00:10 | 0 | 0 | 1 | 1 | 1 | 0 | 0 |
| 7 | Dynamic | 150.0 | 10.00 | 30.00 | 00:28 | 1 | 0 | 1 | 1 | 0 | 1 | 0 |
| 8 | Emergency | 160.0 | | | | | 0 | 1 | 1 | 1 | 0 | 0 |
| ... | StdBy Heat. | 30.0 | 40.00 | | 00:03 | 0 | 0 | 1 | 1 | 1 | 0 | 0 |
| ... | StdBy Iso | 30.0 | | | 00:05 | 0 | 0 | 1 | 1 | 1 | 0 | 0 |
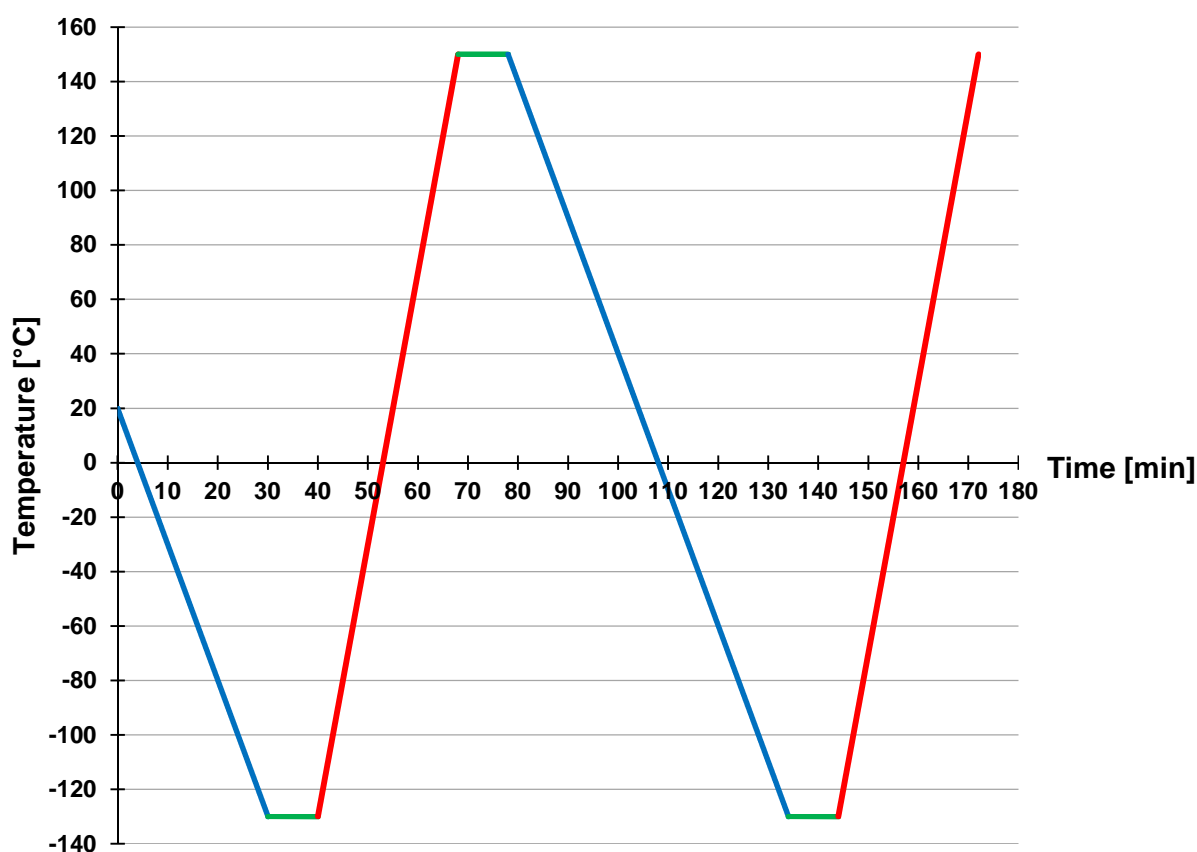


Fig. 19 DSC temperature program.

### 3.8. Electrical measurements on Polymer Electrolyte

Traditionally, investigation of the electrical properties of pure polymers was almost synonymous with the determination of their dielectric properties, since they were only considered as insulators due to their low conductivity. Since 1977 it has been known that pure polymers can also conduct electrons.[4] The authors of that discovery were awarded the Nobel Prize in chemistry in 2000. However, it has also been known for 30 years already, that some of the pure, practically insulating polymers can be used to produce ionically conducting electrolytes[5] and they are the aim of this study.

Characterisation of the basic electrical properties of a polymer electrolyte involves determination of the following:

1) the total conductivity of the electrolyte as a function of temperature,
2) identification of the different charged species contributing to conduction,
3) the transport numbers, i.e. the proportion of the current carried by each charged species, as a function of temperature.

Three major techniques are now widely used in electrical characterisation of polymer electrolytes:

1) direct current (DC) measurements
2) alternating current (AC) measurements
3) transport number measurements

### 3.8.1. Direct Current (DC) Measurements

The DC techniques represent the most straightforward method which may be employed to measure ionic conductivity in polymers. Their use to date is significantly less than that of AC techniques, but is still of considerable value.

Let us, as an example, consider an electrolyte in which conduction occurs by the migration of $Li^+$ only. The polymer electrolyte in question is sandwiched between 2 metallic lithium (non-blocking) electrodes, so that on the application of a stable DC voltage a constant current flows around the circuit and through the cell. At electrode 1 electrons from a power source reduce $Li^+$ cations from electrolyte, while at electrode 2 cations are generated by oxidation and injected into the electrolyte phase as the electrons flow towards the power supply. The electric field generated by the electrodes causes migration of ions through the electrolyte. By simple measurements of the applied potential ($V$) and generated current ($I$), the resistance of the electrolyte ($R_b$) may be calculated according to the Ohm's law:

$$R_b = \frac{V}{I}$$

Knowing the cross section area of the electrolyte (*A*) and the distance between the electrodes (*l*) we convert to the specific conductivity ($\sigma$):

$$\sigma = \frac{l}{R_b \cdot A}$$

This simple consideration does not take into account a major difficulty of this method – the current must cross both electrode/electrolyte interfaces which add other 2 resistances ($R_e$). Normally $R_e$ is not negligible in comparison with $R_b$. This problem is difficult to overcome in real systems.

### 3.8.2. Alternating Current (AC) Measurements

The AC methods are currently the most popular approach to the determination of the electrical properties of polymer electrolytes. The main advantage is, undoubtedly, that very simple cells incorporating inert blocking electrodes may be used to determine bulk electrolyte properties, although compared with the DC techniques both the equipment required and the theory necessary to interpret the measurements are much more complex. On the other hand, from AC impedance data it is also possible to gain information about long-range migration of ions and polarisation phenomena occurring in the cell.

In an AC experiment a sinusoidal voltage is applied across a cell and the sinusoidal current passing through the cell as a result of this perturbation is measured. Two parameters are required to relate current to voltage which is the crucial difference from DC perturbations as this only requires one parameter (i.e. resistance). One represents the opposition to the flow of charge and is equal to the ratio of the voltage and current maxima ($V_{max}/I_{max}$) and is analogous to the resistance in DC measurements. The other parameter ($\theta$) is the phase difference between voltage and current (Fig. 20).
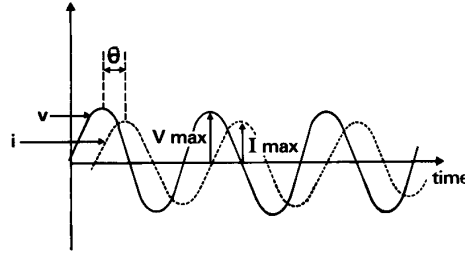
Fig. 20 Representation of sinusoidal voltage and current, at a given frequency associated with the cell.

The combination of these two parameters represents the impedance ($Z$) of the cell. Generally, for an electrochemical cell both the magnitude of the impedance ($/Z/= V_{max}/I_{max}$) and its phase angle ($\theta$) are functions of the applied frequency.

The most commonly used AC method for considered application involves measuring the impedance as a function of the frequency of the applied signal over a wide frequency range, typically from 1 mHz to 1 MHz. Since the impedance is frequency dependent, we can extract information about the electrical properties of the cell. The impedance of a cell is a vector quantity and can be represented by a point on a phasor diagram. The impedance for each frequency measured is represented by a separate point on the vector diagram (Fig. 21).
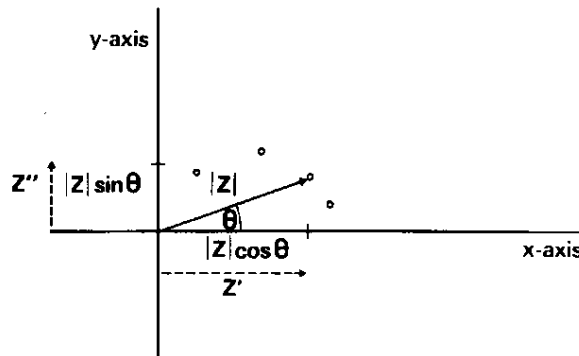


Fig. 21 Representation of the impedance ($Z$) of a cell on a vector diagram.

The distance between the point and the origin, and the angle formed with the x-axis correspond to the magnitude of the impedance and phase difference between the voltage and current accordingly. This is analogous to the representation of a complex number in the complex plane, so that the impedance may be conveniently represented by a complex number. If that is the case, this is often termed the complex impedance ($Z^*$). Its $x$ and $y$ components equal $/Z/cos\theta$ and $/Z/sin\theta$ respectively.

A typical AC experiment consists of determining the complex impedance of the cell as a function of the signal frequency and presenting the results in the form of a complex impedance plot.

### 3.8.2.1. AC response of cells with blocking electrodes

In a cell with blocking electrodes the mobile species in the electrolyte do not participate in any electrode reactions and type 1 polymer electrolytes have only one mobile ionic species. Consider this type of polymer electrolyte sandwiched between two platinum electrodes with a lithium ion conducting polymer electrolyte. Assuming an idealised lithium ion conducting polymer and platinum electrodes, AC voltage is applied to the cell and the frequency is varied. The equivalent circuit to the cell is given in Fig. 22.
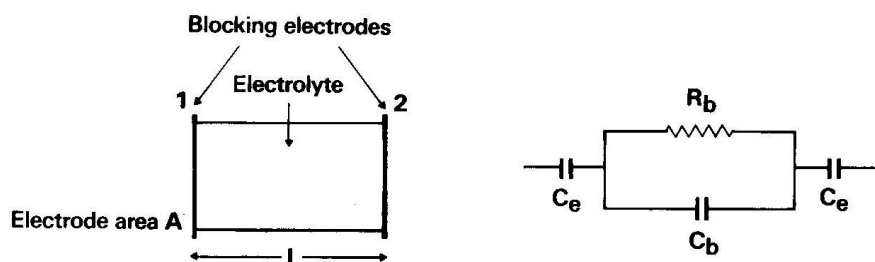


Fig. 22 Schematic representation of a polymer electrolyte/blocking electrode cell.

We can assume that an idealised lithium ion conducting polymer with platinum electrodes will represent such a circuit. An AC voltage is applied to the cell and frequency is varied, so the electrodes become alternatively positively and negatively charged. As a result the alternating field across the electrolyte causes the $Li^+$ ions to migrate back and forth in phase with the voltage. This migration is represented by the resistor $R_b$. At the same time the immobile polymer matrix becomes polarised in that field as a typical dielectric material what is represented by the capacitor $C_b$.

As the $Li^+$ ions move in the alternating field they are alternatively accumulated and then depleted at each electrode. On each half-cycle, ionic charge builds up within the electrolyte near the electrodes, these charges being balanced by an equal and opposite electronic charge on the electrodes. Each electrode is similar to a parallel plate capacitor and can be represented by $C_e$. This representation is a reasonable approximation when the ion concentration in the electrolyte is high, $\geq 1$ M

The bulk polarisation and ionic migration are physically in parallel hence their representative components ($R_b$ and $C_b$) are connected in parallel and both are in series with the electrode capacitance ($C_e$). Since both electrodes are identical, they are combined into one overall capacitance term, $1/C_e = 1/C_{e1} + 1/C_{e2}$. $C_b$ is related to the dielectric constant of the polymer according to the equation:

$$C_b = \frac{\varepsilon \varepsilon_0 A}{l}$$

in which $\varepsilon$ is the relative dielectric constant of the polymer and $\varepsilon_0$ ($8.85 \cdot 10^{-12}$ F/m) is the vacuum permittivity, $A$ is the cross sectional surface area and $l$ is the distance between the two plates. $R_b$ varies with the temperature and the particular polymer and geometric parameters used in the experiment.

Since $C_e$ is in series with a parallel combination of $R_b$ and $C_b$ the total impedance can be calculated by adding the impedance of the capacitor $C_e$ to the impedance of the parallel $RC$ combination. To do this it is necessary to know the relationship between resistance, capacitance and their respective impedances.

In a resistor the phase difference between the voltage and the current is zero. Hence the magnitude of the impedance equals the resistance ($|Z|=R$). With a capacitor the phase difference between applied voltage and the current is -90° out of phase ($\theta = -\pi/2$). Hence $|Z| = 1/(\omega C)$, as this occurs along the imaginary axis and by convention capacitances are treated as negative values, $|Z| = -j/(\omega C)$. In a series circuit impedances are directly additive. However, in a parallel only their reciprocals (admittances, Y) can be added.

Hence:

$$Y^* = Y^*_1 + Y^*_2 + Y^*_3 + \ldots\ldots$$

and

$$Y^* = Y' + jY'' = \frac{1}{Z' - jZ''}$$

Thus:

$$Y' = \frac{Z'}{Z'^2 + Z''^2}, \qquad Y'' = \frac{Z''}{Z'^2 + Z''^2}$$

So total admittance of a parallel combination of a resistor and capacitor is given by:

$$Y_{total} = \frac{1}{R} + j\omega C$$

and hence the total impedance of such combination:

$$Z_{total}^* = \frac{1}{\left(\dfrac{1}{R} + j\omega C\right)} = R\left[\frac{1}{1+(\omega CR)^2}\right] - jR\left[\frac{\omega CR}{1+(\omega CR)^2}\right]$$

Now back to the original circuit depicted in Fig. 22, it can be shown that:

$$Z_{total}^* = R_b\left[\frac{1}{1+(\omega C_b R_b)^2}\right] - j\left\{R_b\left[\frac{\omega C_b R_b}{1+(\omega C_b R_b)^2}\right] + \frac{1}{\omega C_e}\right\}$$

The complex impedance plot given by this equation is shown in Fig. 23.
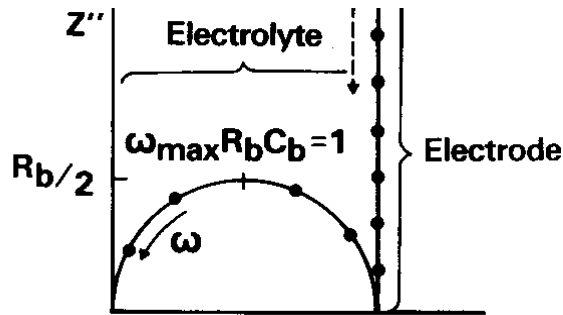


Fig. 23 Simulated complex impedance plot for the circuit of a polymer electrolyte/blocking electrode cell.

The magnitude of all fundamental electrical properties of the cell can be obtained from the complete impedance data, in particular the DC resistance ($R_b$). From that value it is possible to calculate the specific conductivity of the material being measured using equation from 3.8.1.

### 3.8.2.2. Results evaluation

The reliability of any conductivity measurement is dependent not only on the polymer under study but on the complete measuring cell – the two measuring electrodes as well as the tested material sandwiched between them. The characteristics of the electrodes themselves rarely affect the measurements, but the electrode/electrolyte interfaces often do for the reasons described below.

- Processes occurring at the interface (non-blocking electrodes)

The processes taking place at the electrodes involving ions can impede the rapid flow of current and affect the measurement. The main processes are:

    a) Diffusion of ions to the surface of the electrode

    b) Adsorption onto the surface

    c) Diffusion across surface to suitable site

    d) Charge transfer.

- Blocking Electrodes

In the case of blocking electrodes the conducting ions cannot cross the electrode/electrolyte interface. In all electrode systems a double layer capacitance is formed at the interface before any reaction can take place. With blocking electrodes this double layer is formed with no subsequent electrochemical transformation taking place affecting the measurement.

- There may be incomplete electrode contact

In the typical case of an electrical contact between two solids there is rarely 100% contact since both surfaces will not be perfectly flat. Polishing can reduce the problem of irregularities on the electrode surface, and also reduce the possibility of it being coated with a resistive layer of an impurity.  Heating the polymer when in contact with the electrodes can also facilitate greater electrical contact by increasing the likelihood of plastic deformation of the polymer around any imperfections on the electrode surface. Applying pressure to the electrodes has also been used successfully to increase electrode contact.

The samples measured by AC impedance throughout the course of my project were sandwiched between two stainless steel electrodes in a spring loaded PTFE cell. The measurements were carried out in an argon filled stainless steel PTFE lined gas-sealed can.

### 3.8.3. Transport Number Measurements

When a polymer electrolyte possess more than one mobile charged species it is important to determine not only the total conductivity, but also the proportion of the current which is carried by each species. This proportion is given by the transport number ($t$). Consider an electrolyte consisting of $n$ mobile species, then:

$$\sigma_{total} = \sigma_1 + \sigma_2 + \ldots + \sigma_n$$

$$t_n = \sigma_n / \sigma_{total}$$

It is important to remember that both ions and electrons may contribute to the total conductivity. There is a wide variety of diverse methods to measure the transport number. The most commonly used one is the *Bruce and Vincent* method which is based on AC impedance measurements.[6] However, the methods will not be described in detail here, because they have not been used in this project yet.

### References

1. S. Berger, S. Braun, *200 and more NMR experiments : a practical course*, 3rd rev. and expanded ed., Wiley-VCH, Weinheim, **2004**.

2. V. K. Pecharsky, P. Y. Zavalij, *Fundamentals of powder diffraction and structural characterization of materials*, 2nd ed., Springer, New York, **2009**.

3. G. Höhne, W. Hemminger, H. J. Flammersheim, *Differential scanning calorimetry: an introduction for practitioners*, 2nd rev. and enl. ed., Springer, Berlin ; New York, **2003**.

4. C. K. Chiang, C. R. Fincher, Y. W. Park, A. J. Heeger, H. Shirakawa, E. J. Louis, S. C. Gau, A. G. Macdiarmid, *Electrical Conductivity in Doped Polyacetylene.* Physical Review Letters, 1977, **39**(17): p. 1098-1101.

5. M. B. Armand, J. M. Chabango, M. J. Duclot, *Poly-ethers as solid electrolytes,* in *Fast ion transport in solids: electrodes, and electrolytes* (Eds.: P. Vashishta, J. N. Mundy, G. K. Shenoy), North Holland, Amsterdam, **1979**, pp. 131-136.

6. J. Evans, C. A. Vincent, P. G. Bruce, *Electrochemical measurement of transference numbers in polymer electrolytes.* Polymer, 1987, **28**(13): p. 2324-2328.

## 4. MONODISPERSED PEG SYNTHESIS

The syntheses of monodispersed PEG have been explored in detail because of the following:

- the majority of the required polymers are not commercially available,
- synthetic methods described in the literature deliver products of inferior purity.

### 4.1. History

Poly(ethylene glycols) (PEGs) are a class of molecules that have many applications in chemistry, biochemistry, medicine and materials science. For some of those applications it is very important that all macromolecules are of the same length (monodispersed). Well-controlled anionic polymerisation can produce monofunctional PEG with polydispersity indices (PDIs) approaching 1.04.[1]

Many research groups have already tried to synthesise monodispersed PEGs of different chain lengths.[2-7] First such attempt was reported in 1939 by *Hibbert et al.*[2] However, the method they used could only produce (semi)discrete oligomers, as many side reactions occurred leading to inseparable by-products and ruining monodispersity. Once more sophisticated synthetic and diagnostic methods became available, new approaches to monodispersed PEGs were undertaken. A common feature in the majority of new approaches is strategic desymmetrisation (e.g. protection) which prevents uncontrolled polymerisation during the ether coupling. There are four conceptual ways to elongate ethylene glycol (EG)[5]:

    A. iterative coupling of mono-protected building block to one end, $L=x(1+g)$

    B. iterative coupling of mono-protected building block to both ends, $L=x(1+2g)$

    C. chain doubling, $L=2^g x$

    D. chain tripling, $L=3^g x$

where: $L$ – oligo/polymer length, $g$ – number of generations of coupling, $x$ – number of monomeric units in starting oligomer.

From a mathematical point of view mode D is the fastest way to obtain poly/oligomers if $g > 1$. Mode C provides faster growth than linear modes A/B if $g > 2$. Although it is useful to synthesise the desired poly/oligomer in the shortest possible time, our requirements for specific lengths (e.g. 23 EO units in chain) cannot be achieved by methods C or D. Moreover, those methods look very elegant in theory, but in practice the number of processes required to synthesise the product is much greater, as each generation of coupling requires additional steps of preparation (e.g. at least 2 different types of

protection/deprotection reactions)[5], so the actual time needed from $g = 0$ to the end product can be much longer than the linear modes (A, B) especially for small $g$'s. Thus the modes A or B are the most appropriate methods of choice in our case. It is also very likely that $g$ will not be larger than 3 and hence mode B was chosen.

The procedure described by *Loiseau et al*[3] seems to be very robust and gives most of the necessary details to enable repetition. However, the newer procedure by *Tanaka et al*[4], which is based on similar chemistry, benefits from fewer purification steps, especially those involving preparative chromatography columns for large quantities (tens of grams), which are very time and resources consuming. The procedure described by *Springer et al*[6] uses the combination of both *Loiseau's* and *Tanaka's* methods with marginal modifications. *Tanaka's* procedure allows any lengths of PEG (up to 44 EO units) to be synthesised. However, it will be shown in following chapters that the purity of products synthesised using this procedure can be improved by means of modifications suggested by *Davis et al*[5] and then even more by our further improvements. Thus, the combination of both *Tanaka's* and *Davis's* recipes along with further optimisation are the most appropriate for our application where both high purity and reasonably high yields are required.

## 4.2. Analytical challenges

Development of the most efficient procedure to synthesise a monodispersed polymer relies heavily on analytical techniques, each of which has its own advantages and limitations. It has to be noted that the most important difference between non-polymeric organic molecules and polymers is that qualitative analysis is not enough to evaluate monodispersed purity. This is simply because, independently of molecular weight, polymeric macromolecules, which differ only in the number of repeating units, are practically identical in terms of their physicochemical properties. Hence the analytical methods to be applied must not only provide information regarding elemental and structural purity, but must also be size sensitive and, moreover, be able to quantify molecules of different sizes.

In terms of organic impurities and by-products which are chemically different than the desired product, it is often enough to analyse a material by ^{1}H NMR which is a very powerful qualitative and quantitative tool not only for organic but also for polymer chemistry.[8,9] However, for dispersity evaluation the NMR analysis alone is not sufficient, especially for poly(ethylene glycol) in which all the protons and carbons (except those at the chain ends and the adjacent $-O-CH_2-$ groups) produce overlapping peaks. Evaluation based on the ratio

between the protons from chain ends and the protons from actual chains can also be very misleading because the numbers calculated from peak areas are ambiguous for polymers. For example, a polydispersed dimethoxy PEG may show exactly the same ratio between the protons from the chain to those from the chain ends as a monodispersed PEG. As an example $^1$H NMR spectrum of polydispersed poly(ethylene glycol) of 1000 Da molecular weight is shown (Fig. 24). The peak areas may well correspond to the monodispersed 23 repeating units dimethoxy poly(ethylene glycol) (BMP23EO) in which there are 6 equivalent protons from the end groups 3.38 ppm (6 H, s, -OCH$_3$) and 92 protons from methylene groups 3.53-3.70 ppm (92 H, m, -CH$_2$-).
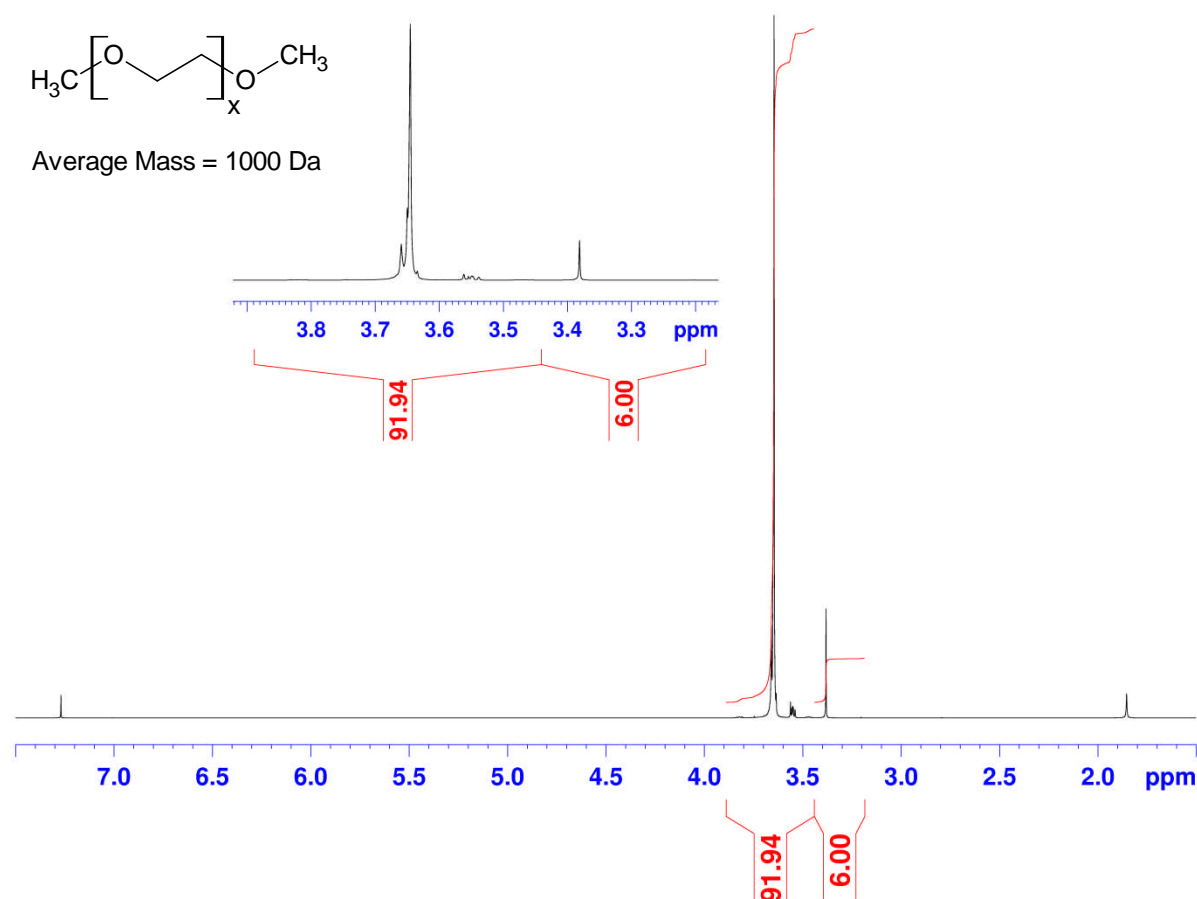


Fig. 24 $^1$H NMR spectrum of poly(ethylene glycol) Mw=1000Da.

Let us now consider elemental analysis (CHNX). The general molecular formula of a dimethoxy PEG is CH$_3$O(C$_2$H$_4$O)$_x$CH$_3$. It implies that carbon/hydrogen/oxygen ratios change very insignificantly throughout different Mws (Fig. 25). For example, dimethoxy monoethylene glycol (BMP1EO) composition is: C (53.31%), H (11.18%), O (35.51%) while

dimethoxy 30(ethylene glycol) (BMP30EO) gives: C (54.45%), H (9.29%), O (36.27%). As the value of $x$ in $CH_3O(C_2H_4O)_xCH_3$ increases, the terminus methyl or methoxy groups become more negligible and the composition of $CH_3O(C_2H_4O)_\infty CH_3$ is: C (54.53%), H (9.15%), O (36.32%).

(a)



(b)
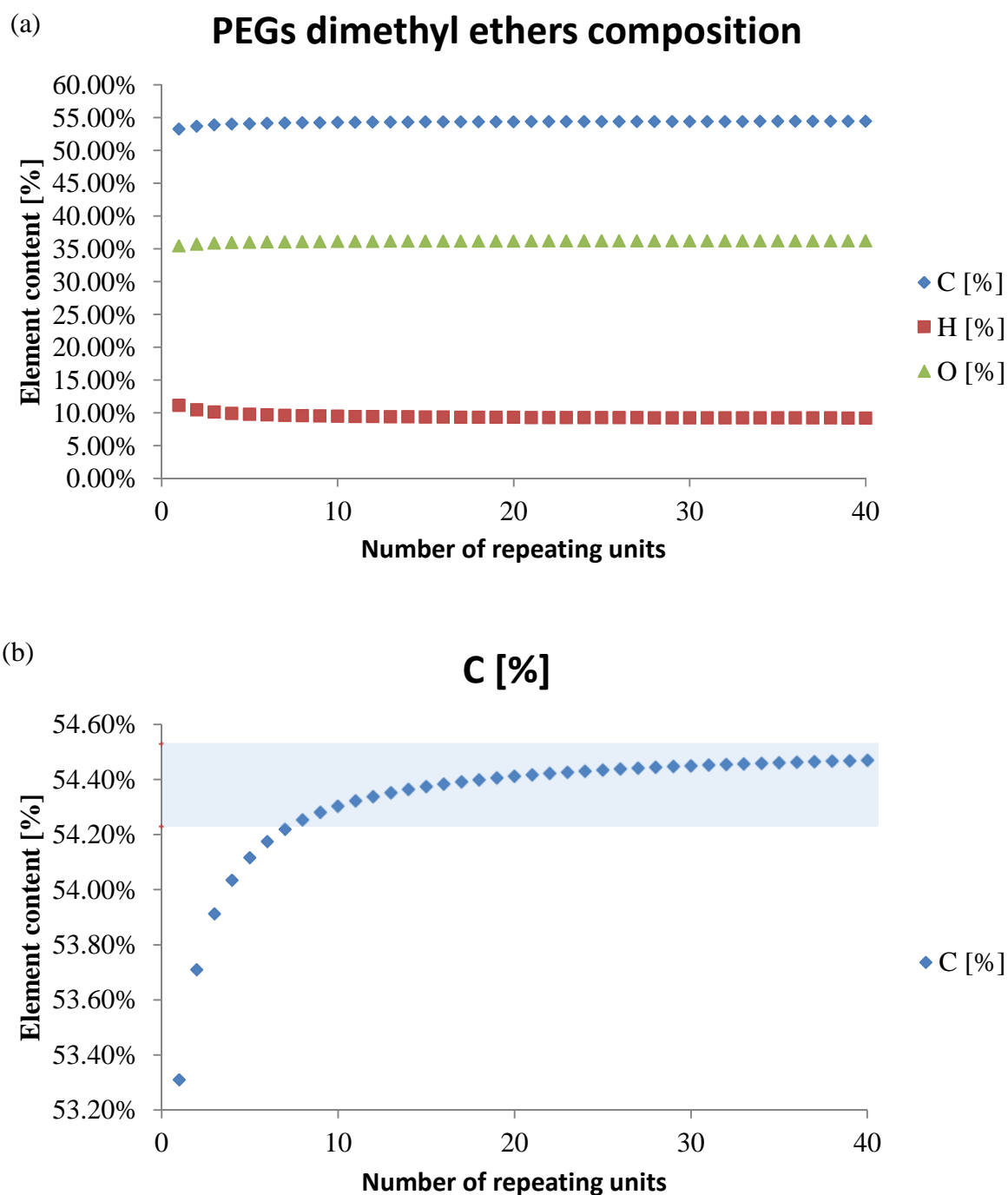


Fig. 25 Theoretical elemental composition of the series of dimethoxy PEGs (a) and change of carbon content throughout that series (b). The light blue band indicates the error margins of the elemental analysis.

The range of different chain lengths covered by the accuracy (±0.3%) of the CHNX analysis for carbon is represented by the light blue band in Fig. 25(b) which stretches to $x = \infty$. Thus an infinitely long polymer in which the carbon content is C (54.53%) cannot be reliably distinguished from dimethoxy PEG molecule consisting of just 7 or 8 repeating units C (54.22%, 54.25% respectively). A similar confusion arises when the contents of hydrogen and oxygen are analysed. In general the CHNX method cannot distinguish between dimethoxy PEGs when $x > 12$. Thus the elemental analysis can be used only to confirm elemental purity but, like ^{1}H NMR, does not provide reliable information regarding the monodispersity.

Characterisation and quantification of polymers is possible using size-exclusion chromatography (SEC) which reveals molar mass distribution.[10,11] However, in case of the synthesis of a monodispersed PEG it is necessary to quantify the discrete molecules. To find out whether SEC can provide sufficient resolution for such quantification of PEGs, a number of different samples consisting of either an individual monodispersed moiety or a mixture of 2 monodispersed PEGs were analysed. Since the goal of this project is to focus on chain lengths between 19 and 25 repeating units, 2 consecutive monodispersed PEGs were selected for analysis – 20 units (20EO) and 21 units (21EO). They were analysed on SEC both individually and in an equimolar mixture (Fig. 26). The results show that SEC fails to resolve signals from 20EO and 21EO. The mixture of those 2 polymers produces only 1 peak with the maximum positioned in the middle between the maxima of 20EO and 21EO.

However, once the difference in chain length of the component PEGs in the mixture is higher than a single repeating unit, SEC analysis becomes a useful quantitative tool. Let us consider an example which is related to the synthesis of monodispersed PEGs. The process is based on the chain extension reactions of shorter PEGs, thus for example, 20EO can be obtained from 12EO. As Fig. 27 shows, the retention volumes for 12EO and 20EO are sufficiently different to determine whether any of the starting material (12EO) is present in the targeting product (20EO).

Fig. 26 SEC results of: 20EO (red), 21EO (blue), equimolar mixture of 20EO and 21EO (black).



Fig. 27 Comparison of SEC data for 20EO (red) and 12EO (green).

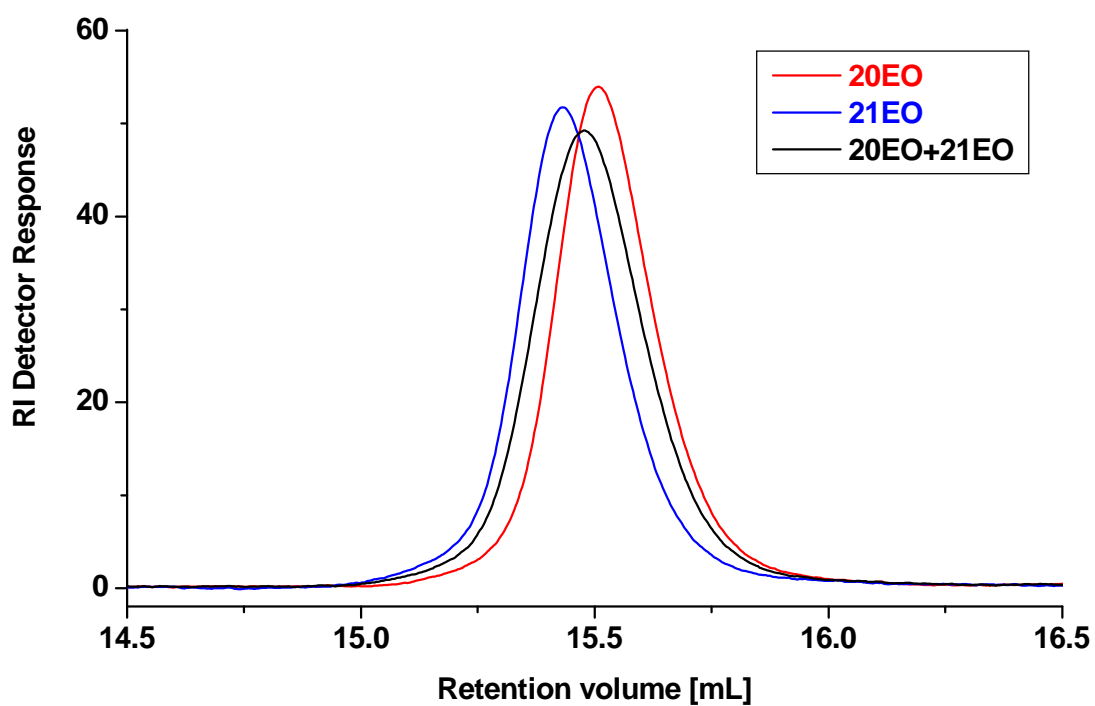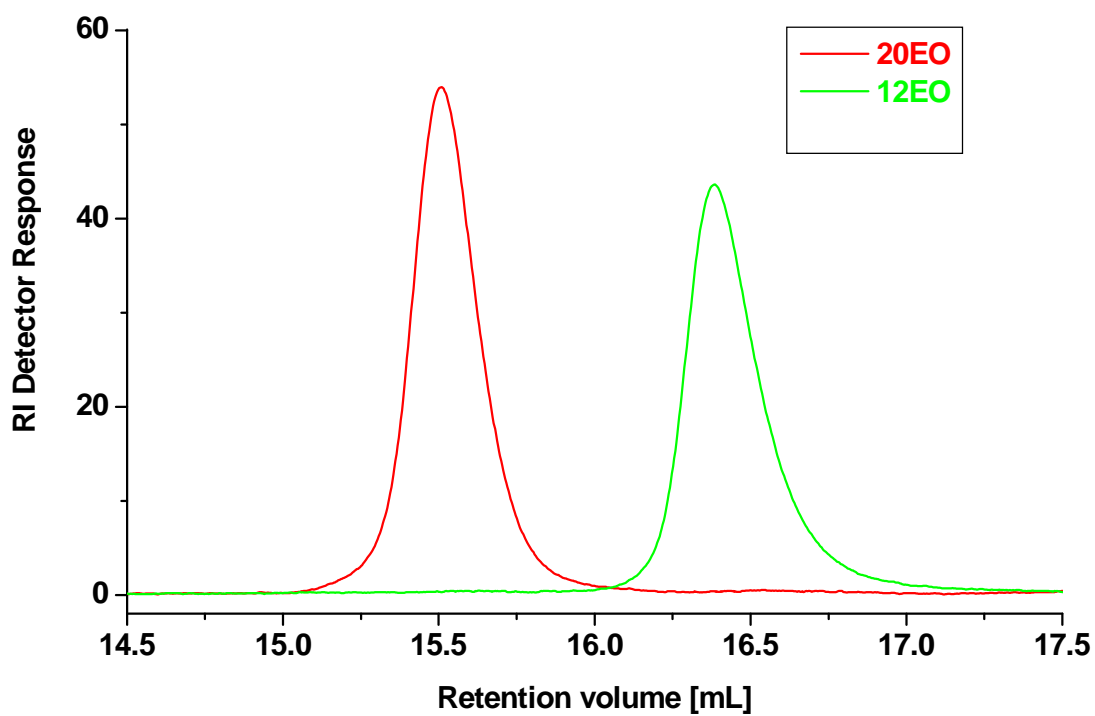SEC is the only direct liquid-chromatography-based method to assess the chain lengths and their distribution. Other methods rely on difference in polarity of analysed molecules. Silica-gel based chromatography can be used when the chains of different lengths possess sufficiently different polarity.

PEG is a very polar polymer because of both its chain structure and terminal (-OH) groups[12]. It is even extracted from chloroform (already a relatively polar solvent[13]) with 5% HCl[4] which demonstrates its affinity to polar species. For a polymer like PEG, protection of highly polar -OH end groups with non-polar (e.g. methyl- or benzyl-) groups gives the opportunity of varying polarity across different chain lengths, thus opening the possibility of using silica-gel based chromatography. However, similarly to SEC, the larger the polymer chains are, the less pronounced is the difference in their retention factors ($R_f$) making the separation of 2 consecutive chain lengths all but impossible regardless of the type of eluent used. Further details are provided in the synthesis chapter.

All the above methods are useful for evaluating the purity but not sufficiently accurate on their own for reliable determination of monodispersity. Because of that, mass-spectrometry (MS) based methods were also employed to determine the purity of monodispersed PEGs[3,5,6]. It is important to note that for quantification only soft ionization techniques are suitable, because all the other ones are highly energetic and inevitably lead to decomposition of analysed compounds[14,15]. That is why electrospray ionization (ESI) and matrix-assisted laser desorption/ionization (MALDI) analyses were chosen, in which time of flight (TOF) was measured to determine molecular weights and presence of impurities. There have been investigations of whether these techniques can provide quantitative data for PEGs and their derivatives of different Mws[16-21], but only one group used them to analyse monodispersed PEGs[17]. The general conclusion from the literature is that there is a good agreement in Mw determination and its distribution between MS techniques and SEC, but changes in experimental setup parameters can affect the results of dispersity evaluation. Our own study of 12EO synthesised according to the procedure developed by *Tanaka et al*[4], using ESI-MS-TOF clearly showed 1 species with the main peak at 569.16 Da (and its isotopic 570.25 Da) which corresponds exactly to 12EO+Na$^+$. Since no other molecules were detected at all, high purity was assumed. However, when the same material was run on MALDI-TOF-MS 2 species were detected: the desired 12EO+Na$^+$ (569.24 Da, intensity = 100%) and 11EO+Na$^+$ (525.21 Da, intensity = 8%). Such discrepancy between ESI and MALDI was not acceptable and it became important to find out which method is more reliable. There were reports in the literature that under MALDI conditions PEGs may decompose[22], however no

molecules which would be the results of such a decomposition pathway were observed in our spectra. No matter whether the analysed $x$EO was -OH, methyl- or benzyl- protected, ($x$-$1$)EO side-product was always found. Moreover, when benzyl groups had been cleaved by means of catalytic hydrogenation, the MALDI results showed very similar amounts of ($x$-$1$)EO in both substrate and product. These results led to the conclusion that under our MALDI operating conditions decomposition is not observed and the ($x$-$1$)EO by-products must be generated over the course of the synthesis. A possibility of reaction between the matrices used in MALDI and PEG derivatives has also been reported[18,23], but for -OH, -CH$_3$ and benzyl- terminated PEGs the side reactions were not observed in our measurements. *Shimada et al*[17] attempted to evaluate the quantitative capability of MALDI for an equimolar mixture of monodispersed PEGs of $x$ = 6–40. In their investigation laser power (LP) and species of adduct cations were the variables. Although the general conclusion was that MALDI is not a quantitative method, when sodium is added and LP is not higher than 5.0, the discrimination effects are moderate and, in the worst case the intensity of 26EO was 25% greater than 30EO. Assuming that 25% difference is spread over 5 consecutive PEGs (26–30), the error between 2 subsequent chain lengths should be much smaller. When coming back to the 12EO sample discussed above: even if the analysis error was 25%, the amount of 11EO present in the sample would be 6-10% which was not seen at all by ESI. Hence, from the purity requirements point of view it was definitely more favourable to rely on MALDI as it was much more sensitive than ESI towards impurities even if the amounts were over or under estimated. In fact, it will be shown in further chapters that after optimisation of MALDI conditions results of the analysis are very reproducible.

### 4.3. Optimisation of MALDI-MS

It was necessary to optimise MALDI-MS technique in order to achieve quantitative and reproducible results. According to the literature the most suitable matrix for synthetic polar polymers, such as PEO, is 2,5-dihydroxybenzoic acid (DHBA, or sometimes abbreviated DHB)[17,24,25]. Sodium as an ionising agent in this case is superior to other 1$^{st}$ group cations (Li$^+$, K$^+$, Rb$^+$, Cs$^+$) in terms of intensity produced in MALDI spectra[25]. Aqueous ethanol was selected as the solvent. Table 2 shows the proportions of ingredients which provide reliable MALDI-MS analysis for PEOs.

| | |
|---|---|
| **DHBA [g]** | 0.0094 |
| **Ethanol [ml]** | 0.90 |
| **Water [ml]** | 0.10 |
| **NaCl [g]** | 0.0024 |
| **sample [g]** | 0.0005 |

Table 2: Optimised solution for MALDI-MS.

Since the ability for ion complexation by PEOs varies depending on the end groups and is likely to be different than that of the crown ether, MALDI-MS is not suitable for relative quantification of those.

MALDI-TOF analysis of a monodispersed PEG typically reveals the product (*target*) peak and the 44 Da lighter *target-(1 EO)* impurity. A small peak at *target-(90 Da)* observed in purified bis benzyl protected PEGs is associated with the product losing 1 benzyl group during MALDI analysis (possibly reaction with DHBA). Occasionally a very small peak is also observed at *target+(152 Da)* independent of the type of the PEG end groups. The peak is sporadic and does not always appear in repeated runs, suggesting a methodological error. It could be associated with the DHBA matrix molecule losing 2 protons and agglomerating with $Na^+$ cation and the analysed compound. Some small peaks below 600 Da, which also appear sporadically, are also associated with the decomposition of the matrix. The peak appearing at *target+(16 Da)* is associated with the product coordinating $K^+$ cations (possibly from reaction as KOtBu is used as a base) rather than $Na^+$.

All the intensities in MALDI spectra are given in percents, relative to the intensity of the strongest peak.

### 4.4. Monodispersed PEG availability

At the time of writing only a few monodispersed poly/oligo(ethylene glycols) were available commercially and even then not with sufficient purity (Table 3). The required chain lengths, 19-24 EO units, were not available.

| PEG | | purity [%] | supplier | quantity | price £ |
|---|---|---|---|---|---|
| $HOCH_2CH_2OH$ | Ethylene glycol $C_2H_6O_2$ | 99.8 | Sigma Aldrich | 1 L | 34.00 |
| $H(OCH_2CH_2)_2OH$ | Diethylene glycol $C_4H_{10}O_3$ | $\geq 99$ | Sigma Aldrich | 1 L | 52.30 |
| $H(OCH_2CH_2)_3OH$ | Triethylene glycol $C_6H_{14}O_4$ | $\geq 99$ | Sigma Aldrich | 500 mL | 40.60 |
| $H(OCH_2CH_2)_4OH$ | Tetraethylene glycol $C_8H_{18}O_5$ | 99.5 | Fisher Scientific | 1 L | 30.70 |
| $H(OCH_2CH_2)_5OH$ | Pentaethylene glycol $C_{10}H_{22}O_6$ | 98 | Fisher Scientific | 25 g | 150.10 |
| $H(OCH_2CH_2)_6OH$ | Hexaethylene glycol $C_{12}H_{26}O_7$ | 97 | Sigma Aldrich | 25 g | 110.10 |
| $H(OCH_2CH_2)_8OH$ | Octaethylene glycol $C_{16}H_{34}O_9$ | $\geq 95$ | Polypure | 25 g | 455.30 |
| $H(OCH_2CH_2)_{12}OH$ | Dodecaethylene glycol $C_{24}H_{50}O_{13}$ | $\geq 95$ | Polypure | 25 g | 780.50 |
| $H(OCH_2CH_2)_{28}OH$ | Dodecaethylene glycol $C_{56}H_{114}O_{29}$ | $\geq 95$ | Polypure | 5 g | 351.20 |
| $H(OCH_2CH_2)_{12}OH$ | Dodecaethylene glycol $C_{24}H_{50}O_{13}$ | > 99 (claimed) | Quanta Biodesign | 1 g | 490.00 |

Table 3: Commercial monodispersed poly/oligo(ethylene glycols)

## 4.5. Monodispersed PEG synthesis procedure development and optimisation

As mentioned in chapter 4.1 the combination of both *Tanaka's*[4] and *Davis's*[5] synthesis recipes, combined with further optimisation, is the most appropriate for our application, when both high purity and high yields are required. In terms of exact synthetic procedure, method *B* (Fig. 28) allows the synthesis of a polymer in which the number of mers equals the multiplicity of the number of repeating units ($x$) in the starting material. However, if two different starting materials are used (mode *Bm*) and the glycol is built of $m$ mers, while elongating (coupling) agent contains $x$ mers, any number of repeating units in the final product can be achieved, according to the formula: $L=m+2xg$ (Fig. 28, mode *Bm*).
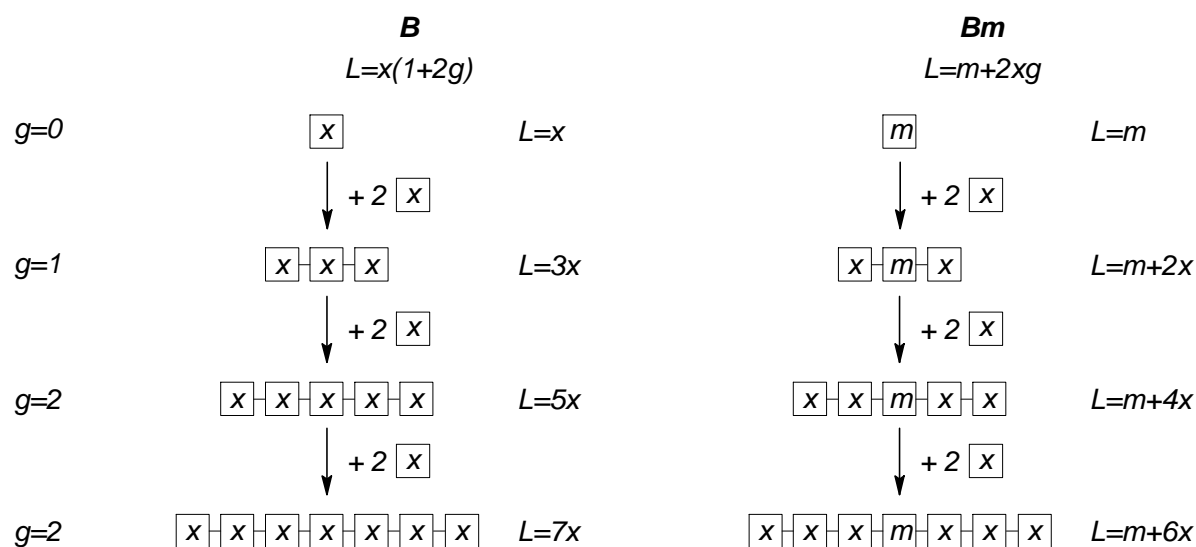


Fig. 28 Algorithm of the synthesis of monodispersed PEGs in mode *B* and its modification mode *Bm*. *L* – oligo/polymer length, *g* – number of generations of coupling, *x* – number of monomeric units in starting oligomer.

The basis of the synthetic process is the reiteration of *Williamson's* ether synthesis[26] which usually proceeds via the nucleophilic substitution $S_N2$ reaction[27] (Fig. 29).
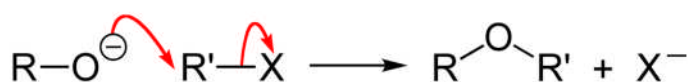


Fig. 29 Williamson's ether synthesis.

The synthesis route for monodispersed PEGs is shown in Fig. 30. Diols are symmetric molecules with 2 reactive hydroxyl- groups. Hence, in order to control the growth of polymeric chains, the *m*EO is reacted with an elongating agent on both ends (Fig. 30b). The agent is a mono-protected (**Pr**) mono-functionalised (**X**) *x*EO (Fig. 30a). The functionalised end is reactive towards hydroxyl- groups of the *m*EO. Although there is a possibility to functionalise *m*EO on both ends and react it with monoprotected *x*EO, such route was ruled out by *Tanaka et al*[4] because of higher probability of generating side products. The product of such ether coupling reaction is an elongated PEG, protected on both ends. Removal of protective groups (Fig. 30c) leads to the next generation of PEG, consisting of *(m+2x)* mers, which can be used as a substrate for reiteration of the ether coupling.
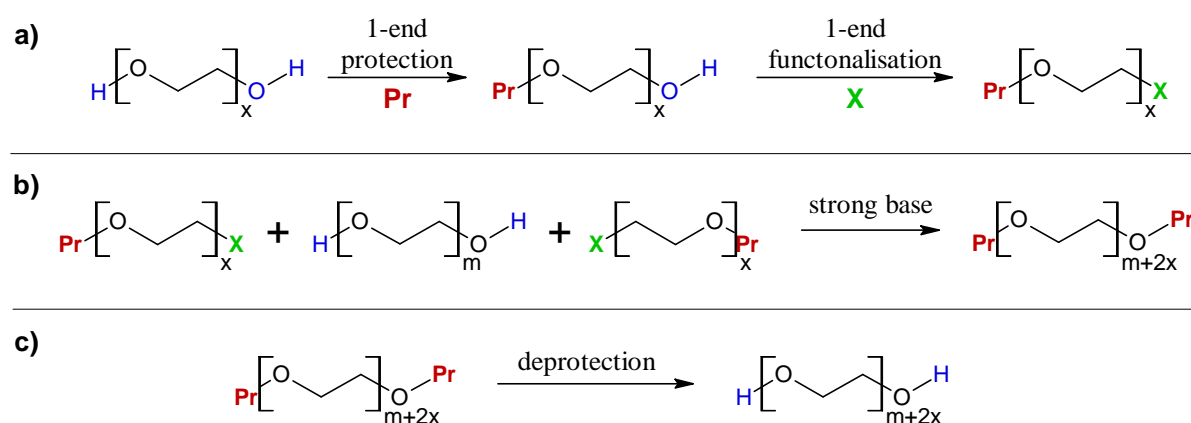


Fig. 30 Monodispersed PEG synthesis route: a) synthesis of an elongating agent by mono-protection and subsequent mono-functionalisation of *x*EO; b) chain elongation via ether coupling reaction; c) removal of protective group.

Considering the availability, price, purity, desire to minimise the number of synthetic steps and the fact that the ether coupling reagent **Pr**-$(OCH_2CH_2)_x$-**X** should be used in excess to the *m*EO, tetraethylene glycol appears to be the best candidate for that.

### 4.5.1. Selective monoprotection

The protective group must be stable under both functionalisation and ether coupling reactions conditions. Its removal (cleavage) should be selective, not destructive to the PEG chain and efficient, in order to deliver as much as possible of the desired product. Monotetrahydropyranyl- (THP-), *tert*-butyl- (*t*-Bu-), monotrityl- (Ph$_3$C-) and benzyl- (Bn-)

protective groups have already been examined by many reasearchers[3-5,7] for the synthesis of monodispersed PEGs and only Bn- was stable under both ether coupling and functionalisation conditions[4]. Moreover, Bn- group can be selectively cleaved under neutral conditions by means of catalytic hydrogenolysis, which has a yield of 95-98%[4,28].

Formation of benzyl- ether can be achieved through a variety of methods[28,29], many of which being variations of the *Williamson's* synthesis (Fig. 29). Mono-protection is achieved by using large excess of a diol, which can be easily removed by simple extraction, because the diol has stronger affinity to the aqueous phase than to a non-polar organic solvent (Fig. 31)[4,5].
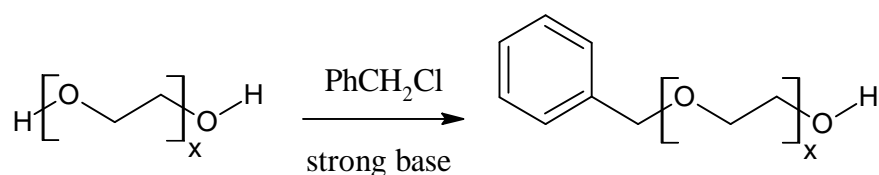


Fig. 31 Monobenzylation of PEGs.

Although the excess of a diol minimises formation of bisbenzyl protected (BBP) diol, some always forms. Fortunately, the latter can be easily removed using column chromatography[5]. The BBP diol remains intact during consecutive functionalisation and if its content in the crude product is lower than 10%, there is no need for purification at that stage, providing that the product of the ether coupling elongation reaction is separable from the BBP diol[4]. The formation of BBP is observed in $^1$H NMR (400 MHz, in CDCl$_3$). Benzyl protons of tetraethylene glycol monobenzyl and bisbenzyl ethers manifest themselves in NMR peaks with different chemical shifts, 4.57 and 4.56 ppm respectively. The intensities of the peaks can be used to determine the molar ratio.

Highly selective silver(I)-oxide-mediated procedure for monoprotection of symmetrical diols was suggested by *Bouzide et al*[29] and also applied by *Loiseau et al*[3]. The product was obtained in 90% yield and contained 5-10% molar of BBP diol.

Compared to the procedures involving excess of a diol, the silver(I)-oxide-mediation is more labour-intensive (requires preparation of fresh Ag$_2$O, filtration), more difficult (overhead stirrer necessary due to high viscosity of the reacting mixture), more expensive and environmentally unfriendly (uses substantial amounts of Ag$_2$O).

Since both of the above procedures produce BBP diol as a side product the easier and cheaper excess-of-diol method has been chosen.

### 4.5.2. Functionalisation by tosylation

Functionalisation of the hydroxyl group in a mono protected diol has been extensively studied by a number of research groups[3-5]. The functional group must both attach and leave with highest possible yields and without destroying the substrate. Those requirements are met by both mesyl- (Ms-) and tosyl- (Ts-) groups and although the former was found to perform marginally better in subsequent reactions, the latter was attached with excellent yields (over 96%) in a less toxic environment (THF/$H_2O$ instead of pyridine) (Fig. 32). Hence, tosyl-group was selected and no further improvements of the procedure were required at this stage[4]. Purification by extraction was adequate. Impurities and unreacted substrates were beyond detectable levels and the use of column chromatography did not affect the yield of the purified product.
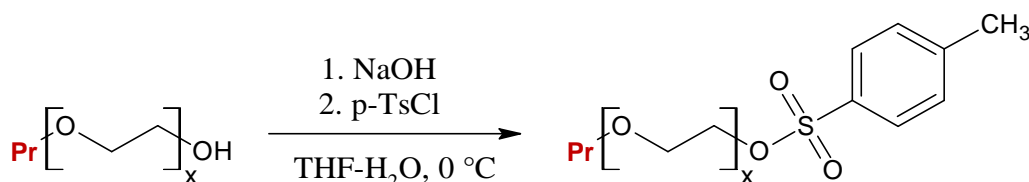


Fig. 32 Tosylation of monoprotected PEGs.

### 4.5.3. Chain elongation – ether coupling.

The ether coupling reaction (Fig. 33) is another variation of the Williamson's ether synthesis.
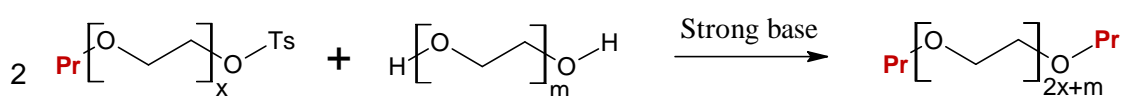


Fig. 33 Ether coupling reaction.

Following the *Bm* algorithm (Fig. 28), 2 molecules of the ether coupling reagent react with 1 molecule of *m*EO. The *m*EO is deprotonated with a strong base and the resulting alkoxide (nucleophile) attacks the ether coupling reagent. Despite being commonly used in organic chemistry, in this particular case this reaction requires extensive optimisation because of the reported depolymerisation of alkoxides formed from PEGs[5,30]. Indeed, the depolymerisation has been observed in this work too and the *(m+2x-1) – target-(1 EO) –* practically inseparable side product always formed during the ether coupling, but as shown later in this chapter the procedure has been refined to minimise the amount of it. Additional

difficulties in purification may arise due to formation of mono-ether coupled product, although for the target chain lengths of this project ($\leq$ 24 EO units) they were separable from the product by means of column chromatography.

In *Tanaka's* procedure NaH, *m*EO and dry THF were put into a flask and a solution in dry THF of monobenzyl protected *x*EO tosylate (MBP*x*EOTos) was added dropwise. Then the reaction mixture was refluxed for 24 hrs and cooled to room temperature. Excess of NaH was quenched with MeOH and then $H_2O$. After evaporation of THF, the product was extracted with 5 wt % aqueous HCl and $CHCl_3$. The crude product obtained by solvent evaporation was purified by gel permeation chromatography (GPC). However, GPC was unable to separate the *target-(1 EO)* from the product (Fig. 26). All the attempts to reproduce the *Tanaka's* procedure in our laboratory have revealed at least 5-10% of the *target-(1 EO)* formed after 1st generation of the ether coupling reaction. Unfortunately neither mass spectroscopy nor analytical GPC data are presented in *Tanaka's* publication, while the NMR spectra alone are insufficient to quantify the side products of different chain lengths.

Improvements to the *Tanaka's* method have been reported by *Davis et al*[5]. The authors highlight the depolymerisation problem and attempt to resolve it. The procedure proposed by *Davis* has been tried in this work together with the *Bm* algorithm and is described below.

*m*EO (1 eq), MBP*x*EOTos (2.6 eq) and 18-crown-6 (1.1 eq) were dried into a vessel by co-evaporation with toluene. The mixture was taken up in dry DMF (1.5 mass of reactants) and a solution of potassium tert-butoxide (KOtBu) (1.3 eq) in dry DMF (3 ml per gram) was added at the slowest rate possible using a syringe pump such that the whole addition took around 20 hours whilst the reaction was stirred vigorously under argon. For work up, the reaction mixture was poured into a large flask containing 50 ml of water and evaporated under high vacuum to remove DMF. The residue was dissolved in DCM and poured into ammonium chloride solution. After separating the DCM phase, the aqueous portion was extracted with five portions of chloroform. The combined organic extracts were dried over sodium sulfate to give a crude product for purification by normal or reversed phase column chromatography. Although the ESI-MS data presented by the authors of the procedure showed excellent purity (often over 99.5%), MALDI-TOF of the product synthesised in our laboratory using their method showed at least 1.8% of *target-(1 EO)*. Moreover, it turned out to be practically impossible to separate the product from the 18-crown-6 ether which was added in rather substantial amount in order to improve solubility of KOtBu in DMF. The crown ether was clearly observed on both MALDI-TOF (18%) and

^{1}H NMR (27%) [δ ppm 3.69 (24H, s, $CH_2$)] analyses – the discrepancy in quantification is not surprising and can be explained as described in chapter 4.2. Even after subsequent removal of protective groups and another run through chromatography column in a different solvent system the 18-crown-6 was still found in the product.

### 4.5.3.1. Crown ether

In view of the above, the first step in process optimisation was to eliminate the crown ether from the reaction. The reaction was repeated using exactly the same conditions, but without the 18-crown-6. According to MALDI-TOF analysis, the resulting crude product contained slightly greater amount of *target-(1 EO)* (2.8%). There was no significant increase in the amount of impurities suggesting that the removal of 18-crown-6 from the procedure is possible with further optimisation.

### 4.5.3.2. Optimisation of parameters

Since alkoxides formed from PEGs can undergo depolymerisation, the shorter they are present in the reaction mixture, the smaller the amount of *target-(1 EO)* will be. Thus, it is advantageous to increase the rate of the ether coupling reaction as much as possible, without increasing the rate of depolymerisation.

The rates of $S_N2$ reactions strongly depend on the choice of solvents[31]. The requirements are that the solvent must be polar enough to dissolve the reagents, but not too polar, because highly polar solvents solvate anionic nucleophiles and slow down the reactions.[9] It is energetically favourable to destabilise the nucleophile by using less polar solvent.

DMF used in the *Davis's* procedure is a polar aprotic solvent which is often selected for $S_N2$ reactions[9,31]. However, there are several disadvantages of using DMF (Table 4), and THF was proposed as a replacement, because it has also been commonly used for ether coupling of PEGs[3,4,6,7,32]. The main problem with using THF is a possibility of forming peroxides, hence it should be kept away from both light and oxygen[32,33].

|  | DMF | THF |
|---|---|---|
| boiling point | 153°C – difficulties in complete solvent evaporation after the reaction, especially from a polymer soluble in DMF (such as PEG) | 65-67°C – volatile, easily removed from the product after reaction |
| hygroscopicity | hygroscopicity together with high b.p. cause difficulties in obtaining DMF water free which is necessary in order to favour $S_N2$ reaction | dry THF is obtained using a MBRAUN GmbH MB SPS-800 solvent purification system (by passing the solvent through two drying columns then dispensing under an Ar or $N_2$ atmosphere), or from shared distillation rigs. |
| toxicity | thought to cause birth defects[34] and therefore in some sectors of industry women are banned from working with DMF. It can accumulate in the body and it is a possible carcinogen (MSDS) | considered a relatively nontoxic solvent (MSDS) |

Table 4: DMF vs. THF for ether coupling reaction.

The monodispersity of the polymers synthesised using THF was better than when using DMF (+crown ether) reaching *target-(1 EO)* level of 1.2%. The amounts of other impurities varied but they were all separable from the main product by means of column chromatography.

Because of the possible formation of peroxides in THF, *Booth et al*[32] proposed chlorobenzene as an alternative solvent. They used it with KOH at 0°C. When the reaction was reproduced in our laboratory using the same substrates as for earlier comparison of DMF and THF, the amount of *target-(1 EO)* found in the product was significantly larger (7.2%) than for the reaction performed in THF with KOtBu. *Target-(2 EO)*, *target-(3 EO)* and *target-(4 EO)* were also observed bringing the overall monodispersed purity well under 90%.

The experiments prove that THF is a suitable replacement for DMF and also produces significantly higher purity products than chlorobenzene does.

In the *Davis's* procedure ether coupling reaction was performed at room temperature, probably in a non-air conditioned laboratory thus adding another variable to the synthesis. In order to control this parameter the synthesis was carried out at 40°C. The resulting product contained greater amount of *target-(1 EO)* (3.7%) and significantly more other impurities than in the room temperature process. This outcome led to the conclusion that lowering the reaction temperature could be beneficial for improving the purity of the product. Indeed, when reaction was performed at 0°C, the overall purity of the product was higher and *target-(1 EO)* content dropped to 0.9%.

*Davis et al* also highlighted that changing the sequence of added reagents to the reaction vessel affected the purity. They suggested that a PEG diol and a tosylate should be

premixed first and then the base was added at a slowest possible rate. Such approach was aimed at minimising the life time of an alkoxide which could depolymerise. However, the elimination reaction occurs (via E2 mechanism) more readily under these conditions because it is competitive to the desirable $S_N2$[9,31]. Both *Tanaka* and *Davis* reported elimination of tosylates, while Davis also claimed that in their sequence of addition, the amount of the eliminated side product was larger than in other synthesis procedures. We have investigated three different sequences in order to improve the process in terms of purity and yield of the product (Table 5). The best purity and yield were achieved when PEG diol was added to a solution of KOtBu followed by addition of tosylate.

| sequence | purity of crude product | yield | other problems |
|---|---|---|---|
| 1.diol+tosylate 2.base | good, *target-(1 EO)* (1.2%) | ≤70% | difficulties in addition of the base solution |
| 1.base 2.tosylate 3.diol | low, *target-(1 EO)* (>6%), significant amount of other impurities | N/A | E2 elimination occurs |
| 1.base 2.diol 3.tosylate | good, *target-(1 EO)* (0.9%) | ≤80% | - |

Table 5: Sequence of adding reagents.

The rate of addition was optimised to minimise the life time of alkoxide and to prevent heating of the mixture due to addition of the chemicals.

The ratio of the reagents in the ether coupling reaction has been also investigated and optimised. KOtBu was selected as a base because it was producing the product of higher purity than NaH. One could think that using large excess of base would increase the yield of the product, as it guarantees that both hydroxyl- groups from a PEG diol are deprotonated and become attacking nucleophiles. Indeed, high yields are observed when methyl iodide ($CH_3I$) is used as coupling reagent, but it has to be noted that $CH_3I$ cannot undergo elimination reaction E2. However, when the leaving functional group (**X**) of a coupling reagent is attached to a primary carbon, elimination can occur, especially if *tert*-butoxide, a large nucleophile anion is used as a base. The best yields, approaching 80%, are obtained with the following ratio of reagents: PEG diol (1 eq), KOtBu (2.8 eq), tosylate (2.6 eq).

Table 6 shows optimised conditions for the ether coupling reaction, along with the products' purity after the first generation vs the conditions and results presented by *Tanaka* and by *Davis*.

|  | *Tanaka's* | *Davis's* | **optimised** |
|---|---|---|---|
| strong base | NaH | KOtBu + 18-crown-6 | **KOtBu** |
| solvent | THF | DMF | **THF** |
| temperature | reflux (66-67°C) | room temperature | **0°C** |
| sequence | 1.base 2.diol 3.tosylate | 1.diol+tosylate 2.base | **1.base 2.diol 3.tosylate** |
| eluent for flash chromatography | MeOH in CHCl$_3$ | various systems | **Acetone + DCM** |
| inseparable *target-(1 EO)* | 5-10% | <5% | **<2%** |
| other inseparable impurities | - | 18-crown-6 | **-** |
| yield | ≤73% | ≤70% | **≤80%** |

Table 6: Ether coupling reaction summary

### 4.5.4. Deprotection – hydrogenolysis

As mentioned in chapter 4.5.1, the benzyl protective group was chosen for this work due to its excellent stability in various (particularly basic) conditions and selective, high yield removal. The benzyl group can be cleaved using several methods.[28] Both *Tanaka* and *Davis* chose hydrogenolysis catalysed by Pd/C in ethanol (Fig. 34) because it provided high yields (>95%) and did not destroy the PEG chains.
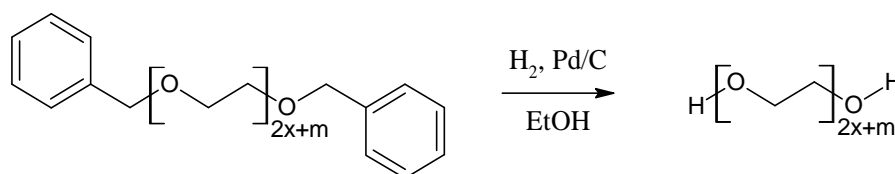


Fig. 34 Benzyl group cleavage.

Table 7 compares the hydrogenolysis reaction conditions and results given by *Tanaka* and *Davis* with the optimised conditions and results of this work. Lower temperature of the reaction is safer, especially since thermal degradation of PEGs has been reported[35-37]. It was found that lowering the temperature from 100°C to room temperature (~25°C) did not decrease the yield or the purity of the product when 15-20 bar H$_2$ and Pd/C (10%wt) were used.

| | *Tanaka's* | *Davis's* | **optimised** |
|---|---|---|---|
| solvent | Ethanol | Ethanol | **Ethanol** |
| temperature | 100°C | room temperature | **room temperature** |
| $H_2$ pressure | 8 bar | ~1 bar | **15-20 bar** |
| catalyst | Pd/C (5%wt) | Pd/C (10%wt) | **Pd/C (10%wt)** |
| appearance | colourless oil/white solid | colourless oil/white solid | **colourless oil/white solid** |
| typical yields | 91-98% | 75-99% | **95-98%** |
| purification | N/A | N/A | **extraction or column chromatography** |

Table 7: Hydrogenolysis reaction conditions and results

According to *Tanaka* and *Davis*, high yields of hydrogenolysis lead to high purity of the product after simple filtration of catalyst followed by solvent evaporation and no additional purification was necessary. However, we have found that both MALDI-MS and ^{1}H NMR detected 2-5% of a side product which was identified as a mono methylcyclohexyl PEG. It was 96 Da larger than the target and produced a characteristic doublet at 3.25 ppm in ^{1}HNMR spectra corresponding to the -OC$\underline{H}_2$C$_6$H$_{11}$ protons. Formation of such side product can be explained by hydrogenation of the aromatic ring of a benzyl group[28]. This was also confirmed when the impurities from the crude 13EO, 19EO and 21EO were isolated and analysed. It was preferred to remove those impurities before proceeding to next steps of the process as the purification at this point was relatively easy, while it could be significantly more difficult or even impossible after another ether coupling reaction. However, if the subsequent synthesis step was the chain elongation followed by another hydrogenolysis reaction, the impurity could be readily removed after the last benzyl cleavage.

### 4.5.5. End-capping

This project requires dimethoxy PEGs rather than hydroxyl- terminated. Hence, the final step in the synthesis of monodispersed bis-methyl protected (BMP) PEG is an end-capping reaction. In terms of mechanism, this is another ether coupling reaction, with the only difference that the product cannot be selectively deprotected without uncontrolled chain degradation. The examples of end-capping reactions are shown in Fig. 35.
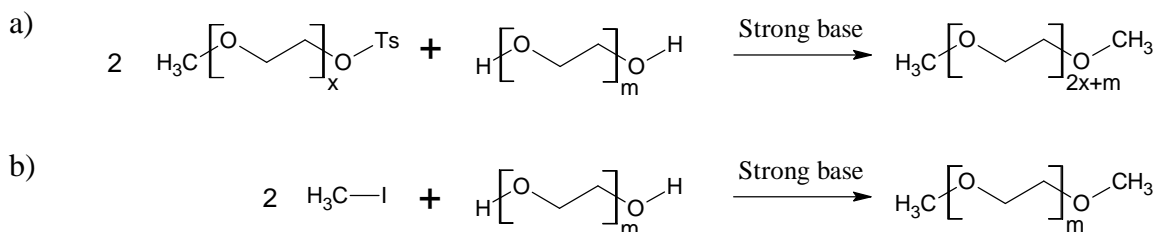
a)



b)



Fig. 35 End-capping reactions: a) with chain elongation using a tosylate (Ts), b) without chain elongation using methyl iodide

### 4.5.6. Purification by column chromatography

Almost all of the synthesised products had to be purified by means of column chromatography. It was necessary to remove both unreacted substrates and by-products with different chain lengths. *Davis's* procedure uses both normal and reversed phase column chromatography. In this work however the latter was not employed, since the products were found pure enough just after normal phase silica gel column. Due to high polarity of the synthesised products, relatively polar eluents had to be selected. Many different eluents are suggested in literature for purification of PEGs and benzyl protected PEGs. The following eluents were used by different groups:

1)  *Loiseau et al*[3]: EtOAc/acetone or EtOAc/MeOH
2)  *Tanaka et al*[4]: CHCl$_3$/MeOH
3)  *Davis et al*[5]: MeOH/DCM, MeOH/acetone/toluene, EtOAc/MeOH

However, our extensive study of the influence of composition of eluents on the separation of end-protected PEGs shows that the eluents containing MeOH as a strong solvent provide significantly poorer resolution than the eluents containing acetone (Fig. 36). In both cases the best results are obtained if DCM is used as a weak solvent. THF provides similar resolution to acetone and is slightly stronger towards the PEGs, however it easily oxidises during the course of the column chromatography introducing heavily boiling impurities. Wherever possible, the mixtures of acetone and DCM were applied for column chromatography in this work. Only in case of hydroxyl- or methyl terminated PEGs mixtures of MeOH and DCM were used, since those with acetone were not strong enough.

The main disadvantage of using such polar eluents is that silica in the column can slightly dissolve and appear in the purified product. This was occasionally observed, because some materials turned hazy in appearance after evaporation of solvents. In order to get rid of the unwanted silica, the materials were redissolved in toluene, left for 0.5 hr and then the

solution was filtered through 0.2 μm PTFE filter. As the result, no silica was detected by any analytical method ($^1$H NMR, CHNX, SEM-EDX).
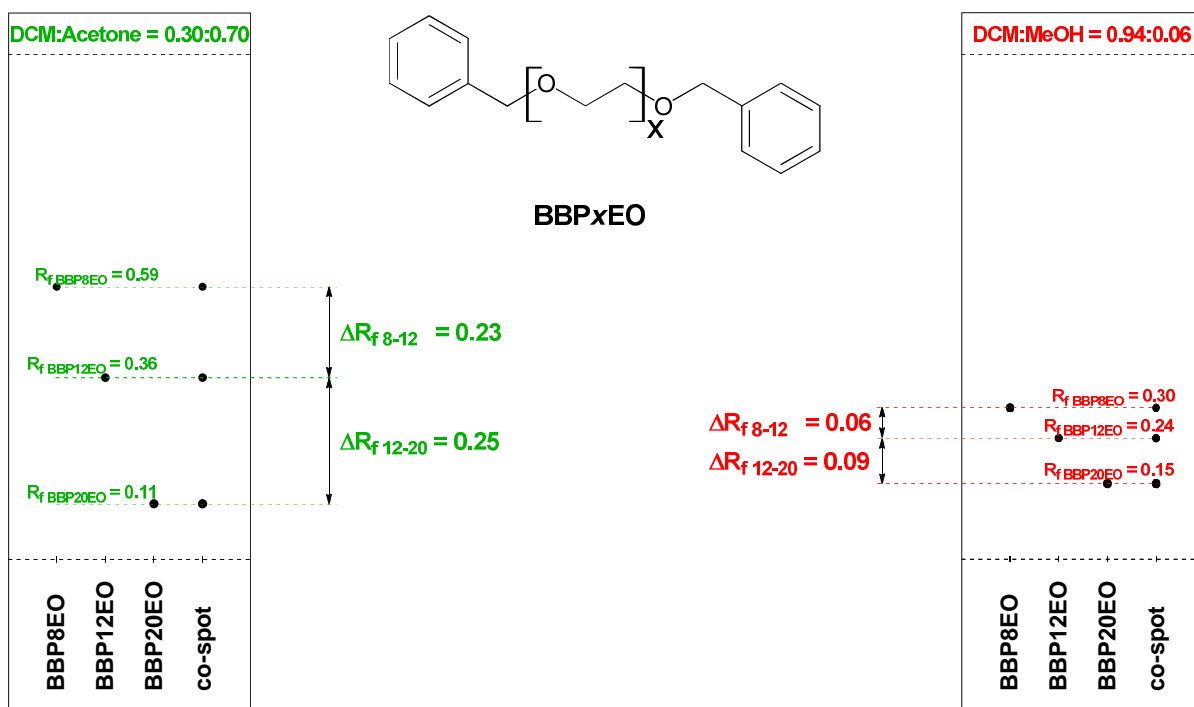


Fig. 36 Comparison of resolution of two eluents: DCM/acetone (left) and DCM/MeOH (right) during the separation of mixtures of bis-benzyl protected PEGs (BBP*x*EO).

### 4.5.7. Synthetic strategy

As stated in 4.5.1, tetra(ethylene glycol) is the most suitable starting material to become the chain elongating reagent. Fig. 37 shows application of *Bm* algorithm leading to the series of desired monodispersed dimethoxy PEGs ranging from 19 to 24 repeating EO units.
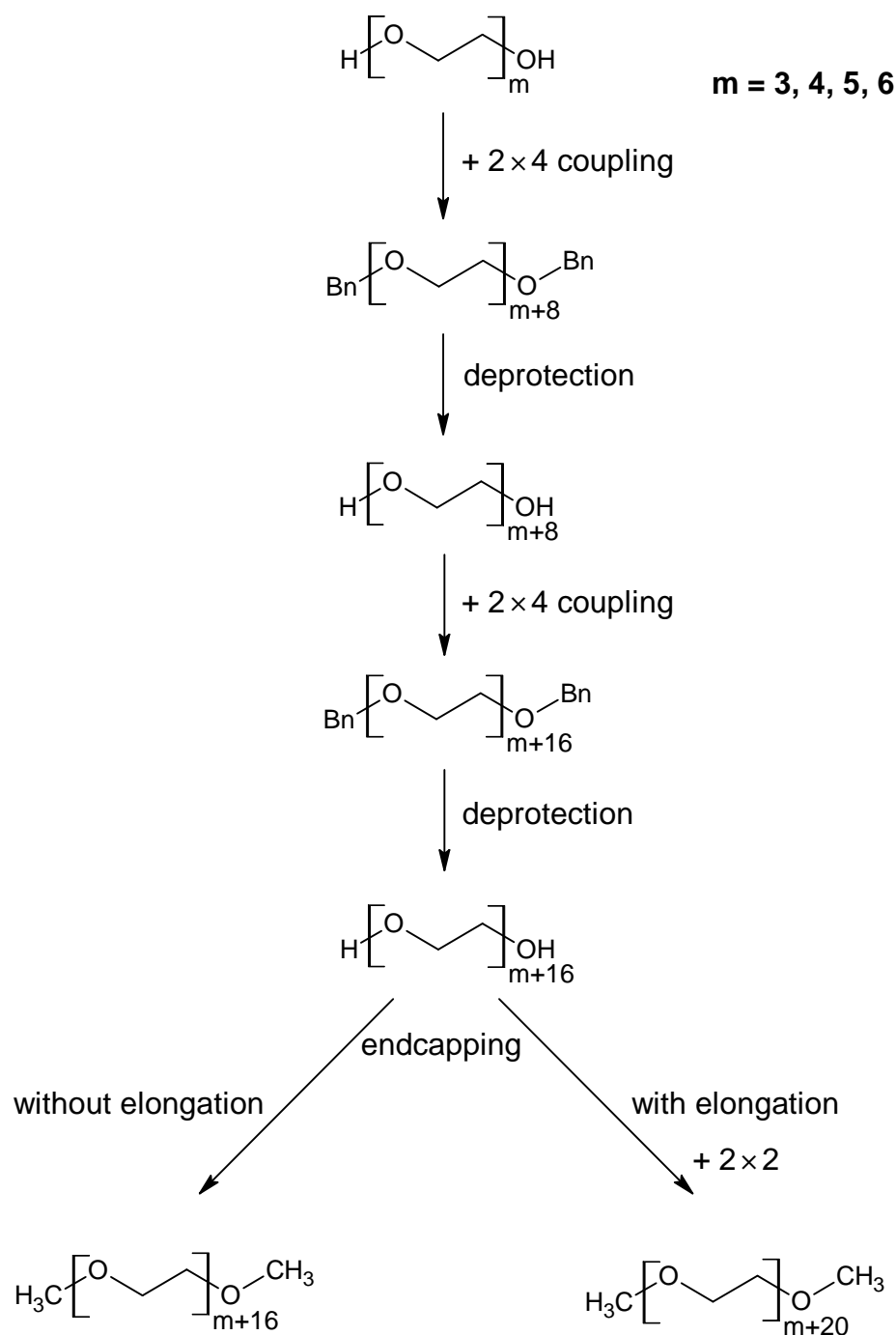


Fig. 37 Synthetic strategy – the route to monodispersed dimethoxy PEGs with 19-24 repeating EO units

### 4.6. Syntheses and characterisation of specific monodispersed PEGs

This chapter presents the optimised general procedures employed in this work and all details for preparation of particular batches which provided products of satisfactory yield and purity. The purity of the substrates is not included in the calculation tables if it is both higher than 99% and has no influence on purity or yield of the product (e.g. when it is used in excess).

#### 4.6.1. Monobenzylation of tetra(ethylene glycol)

This product was always synthesised using the same amounts of the reagents for each batch (Fig. 38).
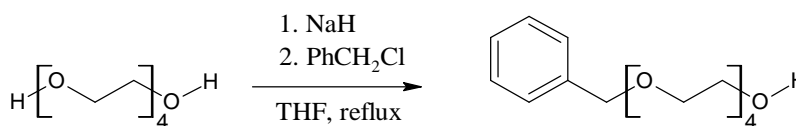


| Compound | purity | n [mol] | m [g] | V [cm$^3$] | d [g/cm$^3$] | M [g/mol] |
|---|---|---|---|---|---|---|
| 4EO | 99.5% | 0.400 | **78.08** | 69.4 | 1.125 | 194.23 |
| NaH | 95.0% | 0.400 | 10.10 | | | 24.00 |
| THF | | | 622.28 | 700.0 | 0.889 | |
| Benzyl chloride | 99.0% | 0.100 | 12.79 | 11.6 | 1.100 | 126.58 |
| THF for BnCl | | | 48.71 | 54.8 | 0.889 | |

Fig. 38 Monobenzylation of tetra(ethylene glycol)

NaH (10.10 g, 400 mmol, 95%) and THF (700 ml) were placed into a three-necked flask, and then, tetraethylene glycol (78.1 g, 400 mmol, 99.5%) was then added slowly. The mixture was heated to reflux (66-67°C), and THF solution (80 ml) of benzyl chloride (12.8 g, 100 mmol, 99%) was added dropwise. The reaction mixture was stirred for 3 hrs at reflux, and then, it was allowed to cool at room temperature. Methanol was added to the reaction mixture to quench the excess NaH, and 1 M HCl (50 ml) was added. After evaporation of THF, the product was extracted using 1M HCl (60 ml) and DCM (4×200 ml). Then DCM phase was washed with 1M HCl (3×100ml) and distilled H$_2$O (3×80ml). The combined DCM extracts were evaporated under reduced pressure to give 28 g of crude product (brown, free

flowing oil) which was purified in portions by gradient flash chromatography on a Biotage® SP1 system running at 40 ml/min; SNAP 100 g KP silica cartridge; for each column 5 g of crude product deposited on 12 g of silica and dry loaded; weak solvent A = DCM, strong solvent B = acetone, column equilibrated with DCM (3 CV); 4 CV at 8%, then a linear gradient over 10 CV to 60% B.

Pure product: monobenzyl protected tetra(ethylene glycol), 25.70 g (90.5% yield), clear colourless oil. TLC (Silica gel 60): $R_{f\,MBP4EO} = 0.28$, 30% acetone in DCM (side product – bis benzyl protected tetra(ethylene glycol): $R_{f\,BBP4EO} = 0.73$). ^{1}H NMR (400 MHz, CDCl$_3$) δ ppm 7.38-7.24 (5 H, m, Bn aromatic CH), 4.57 (2 H, s, Bn CH$_2$), 3.76-3.57 (16 H, m, 8×ethylene glycol CH$_2$), 2.64 (1 H, t, J = 6.3 Hz, OH); ^{13}C NMR (101 MHz, CDCl$_3$) δ ppm 138.19 (Bn 4° C), 128.38, 127.80 and 127.63 (5×Bn aromatic CH), 73.26 (Bn $\underline{C}$H$_2$), 72.57 (HOCH$_2\underline{C}$H$_2$...), 70.65-70.59 (multiple CH$_2$), 70.36 (CH$_2$), 69.41 (CH$_2$), 61.76 (HO$\underline{C}$H$_2$CH$_2$...); m/z ESI-TOF found 307.16 {[M+Na^{+}] expected 307.15}. No impurities were detected in purified product by ^{1}H NMR, chromatography or mass spectroscopy, hence purity can be assessed > 99%.

### 4.6.2. Tosylation of monoprotected PEGs

The reaction scheme is shown in Fig. 32. Sodium hydroxide (3.5 eq) was dissolved in water (5 ml H$_2$O per gram NaOH) and chilled in an ice bath. A solution of monoprotected PEG (1 eq in 2.5 ml THF per gram) was added dropwise. A solution of paratoluyl sulfonyl chloride (1.2 eq in 3 ml THF per gram) was then added dropwise, after which the mixture was allowed to warm gradually to room temperature with stirring over 15 hours.

The mixture was put back on ice and 1 M HCl (to neutralise the excess of NaOH) was also chilled on ice for 0.5 h. Then reaction mixture was poured to 1 M HCl cooled at 0°C, THF was evaporated (at 30°C) and the product was extracted with DCM (3×200 ml). The combined extracts were washed with 10% Na$_2$CO$_3$ (2×100 ml) and then with distilled water until neutral (4×50 ml). The organic phase was dried over sodium sulfate and evaporated to provide pure tosylate, which was additionally dried by evaporation with toluene at 60°C. Then the product was stored under Ar and shielded from light. Typical yield > 96%.

#### 4.6.2.1. Monobenzyl protected tetra(ethylene glycol) tosylate

Monobenzyl protected tetra(ethylene glycol) tosylate (MBP4EOTos) was synthesised using the procedure described in 4.6.2. The details of tosylation of MBP4EO are shown in Fig. 39.



| Compound | purity | n [mol] | m [g] | V [cm$^3$] | d [g/cm$^3$] | M [g/mol] |
|---|---|---|---|---|---|---|
| MBP4EO | 99.0% | 0.088 | **25.28** | | | 284.35 |
| NaOH | | 0.308 | 12.32 | | | 40.00 |
| THF for MBP4EO | | | 56.18 | 63.2 | 0.889 | |
| H$_2$O | | | 61.61 | 61.6 | 1.000 | |
| p-TsCl | 99.0% | 0.106 | 20.34 | | | 190.65 |
| THF for p-TsCl | | | 53.70 | 60.4 | 0.889 | |
| HCl 1M (neutralise) | | 0.20 | | 202.436 | | |

Fig. 39 Tosylation of MBP4EO

Pure product: monobenzyl protected tetra(ethylene glycol) tosylate (MBP4EOTos), colourless free flowing oil, 38.70 g (99.6%). TLC (Silica gel 60): $R_{f\ MBP4EOTos}$ = 0.30, 6% acetone in DCM (substrate: $R_{f\ MBP4EO}$ = 0.05). $^1$H NMR (400 MHz, CDCl$_3$) δ ppm 7.80 (2 H, d, J = 8.3 Hz, Ts aromatic H), 7.38-7.24 (7 H, m, Bn and Ts aromatic CH), 4.56 (2 H, s, Bn CH$_2$), 4.15 (2 H, t, J = 4.8 Hz, Ts-C$\underline{H}_2$CH$_2$O...) 3.73-3.55 (14 H, m, 7×ethylene glycol CH$_2$), 2.44 (3 H, s, CH$_3$); $^{13}$C NMR (101 MHz, CDCl$_3$) δ ppm 144.79 (Ts $\underline{C}$-S), 138.26 (Bn 4° C), 133.01 (Ts 4° C), 129.83 and 128.00 (4×Ts aromatic CH), 128.37, 127.76 and 127.62 (5×Bn aromatic CH), 73.25 (Bn CH$_2$), 70.85-70.45 (multiple CH$_2$), 69.44 (CH$_2$), 69.25 (Ts-$\underline{C}$H$_2$CH$_2$O...), 68.68 (Ts-CH$_2$$\underline{C}$H$_2$O...), 21.66 (Ts CH$_3$); m/z ESI-TOF found 461.11, MALDI-TOF found 461.17 {[M+Na$^+$] expected 461.16}. No impurities were detected in purified product by $^1$H NMR, chromatography or mass spectroscopy, hence purity can be assessed as > 99%.

### 4.6.2.2. Monomethyl protected di(ethylene glycol) tosylate

Monomethyl protected di(ethylene glycol) tosylate (MMP2EOTos) was synthesised according to the procedure 4.6.2. The details of tosylation of MMP2EO are shown Fig. 40.



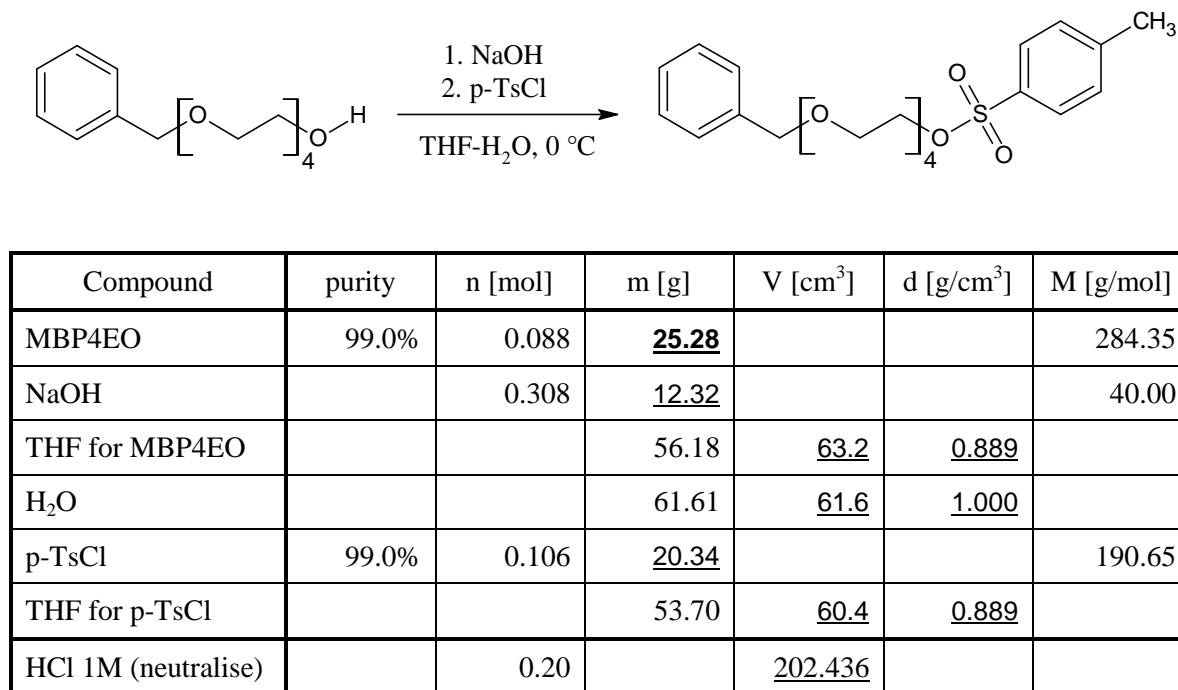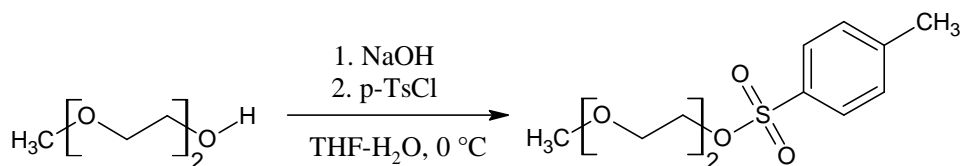| Compound | purity | n [mol] | m [g] | V [cm$^3$] | d [g/cm$^3$] | M [g/mol] |
|---|---|---|---|---|---|---|
| MMP2EO | 99.0% | 0.100 | 12.12 | 12.0 | 0.999 | 120.15 |
| NaOH | | 0.350 | 13.98 | | | 40.00 |
| THF for MMP2EO | | | 26.67 | 30.0 | 0.889 | |
| H2O | | | 69.91 | 69.9 | 1.000 | |
| p-TsCl | 99.0% | 0.120 | 23.08 | | | 190.65 |
| THF for p-TsCl | | | 60.94 | 68.6 | 0.889 | |
| HCl 1M (neutralise) | | 0.23 | | 229.700 | | |

Fig. 40 Tosylation of MMP2EO

Pure product: monomethyl protected di(ethylene glycol) tosylate (MMP2EOTos), colourless free flowing oil, 26.51 g (96.8%). TLC (Silica gel 60): $R_{f\ MMP2EOTos}$ = 0.36, 5% acetone in DCM (substrate: $R_{f\ MMP2EO}$ = 0.00). $^1$H NMR (400 MHz, CDCl$_3$) δ ppm 7.80 (2 H, d, J = 8.3 Hz, Ts aromatic CH), 7.34 (2 H, d, J = 8.3 Hz, Ts aromatic CH), 4.17 (2 H, t, J = 4.8 Hz, Ts-C$\underline{H}_2$CH$_2$O...), 3.69 (2 H, t, J = 4.8 Hz, Ts-CH$_2$C$\underline{H}_2$O...), 3.58 (2 H, m, H$_3$COCH$_2$C$\underline{H}_2$...), 3.48 (2 H, m, H$_3$COC$\underline{H}_2$CH$_2$...), 3.35 (3 H, s, $\underline{H}_3$CO...), 2.45 (3 H, s, Ts CH$_3$); $^{13}$C NMR (101 MHz, CDCl$_3$) δ ppm 144.81 (Ts C-S), 132.98 (Ts 4° C), 129.82 and 128.01 (4×Ts aromatic CH), 71.82 (H$_3$CO$\underline{C}$H$_2$CH$_2$...), 70.69 (H$_3$COCH$_2$$\underline{C}$H$_2$...), 69.22 (Ts-$\underline{C}$H$_2$CH$_2$O...), 68.72 (Ts-CH$_2$$\underline{C}$H$_2$O...), 59.06 (H$_3$$\underline{C}$O...), 21.65 (Ts CH$_3$); m/z ESI-TOF found 296.84, {[M+Na$^+$] expected 297.07}. No impurities were detected on $^1$H NMR or chromatography, hence purity can be assessed > 99%.

### 4.6.3. Chain elongation

Monobenzyl protected tetra(ethylene glycol) tosylate (MBP4EOTos) was used for chain elongation along with different chain lengths PEG diols (Fig. 41).
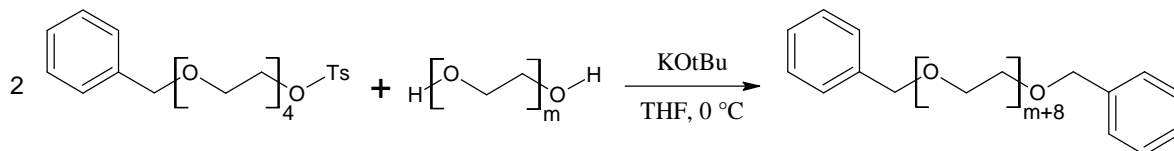


Fig. 41 Chain elongation with MBP4EOTos

KOtBu (2.8 eq) was dissolved in dry THF (8-10ml per gram KOtBu) and left stirred on an ice bath for at least 0.5 h. PEG diol (1 eq) was dried with toluene and then dissolved in dry THF (5-7 ml per gram diol). Monoprotected PEG tosylate (2.6 eq) was dissolved in dry THF (2-4 ml per gram tosylate).

PEG diol solution was added to KOtBu from a glass syringe over 0.5 h at 0°C. Then PEG tosylate solution was added over 2-4 hrs at 0°C and then the reaction mixture was warmed up gradually to room temperature and left stirred for 20hrs. After that, the mixture was cooled down again to 0°C and 1M HCl (also cooled down to 0°C) was added dropwise to neutralise the excess of KOtBu (pH = 7). Next, THF was evaporated and the resulting slurry dissolved in 50 ml of water. Product was extracted from aqueous phase with DCM (4×150ml). Then the organic phase was washed with distilled water (3×75ml) and dried over Na$_2$SO$_4$. After filtration and solvent evaporation, the product was purified by gradient flash chromatography on a Biotage$^®$ SP1 (Table 8).

|  | $g$ = 1 (11-14 EO units) | $g$ = 2 (19-22 EO units) |
|---|---|---|
| cartridge | SNAP 100 g KP silica | SNAP 100 g KP silica |
| flow | 40 ml/min | 40 ml/min |
| dry load | 2 g product on 8 g silica | 2 g product on 8 g silica |
| weak solvent A | DCM | DCM |
| strong solvent B | Acetone | Acetone |
| equilibration | 3 CV with DCM | 3 CV with DCM |
| step 1 | 10 → 10 % B, 4 CV | 15 → 15 % B, 4 CV |
| step 2 | 10 → 60 % B, 9 CV | 15 → 90 % B, 9 CV |
| step 3 | 60 → 60 % B, 2 CV | 90 → 90 % B, 2 CV |

Table 8: Biotage$^®$ SP1 purification conditions for the crude products after $g$ = 1 (11-14 EO units) and $g$ = 2 (19-22 EO units).

### 4.6.3.1. Bis benzyl protected 11-ethylene glycol

Bis benzyl protected 11-ethylene glycol (BBP11EO) was synthesised according to the procedure 4.6.3. The details are shown in Fig. 42.
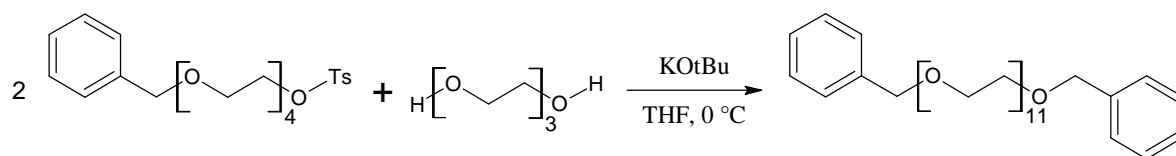


| Compound | purity | n [mol] | m [g] | V [cm$^3$] | d [g/cm$^3$] | M [g/mol] |
|---|---|---|---|---|---|---|
| 3EO | 99.0% | 0.0103 | **1.56** | 1.4 | 1.124 | 150.17 |
| THF for 3EO | | | 9.34 | 10.5 | 0.886 | |
| MBP4EOTos | 99.0% | 0.0267 | 11.82 | 10.0 | 1.180 | 438.53 |
| THF for MBP4EOTos | | | 35.45 | 40.0 | 0.886 | |
| KOtBu | 97.0% | 0.0287 | 3.32 | | | 112.21 |
| THF for KOtBu | | | 29.44 | 33.2 | 0.886 | |
| HCl 1M to neutralise | | 0.0021 | | 2.1 | | |

Fig. 42 Synthesis of BBP11EO

Pure product: bis benzyl protected 11-ethylene glycol (BBP11EO), colourless free flowing oil, 5.52 g (78.8%). TLC (Silica gel 60): $R_{f\ BBP11EO}$ = 0.25, 50% acetone in DCM   ($R_{f\ imp1}$ = 0.59; $R_{f\ imp2}$ = 0.11). $^1$H NMR (400 MHz, CDCl$_3$) δ ppm 7.37-7.25 (10 H, m, Bn aromatic CH), 4.57 (4 H, s, Bn CH$_2$), 3.70-3.61 (44 H, m, 22×ethylene glycol CH$_2$); $^{13}$C NMR (101 MHz, CDCl$_3$) δ ppm 138.29 (Bn 4° C), 128.37, 127.75 and 127.60 (10×Bn aromatic CH), 73.25 (CH$_2$), 70.70-70.50 (multiple CH$_2$), 69.44 (CH$_2$); m/z MALDI-TOF found: 705.35 {[M+Na$^+$], intensity 100%, expected 705.38}, 661.33 {[*target-(1 EO)*+Na$^+$] intensity 0.8%}.

### 4.6.3.2. Bis benzyl protected 12-ethylene glycol

Bis benzyl protected 12-ethylene glycol (BBP12EO) was synthesised according to the procedure 4.6.3. The details are shown in Fig. 43.
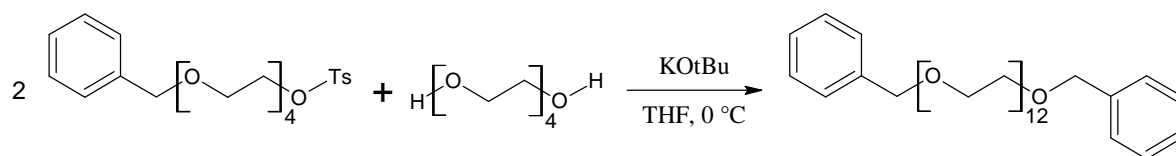


| Compound | purity | n [mol] | m [g] | V [cm³] | d [g/cm³] | M [g/mol] |
|---|---|---|---|---|---|---|
| 4EO | 99.5% | 0.0150 | **2.93** | 2.6 | 1.125 | 194.23 |
| THF for 4EO | | | 14.64 | 16.5 | 0.886 | |
| MBP4EOTos | 99.0% | 0.0390 | 17.28 | 14.6 | 1.180 | 438.53 |
| THF for MBP4EOTos | | | 34.55 | 39.0 | 0.886 | |
| KOtBu | 97.0% | 0.0420 | 4.71 | | | 112.21 |
| THF for KOtBu | | | 33.40 | 37.7 | 0.886 | |
| HCl 1M to neutralise | | 0.0420 | | 42.0 | | |

Fig. 43 Synthesis of BBP12EO

Pure product: bis benzyl protected 12-ethylene glycol (BBP12EO), colourless free flowing oil, 7.57 g (69.4%). TLC (Silica gel 60): $R_{f\ BBP12EO}$ = 0.25, 50% acetone in DCM   ($R_{f\ imp1}$ = 0.59; $R_{f\ imp2}$ = 0.11). $^1$H NMR (400 MHz, CDCl$_3$) δ ppm 7.37-7.25 (10 H, m, Bn aromatic CH), 4.57 (4 H, s, Bn CH$_2$), 3.70-3.61 (48 H, m, 24×ethylene glycol CH$_2$); $^{13}$C NMR (101 MHz, CDCl$_3$) δ ppm 138.29 (Bn 4° C), 128.37, 127.75 and 127.60 (10×Bn aromatic CH), 73.25 (CH$_2$), 70.70-70.50 (multiple CH$_2$), 69.44 (CH$_2$); m/z MALDI-TOF found: 749.38 {[M+Na$^+$], intensity 100%, expected 749.41}, 705.35 {[*target-(1 EO)*+Na$^+$] intensity 1.1%}.

**4.6.3.3. Bis benzyl protected 13-ethylene glycol**

Bis benzyl protected 13-ethylene glycol (BBP13EO) was synthesised during the course of process optimisation according to the procedure 4.6.3, but with the slightly different ratios of the reagents (KOtBu 3.0 eq, MBP4EOTos 2.4 eq) leading to a change in the yield. The details are shown in Fig. 44.
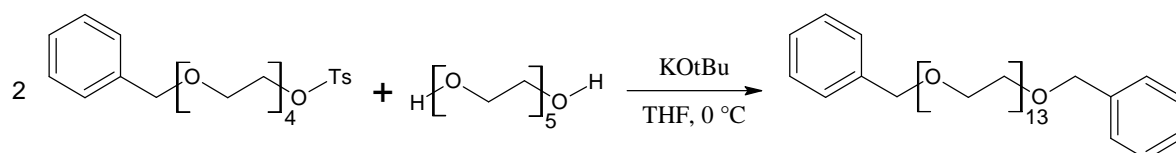


| Compound | purity | n [mol] | m [g] | V [cm$^3$] | d [g/cm$^3$] | M [g/mol] |
|---|---|---|---|---|---|---|
| 5EO | 98.0% | 0.0180 | **<u>4.38</u>** | 3.8 | 1.126 | 238.28 |
| THF for 5EO | | | 21.45 | <u>24.2</u> | 0.886 | |
| MBP4EOTos | 98.0% | 0.0432 | <u>19.33</u> | 16.4 | 1.180 | 438.53 |
| THF for MBP4EOTos | | | 38.66 | <u>43.6</u> | 0.886 | |
| KOtBu | 97.0% | 0.0540 | <u>6.06</u> | | | 112.21 |
| THF for KOtBu | | | 42.95 | <u>48.5</u> | 0.886 | |
| HCl 1M to neutralise | | 0.0108 | | 10.8 | | |

Fig. 44 Synthesis of BBP13EO

Pure product: bis benzyl protected 13-ethylene glycol (BBP13EO), colourless free flowing oil, 7.64 g (55.1%). TLC (Silica gel 60): $R_{f\ BBP13EO}$ = 0.24, 50% acetone in DCM ($R_{f\ imp1}$ = 0.59; $R_{f\ imp2}$ = 0.10). $^1$H NMR (400 MHz, CDCl$_3$) δ ppm 7.37-7.25 (10 H, m, Bn aromatic CH), 4.57 (4 H, s, Bn CH$_2$), 3.70-3.61 (52 H, m, 26×ethylene glycol CH$_2$); $^{13}$C NMR (101 MHz, CDCl$_3$) δ ppm 138.29 (Bn 4° C), 128.37, 127.75 and 127.60 (10×Bn aromatic CH), 73.25 (CH$_2$), 70.70-70.50 (multiple CH$_2$), 69.44 (CH$_2$); m/z MALDI-TOF found: 793.49 {[M+Na$^+$], intensity 100%, expected 793.43}, 749.47 {[*target-(1 EO)*+Na$^+$] intensity 1.3%}.

### 4.6.3.4. Bis benzyl protected 14-ethylene glycol

Bis benzyl protected 14-ethylene glycol (BBP14EO) was synthesised in the course of process optimisation. KOtBu solution was added into the mixture of hexaethylene glycol and MBP4EOTos at room temperature (sequence from *Davis's* procedure, in THF and without 18-crown-6). The details are shown in Fig. 45.
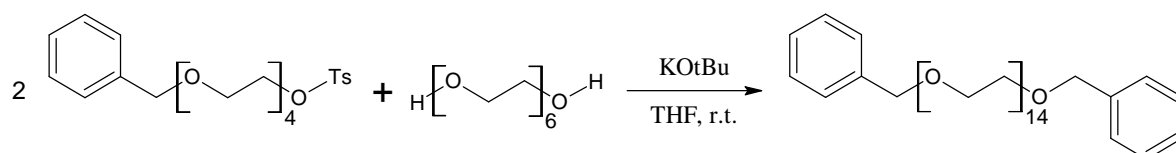


| Compound | purity | n [mol] | m [g] | V [$cm^3$] | d [$g/cm^3$] | M [g/mol] |
|---|---|---|---|---|---|---|
| 6EO | 97.0% | 0.0138 | **4.017** | 3.6 | 1.125 | 282.33 |
| MBP4EOTos | 99.0% | 0.0304 | 13.45 | 11.4 | 1.180 | 438.53 |
| THF for PEG mix | | | 34.93 | 39.4 | 0.886 | |
| KOtBu | 97.0% | 0.0414 | 4.79 | | | 112.21 |
| THF for KOtBu | | | 33.95 | 38.3 | 0.886 | |
| HCl 1M to neutralise | | 0.0110 | | 11.0 | | |

Fig. 45 Synthesis of BBP14EO

Pure product: bis benzyl protected 14-ethylene glycol (BBP14EO), colourless free flowing oil, 7.71 g (68.6%). TLC (Silica gel 60): $R_{f\ BBP13EO}$ = 0.24, 50% acetone in DCM ($R_{f\ imp1}$ = 0.59; $R_{f\ imp2}$ = 0.10). $^1$H NMR (400 MHz, CDCl$_3$) δ ppm 7.37-7.25 (10 H, m, Bn aromatic CH), 4.57 (4 H, s, Bn CH$_2$), 3.70-3.61 (56 H, m, 28×ethylene glycol CH$_2$); m/z MALDI-TOF found: 837.46 {[M+Na$^+$], intensity 100%, expected 837.46}, 793.44 {[*target-(1 EO)*+Na$^+$] intensity 1.2%}.

### 4.6.3.5. Bis benzyl protected 19-ethylene glycol

Bis benzyl protected 19-ethylene glycol (BBP19EO) was synthesised according to the procedure 4.6.3. The details are shown in Fig. 46.
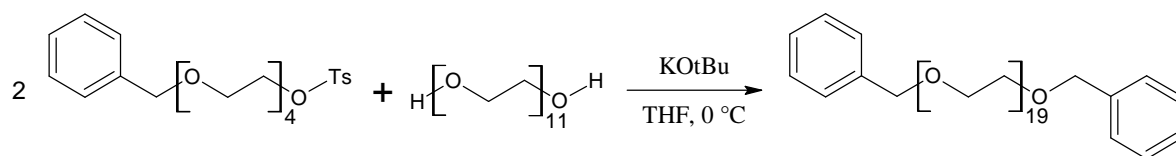


| Compound | purity | n [mol] | m [g] | V [cm$^3$] | d [g/cm$^3$] | M [g/mol] |
|---|---|---|---|---|---|---|
| 11EO | 99.0% | 0.0061 | **_3.102_** | 2.76 | 1.124 | 502.59 |
| THF for 11EO | | | 18.61 | _21.01_ | 0.886 | |
| MBP4EOTos | 99.0% | 0.0159 | _7.04_ | 5.96 | 1.180 | 438.53 |
| THF for MBP4EOTos | | | 21.11 | _23.83_ | 0.886 | |
| KOtBu | 97.0% | 0.0171 | 1.98 | | | 112.21 |
| THF for KOtBu | | | 34.02 | _38.39_ | 0.886 | |
| HCl 1M to neutralise | | 0.0012 | | _1.2_ | | |

Fig. 46 Synthesis of BBP19EO

Pure product: bis benzyl protected 19-ethylene glycol (BBP19EO), white solid, 4.48 g (70.8%). TLC (Silica gel 60): $R_{f\ BBP19EO}$ = 0.11, 70% acetone in DCM ($R_{f\ imp1}$ = 0.59; $R_{f\ imp2}$ = 0.06). $^1$H NMR (400 MHz, CDCl$_3$) δ ppm 7.37-7.25 (10 H, m, Bn aromatic CH), 4.57 (4 H, s, Bn CH$_2$), 3.70-3.61 (76 H, m, 38×ethylene glycol CH$_2$); $^{13}$C NMR (101 MHz, CDCl$_3$) δ ppm 138.29 (Bn 4° C), 128.37, 127.75 and 127.60 (10×Bn aromatic CH), 73.25 (CH$_2$), 70.70-70.50 (multiple CH$_2$), 69.44 (CH$_2$); m/z MALDI-TOF found: 1057.57 {[M+Na$^+$], intensity 100%, expected 1057.59}, 1013.52 {[_target-(1 EO)_+Na$^+$] intensity 1.2%}.

### 4.6.3.6. Bis benzyl protected 20-ethylene glycol

Bis benzyl protected 20-ethylene glycol (BBP20EO) was synthesised according to the procedure 4.6.3. The details are shown in Fig. 47.
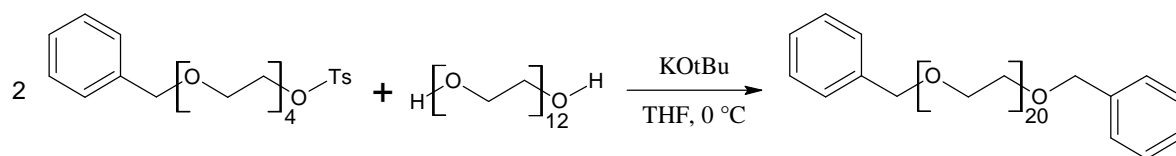


| Compound | purity | n [mol] | m [g] | V [cm³] | d [g/cm³] | M [g/mol] |
|---|---|---|---|---|---|---|
| 12EO | 99.0% | 0.0093 | **5.150** | | | 546.65 |
| THF for 12EO | | | 25.75 | 29.1 | 0.886 | |
| MBP4EOTos | 99.0% | 0.0242 | 10.74 | 9.1 | 1.180 | 438.53 |
| THF for MBP4EOTos | | | 32.22 | 36.4 | 0.886 | |
| KOtBu | 97.0% | 0.0261 | 3.02 | | | 112.21 |
| THF for KOtBu | | | 31.16 | 35.2 | 0.886 | |
| HCl 1M to neutralise | | 0.0019 | | 1.9 | | |

Fig. 47 Synthesis of BBP20EO

Pure product: bis benzyl protected 20-ethylene glycol (BBP20EO), white solid, 6.34 g (63.0%). TLC (Silica gel 60): $R_{f\ BBP20EO}$ = 0.11, 70% acetone in DCM ($R_{f\ imp1}$ = 0.59; $R_{f\ imp2}$ = 0.06). $^1$H NMR (400 MHz, CDCl$_3$) δ ppm 7.37-7.25 (10 H, m, Bn aromatic CH), 4.57 (4 H, s, Bn CH$_2$), 3.70-3.61 (80 H, m, 40×ethylene glycol CH$_2$); $^{13}$C NMR (101 MHz, CDCl$_3$) δ ppm 138.29 (Bn 4° C), 128.37, 127.75 and 127.60 (10×Bn aromatic CH), 73.25 (CH$_2$), 70.70-70.50 (multiple CH$_2$), 69.44 (CH$_2$); m/z MALDI-TOF found: 1101.56 {[M+Na$^+$], intensity 100%, expected 1101.62}, 1057.55 {[*target-(1 EO)*+Na$^+$] intensity 1.3%}.

### 4.6.3.7. Bis benzyl protected 21-ethylene glycol

Bis benzyl protected 21-ethylene glycol (BBP21EO) was synthesised according to the procedure 4.6.3. The details are shown in Fig. 48.
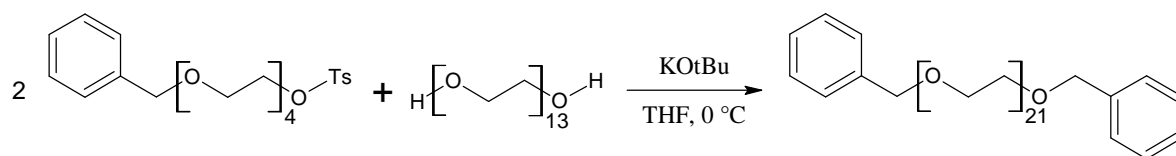


| Compound | purity | n [mol] | m [g] | V [cm$^3$] | d [g/cm$^3$] | M [g/mol] |
|---|---|---|---|---|---|---|
| 13EO | 99.0% | 0.0090 | **5.364** | | | 590.70 |
| THF for 13EO | | | 26.82 | 30.3 | 0.886 | |
| MBP4EOTos | 99.0% | 0.0234 | 10.35 | 8.8 | 1.180 | 438.53 |
| THF for MBP4EOTos | | | 20.71 | 23.4 | 0.886 | |
| KOtBu | 97.0% | 0.0270 | 3.12 | - | | 112.21 |
| THF for KOtBu | | | 21.45 | 24.2 | 0.886 | |
| HCl 1M to neutralise | | 0.0036 | | 3.6 | | |

Fig. 48 Synthesis of BBP21EO

Pure product: bis benzyl protected 21-ethylene glycol (BBP21EO), white solid, 6.67 g (66.0%). TLC (Silica gel 60): $R_{f\ BBP21EO}$ = 0.11, 70% acetone in DCM ($R_{f\ imp1}$ = 0.59; $R_{f\ imp2}$ = 0.06). $^1$H NMR (400 MHz, CDCl$_3$) δ ppm 7.37-7.25 (10 H, m, Bn aromatic CH), 4.57 (4 H, s, Bn CH$_2$), 3.70-3.61 (84 H, m, 42×ethylene glycol CH$_2$); $^{13}$C NMR (101 MHz, CDCl$_3$) δ ppm 138.29 (Bn 4° C), 128.37, 127.75 and 127.60 (10×Bn aromatic CH), 73.25 (CH$_2$), 70.70-70.50 (multiple CH$_2$), 69.44 (CH$_2$); m/z MALDI-TOF found: 1145.60 {[M+Na$^+$], intensity 100%, expected 1145.64}, 1101.57 {[*target-(1 EO)*+Na$^+$] intensity 2.3%}.

### 4.6.3.8. Bis benzyl protected 22-ethylene glycol

Bis benzyl protected 22-ethylene glycol (BBP22EO) was synthesised in the course of process optimisation. KOtBu solution was added into the mixture of 14-ethylene glycol and MBP4EOTos at room temperature (sequence from *Davis's* procedure, in THF and without 18-crown-6). The details are shown in Fig. 49.
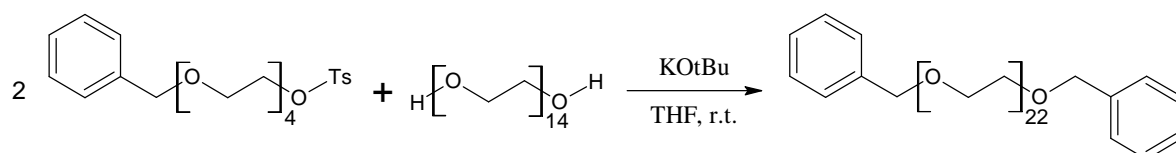


| Compound | purity | n [mol] | m [g] | V [cm$^3$] | d [g/cm$^3$] | M [g/mol] |
|----------|--------|---------|-------|------------|--------------|-----------|
| 14EO | 99.0% | 0.0044 | **2.840** | | | 634.75 |
| MBP4EOTos | 99.0% | 0.0097 | 4.32 | 3.7 | 1.180 | 438.53 |
| THF for PEG mix | | | 14.31 | 16.2 | 0.886 | |
| KOtBu | 97.0% | 0.0133 | 1.54 | | | 112.21 |
| THF for KOtBu | | | 10.57 | 11.9 | 0.886 | |
| HCl 1M to neutralise | | 0.0035 | | 3.5 | | |

Fig. 49 Synthesis of BBP22EO

Pure product: bis benzyl protected 22-ethylene glycol (BBP22EO), white solid, 3.34 g (64.6%). TLC (Silica gel 60): $R_{f\ BBP21EO}$ = 0.11, 70% acetone in DCM ($R_{f\ imp1}$ = 0.59; $R_{f\ imp2}$ = 0.06). $^1$H NMR (400 MHz, CDCl$_3$) δ ppm 7.37-7.25 (10 H, m, Bn aromatic CH), 4.57 (4 H, s, Bn CH$_2$), 3.70-3.61 (88 H, m, 44×ethylene glycol CH$_2$); additional peaks, e.g. broad multiplets found 1.75-2.11 and 3.92-4.00 were some impurities, coming most likely from THF which at this stage of process development was used together with DCM as an eluent for flash chromatography (an extra spot appeared on TLC after the column); m/z MALDI-TOF found: 1189.59 {[M+Na$^+$], intensity 100%, expected 1189.67}, 1145.54 {[*target-(1 EO)*+Na$^+$] intensity 0.6%}.

### 4.6.4. Benzyl group cleavage – hydrogenolysis

The benzyl group cleavage reaction is shown in Fig. 50.
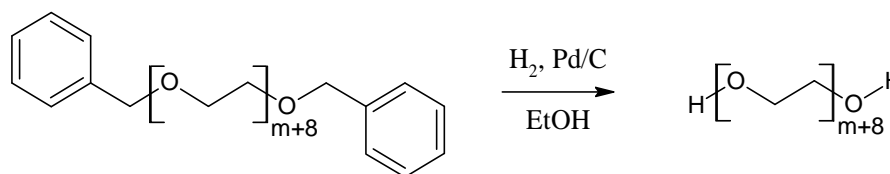


Fig. 50 Benzyl group cleavage

Bis benzyl protected PEG was taken up in ethanol (10-20 ml per gram, depending on solubility) and 10wt.% palladium on carbon (10% of mass of a substrate) was added to the solution, which was degassed thoroughly by repeated cycles of vacuum and Ar, then placed in an autoclave under a hydrogen atmosphere (15-20 bars) and stirred vigorously at room temperature for at least 20 hrs. To work up, hydrogen was removed by repeated cycles of vacuum and Ar, after which the catalyst was removed by filtration through a PTFE 0.2 μm filter and the solvent removed by evaporation under reduced pressure.

In order to get rid of the impurity (methylcyclohexyl end capped) the crude product was dissolved in DCM and extracted with DI water at least 3 times followed by evaporation of water. Alternatively, the purification was performed using gradient flash chromatography under the conditions listed in Table 9.

|  | 11-14 ethylene glycol | 19-22 ethylene glycol |
|---|---|---|
| cartridge | SNAP 100 g KP silica | SNAP 100 g KP silica |
| flow | 40 ml/min | 40 ml/min |
| dry load | 1.5 g product on 8 g silica | 1.5 g product on 8 g silica |
| weak solvent A | DCM | DCM |
| strong solvent B | 30% MeOH in DCM | 30% MeOH in DCM |
| equilibration | 3 CV with DCM | 3 CV with DCM |
| step 1 | 10 → 10 % B, 4 CV | 10 → 10 % B, 4 CV |
| step 2 | 10 → 80 % B, 12 CV | 10 → 92 % B, 10 CV |
| step 3 | 80 → 80 % B, 1 CV | 92 → 92 % B, 1 CV |

Table 9: Biotage® SP1 purification conditions for the crude *n*-ethylene glycols.

### 4.6.4.1. 11-ethylene glycol

11-ethylene glycol (11EO) was synthesised according to the procedure 4.6.4. The details are shown in Fig. 51.
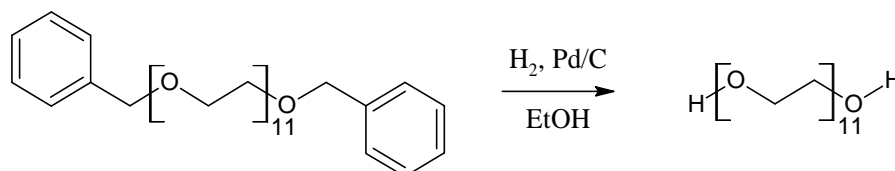


| Compound | purity | n [mol] | m [g] | V [cm$^3$] | d [g/cm$^3$] | M [g/mol] |
|---|---|---|---|---|---|---|
| BBP11EOch | 99.0% | 0.0080 | **5.520** | | | 682.84 |
| Palladium on carbon | 10.0% | 0.000519 | <u>0.552</u> | | | 106.42 |
| Ethanol | | 0.9419 | 43.40 | <u>55</u> | 0.789 | 46.07 |

Fig. 51 Synthesis of 11EO

Crude product: 11-ethylene glycol (11EO), white solid, 4.00 g (99.4%). TLC (Silica gel 60): $R_{f\ 11EO}$ = 0.20, 12% MeOH in DCM ($R_{f\ imp1}$ = 0.36). $^1$H NMR (400 MHz, CDCl$_3$) δ ppm 3.75-3.60 (44 H, m, 22×ethylene glycol CH$_2$), 2.68 (2 H, t, broad, OH); $^{13}$C NMR (101 MHz, CDCl$_3$) δ ppm 72.54 (CH$_2$), 70.70-70.30 (multiple CH$_2$), 61.74 (CH$_2$); m/z MALDI-TOF found: 525.27 {[M+Na$^+$], intensity 100%, expected 525.29}, 481.22 {[*target-(1 EO)*+Na$^+$] intensity 0.9%}. Low intensity (0.03 H) additional peak at 3.25 ppm (d, J = 6.6 Hz, CH$_2$) comes most likely from mono methylcyclohexyl 11-ethylene glycol impurity which is in agreement with MALDI-TOF peak 621.36 Da (4.5%). The product was not purified at this stage because it was used for another chain elongation and purified afterwards.

### 4.6.4.2. 12-ethylene glycol

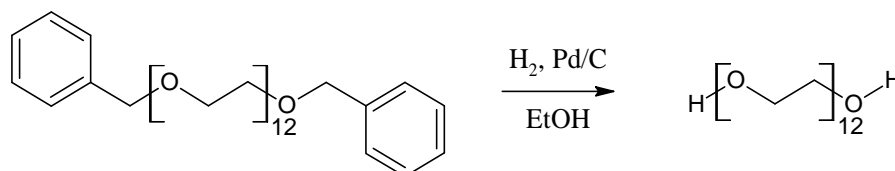12-ethylene glycol (12EO) was synthesised according to the procedure 4.6.4. The details are shown in Fig. 52.



Fig. 52 Synthesis of 12EO

| Compound | purity | n [mol] | m [g] | V [cm³] | d [g/cm³] | M [g/mol] |
|---|---|---|---|---|---|---|
| BBP12EOch | 99.0% | 0.0099 | **7.253** | | | 726.89 |
| Palladium on carbon | 10.0% | 0.000682 | 0.725 | | | 106.42 |
| Ethanol | | 1.2422 | 57.23 | 73 | 0.789 | 46.07 |

Pure product (purified by extraction): 12-ethylene glycol (12EO), white solid, 5.31 g (98.3%). TLC (Silica gel 60): $R_{f\ 12EO}$ = 0.20, 12% MeOH in DCM ($R_{f\ imp1}$ = 0.36). $^1$H NMR (400 MHz, CDCl$_3$) δ ppm 3.75-3.60 (48 H, m, 24×ethylene glycol CH$_2$), 2.89 (2 H, t, broad, OH); $^{13}$C NMR (101 MHz, CDCl$_3$) δ ppm 72.54 (CH$_2$), 70.70-70.30 (multiple CH$_2$), 61.75 (CH$_2$); m/z MALDI-TOF found: 569.27 {[M+Na$^+$], intensity 100%, expected 569.31}, 525.25 {[*target-(1 EO)*+Na$^+$] intensity 1.5%}.

Crude product: low intensity (0.03 H) additional peak at 3.25 ppm (d, J = 6.6 Hz, CH$_2$) most likely originates from mono methylcyclohexyl 12-ethylene glycol impurity which is also confirmed by a peak 665.35 Da found on MALDI-TOF (2.2%).

#### 4.6.4.3. 13-ethylene glycol

13-ethylene glycol (13EO) was synthesised according to the procedure 4.6.4. The details are shown in Fig. 53.



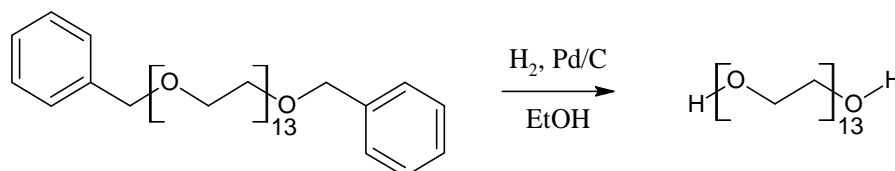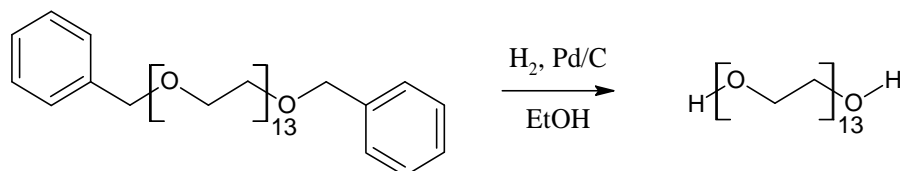| Compound | purity | n [mol] | m [g] | V [cm$^3$] | d [g/cm$^3$] | M [g/mol] |
|---|---|---|---|---|---|---|
| BBP13EOch | 99.0% | 0.098 | **7.640** | | | 770.94 |
| Palladium on carbon | 10.0% | 0.000718 | 0.764 | | | 106.42 |
| Ethanol | | 1.3084 | 60.28 | 76 | 0.789 | 46.07 |

Fig. 53 Synthesis of 13EO

Pure product (purified by extraction): 13-ethylene glycol (13EO), white solid, 5.57 g (96.1%). TLC (Silica gel 60): $R_{f\ 13EO}$ = 0.20, 12% MeOH in DCM ($R_{f\ imp1}$ = 0.36). $^1$H NMR (400 MHz, CDCl$_3$) δ ppm 3.75-3.60 (52 H, m, 26×ethylene glycol CH$_2$), 2.86 (2 H, t, J = 6.2, OH); $^{13}$C NMR (101 MHz, CDCl$_3$) δ ppm 72.56 (CH$_2$), 70.70-70.30 (multiple CH$_2$), 61.74 (CH$_2$); m/z MALDI-TOF found: 613.27 {[M+Na$^+$], intensity 100%, expected 613.34}, 569.25 {[*target-(1 EO)*+Na$^+$] intensity 1.1%}.

Crude product: low intensity (0.04 H) additional peak at 3.25 ppm (d, J = 6.6 Hz, CH$_2$) most likely originates from mono methylcyclohexyl 13-ethylene glycol impurity. The peak intensity indicates approximately 2% of the impurity. MALDI found 709.40 Da (2.7%).

The isolated impurity (DCM phase): mono methylcyclohexyl 13-ethylene glycol (MMCH13EO), colourless oil, 0.1036 g (1.8%). TLC (Silica gel 60): $R_{f\ MMCH13EO}$ = 0.36. $^1$H NMR (400 MHz, CDCl$_3$) δ ppm 3.85-3.45 (52 H, m, 13×ethylene glycol CH$_2$), 3.25 (2 H, d, J = 6.6 Hz, CH$_2$), 2.80 (1 H, broad, OH), 1.79-1.53 (5 H, m, cyclohexyl ring CH and CH$_2$), 1.33-1.09 (4 H, m, cyclohexyl ring CH$_2$), 0.96-0.83 (2 H, m, cyclohexyl ring CH$_2$); $^{13}$C NMR (101 MHz, CDCl$_3$) δ ppm 77.28 (...OCH$_2$C$_6$H$_{11}$), 72.53 (HOCH$_2$CH$_2$O...), 70.80-70.18 (...OCH$_2$CH$_2$O...), 61.68 (HOCH$_2$CH$_2$O...), 37.83 (cyclohexyl ring CH), 30.03, 26.60 and 25.81 (cyclohexyl ring multiple CH$_2$); m/z MALDI-TOF found: 709.41 {[M+Na$^+$], intensity 100%, expected 709.43}.

### 4.6.4.4. 14-ethylene glycol

14-ethylene glycol (14EO) was synthesised in the course of process optimisation. The parameters were similar to those of the procedure 4.6.4, but 5 wt % Pd/C was used instead of 10 wt % with double of the amount. The details are shown in Fig. 54.



| Compound | purity | n [mol] | m [g] | V [$cm^3$] | d [$g/cm^3$] | M [g/mol] |
|----------|--------|---------|-------|-----------|-------------|-----------|
| BBP14EOch | 99.0% | 0.0046 | **3.810** | | | 815.00 |
| Palladium on carbon | 5.0% | 0.000358 | 0.762 | | | 106.42 |
| Ethanol | | 1.3050 | 60.12 | 76 | 0.789 | 46.07 |

Fig. 54 Synthesis of 14EO

Pure product (purified by extraction): 14-ethylene glycol (14EO), white solid, 2.88 g (98.0%). TLC (Silica gel 60): $R_{f\ 14EO}$ = 0.20, 12% MeOH in DCM ($R_{f\ imp1}$ = 0.36). $^1$H NMR (400 MHz, CDCl$_3$) δ ppm 3.75-3.60 (56 H, m, 28×ethylene glycol CH$_2$); m/z MALDI-TOF found: 657.43 {[M+Na$^+$], intensity 100%, expected 657.37}, 613.40 {[*target-(1 EO)*+Na$^+$] intensity 1.0%}.

Crude product: low intensity (0.06 H) additional peak at 3.25 ppm (d, J = 6.6 Hz, CH$_2$) most likely originates from mono methylcyclohexyl 14-ethylene glycol impurity.

#### 4.6.4.5. 19-ethylene glycol

19-ethylene glycol (19EO) was synthesised according to the procedure 4.6.4. The details are shown in Fig. 55.
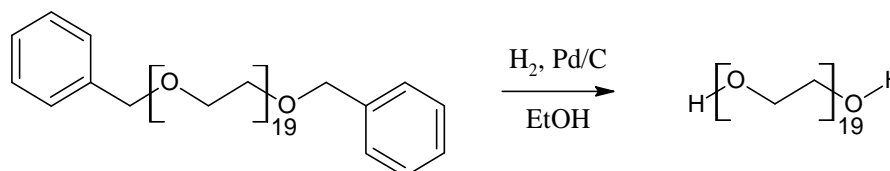


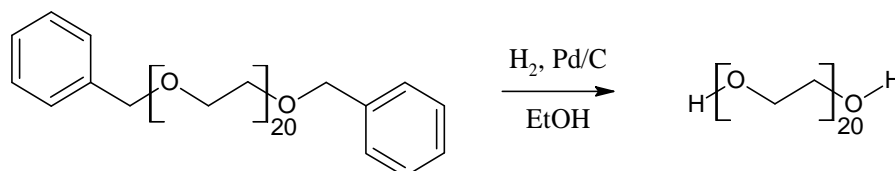| Compound | purity | n [mol] | m [g] | V [cm$^3$] | d [g/cm$^3$] | M [g/mol] |
|---|---|---|---|---|---|---|
| BBP19EOch | 99.0% | 0.0043 | **4.480** | 4.5 | | 1035.26 |
| Palladium on carbon | 10.0% | 0.000421 | 0.448 | | | 106.42 |
| Ethanol | | 0.7672 | 35.35 | 45 | 0.789 | 46.07 |

Fig. 55 Synthesis of 19EO

Pure product (purified by flash chromatography): 19-ethylene glycol (19EO), white solid, 3.51 g (95.8%). TLC (Silica gel 60): $R_{f\ 19EO}$ = 0.20, 12% MeOH in DCM ($R_{f\ imp1}$ = 0.36). $^1$H NMR (400 MHz, CDCl$_3$) δ ppm 3.75-3.60 (76 H, m, 38×ethylene glycol CH$_2$), 2.63 (2 H, broad, OH); $^{13}$C NMR (101 MHz, CDCl$_3$) δ ppm 72.51 (CH$_2$), 70.70-70.20 (multiple CH$_2$), 61.69 (CH$_2$); m/z MALDI-TOF found: 877.44 {[M+Na$^+$], intensity 100%, expected 877.50}, 833.41 {[*target-(1 EO)*+Na$^+$] intensity 1.2%}.

Crude product: low intensity (0.10 H) additional peak at 3.25 ppm (d, J = 6.6 Hz, CH$_2$) most likely originates from mono methylcyclohexyl 19-ethylene glycol impurity. The peak intensity indicates approximately 5% of the impurity. MALDI found 973.54 Da (4.7%).

The isolated impurity: mono methylcyclohexyl 19-ethylene glycol (MMCH19EO), colourless oil, 0.1635 g (4.7%). TLC (Silica gel 60): $R_{f\ MMCH19EO}$ = 0.36. $^1$H NMR (400 MHz, CDCl$_3$) δ ppm 3.85-3.45 (76 H, m, 19×ethylene glycol CH$_2$), 3.25 (2 H, d, J = 6.6 Hz, CH$_2$), 2.74 (1 H, broad, OH), 1.79-1.53 (5 H, m, cyclohexyl ring CH and CH$_2$), 1.33-1.09 (4 H, m, cyclohexyl ring CH$_2$), 0.96-0.83 (2 H, m, cyclohexyl ring CH$_2$); $^{13}$C NMR (101 MHz, CDCl$_3$) δ ppm 77.34 (...OCH$_2$C$_6$H$_{11}$), 72.56 (HOCH$_2$CH$_2$O...), 70.80-70.20 (...OCH$_2$CH$_2$O...), 61.73 (HOCH$_2$CH$_2$O...), 37.87 (cyclohexyl ring CH), 30.07, 26.64 and 25.86 (cyclohexyl ring multiple CH$_2$); m/z MALDI-TOF found: 973.54 {[M+Na$^+$], expected 973.59}.

### 4.6.4.6. 20-ethylene glycol

20-ethylene glycol (20EO) was synthesised according to the procedure 4.6.4. The details are shown in Fig. 56.



Fig. 56 Synthesis of 20EO

| Compound | purity | n [mol] | m [g] | V [cm³] | d [g/cm³] | M [g/mol] |
|---|---|---|---|---|---|---|
| BBP20EOch | 99.0% | 0.0058 | **6.340** | | | 1079.31 |
| Palladium on carbon | 10.0% | 0.000596 | 0.634 | | | 106.42 |
| Ethanol | | 1.0858 | 50.02 | 63 | 0.789 | 46.07 |

Pure product (purified by extraction): 20-ethylene glycol (20EO), white solid, 5.09 g (97.4%). TLC (Silica gel 60): $R_{f\ 20EO}$ = 0.20, 12% MeOH in DCM ($R_{f\ imp1}$ = 0.36). $^1$H NMR (400 MHz, CDCl$_3$) δ ppm 3.75-3.60 (80 H, m, 40×ethylene glycol CH$_2$), 2.64 (2 H, broad, OH); $^{13}$C NMR (101 MHz, CDCl$_3$) δ ppm 72.55 (CH$_2$), 70.70-70.30 (multiple CH$_2$), 61.73 (CH$_2$); m/z MALDI-TOF found: 921.50 {[M+Na$^+$], intensity 100%, expected 921.52}, 877.47 {[*target-(1 EO)*+Na$^+$] intensity 1.4%}.

Crude product: low intensity (0.05 H) additional peak at 3.25 ppm (d, J = 6.6 Hz, CH$_2$) most likely originates from mono methylcyclohexyl 20-ethylene glycol impurity. The peak intensity indicates approximately 2.5% of the impurity. MALDI found 1017.54 Da (1.6%).

#### 4.6.4.7. 21-ethylene glycol

21-ethylene glycol (21EO) was synthesised according to the procedure 4.6.4. The details are shown in Fig. 57.



Fig. 57 Synthesis of 21EO
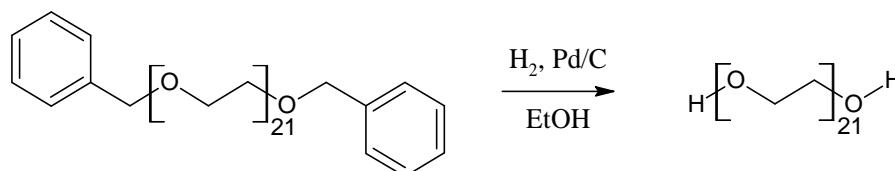
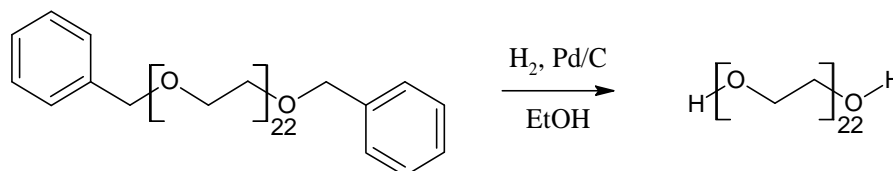| Compound | purity | n [mol] | m [g] | V [cm$^3$] | d [g/cm$^3$] | M [g/mol] |
|---|---|---|---|---|---|---|
| BBP21EO | 99.00% | 0.006 | **6.670** | | | 1123.36 |
| Palladium on carbon | 10.00% | 0.000627 | 0.667 | | | 106.42 |
| Ethanol | | 1.1423 | 52.63 | 67 | 0.789 | 46.07 |

Pure product (purified by flash chromatography): 21-ethylene glycol (21EO), white solid, 5.42 g (97.8 %). TLC (Silica gel 60): $R_{f\ 21EO}$ = 0.20, 12% MeOH in DCM ($R_{f\ imp1}$ = 0.36). $^1$H NMR (400 MHz, CDCl$_3$) δ ppm 3.75-3.60 (84 H, m, 42×ethylene glycol CH$_2$), 2.83 (2 H, broad, OH); $^{13}$C NMR (101 MHz, CDCl$_3$) δ ppm 72.54 (CH$_2$), 70.70-70.30 (multiple CH$_2$), 61.75 (CH$_2$); m/z MALDI-TOF found: 965.50 {[M+Na$^+$], intensity 100%, expected 965.55}, 921.48 {[*target-(1 EO)*+Na$^+$] intensity 2.3%}.

Crude product: low intensity (0.03 H) additional peak at 3.25 ppm (d, J = 6.6 Hz, CH$_2$) most likely originates from mono methylcyclohexyl 21-ethylene glycol impurity. The peak intensity indicates approximately 1.5% of the impurity. MALDI found 1061.62 (1.8%).

The isolated impurity: mono methylcyclohexyl 21-ethylene glycol (MMCH21EO), colourless oil, 0.1222 g (2.2%). TLC (Silica gel 60): $R_{f\ MMCH21EO}$ = 0.36. $^1$H NMR (400 MHz, CDCl$_3$) δ ppm 3.85-3.45 (84 H, m, 21×ethylene glycol CH$_2$), 3.25 (2 H, d, J = 6.6 Hz, CH$_2$), 2.80 (1 H, broad, OH), 1.79-1.53 (5 H, m, cyclohexyl ring CH and CH$_2$), 1.33-1.09 (4 H, m, cyclohexyl ring CH$_2$), 0.96-0.83 (2 H, m, cyclohexyl ring CH$_2$); $^{13}$C NMR (101 MHz, CDCl$_3$) δ ppm 77.32 (...OCH$_2$C$_6$H$_{11}$), 72.54 (HOCH$_2$CH$_2$O...), 70.80-70.20 (...OCH$_2$CH$_2$O...), 61.72 (HOCH$_2$CH$_2$O...), 37.87 (cyclohexyl ring CH), 30.07, 26.64 and 25.85 (cyclohexyl ring multiple CH$_2$); m/z MALDI-TOF found: 1061.62 {[M+Na$^+$], expected 1061.64}.

#### 4.6.4.8. 22-ethylene glycol

22-ethylene glycol (22EO) was synthesised in the course of process optimisation. The parameters were similar to those in the procedure 4.6.4, but 5 wt % Pd/C was used instead of 10 wt % with double the amount. The details are shown in Fig. 58.



Fig. 58 Synthesis of 22EO

| Compound | purity | n [mol] | m [g] | V [cm$^3$] | d [g/cm$^3$] | M [g/mol] |
|---|---|---|---|---|---|---|
| BBP22EOch | 99.0% | 0.003 | **3.340** | | | 1167.40 |
| Palladium on carbon | 5.0% | 0.000314 | 0.668 | | | 106.42 |
| Ethanol | | 1.1440 | 52.71 | 67 | 0.789 | 46.07 |

Pure product (purified by flash chromatography): 22-ethylene glycol (22EO), white solid, 2.51 g (89.8%). TLC (Silica gel 60): $R_{f\ 22EO}$ = 0.20, 12% MeOH in DCM ($R_{f\ imp1}$ = 0.36). $^1$H NMR (400 MHz, CDCl$_3$) δ ppm 3.75-3.60 (88 H, m, 44×ethylene glycol CH$_2$), 2.74 (2 H, t, J= 6.2 Hz, OH); $^{13}$C NMR (101 MHz, CDCl$_3$) δ ppm 72.53 (CH$_2$), 70.70-70.30 (multiple CH$_2$), 61.74 (CH$_2$); m/z MALDI-TOF found: 1009.60 {[M+Na$^+$], intensity 100%, expected 1009.58}, 965.58 {[*target-(1 EO)*+Na$^+$] intensity 1.2%}. Crude product: not analysed.

### 4.6.5. End-capping without chain elongation

KOtBu (6 eq) was dissolved in dry THF (10-20ml per gram KOtBu) and left stirred in an ice bath for at least 0.5 h. PEG diol (1 eq) was dried with toluene and then dissolved in dry THF (5-6 ml per gram alcohol). Iodomethane (8 eq) was dissolved in dry THF (2-2.5 ml per gram $CH_3I$).

PEG alcohol solution was added to KOtBu solution from a glass syringe over 30 minutes at 0°C. Then iodomethane solution was added over 30 minutes at 0°C. The mixture was allowed to warm up to room temperature and left stirred overnight.

The reaction mixture was poured into cold water (50 ml per gram PEG diol) and, if required, neutralised with HCl solution. THF was evaporated and the product was extracted with DCM (3×100ml). Next, organic phase washed with 10% $Na_2CO_3$ (8×50ml) and then with distilled water until neutral (4×25ml). Typically the yields were over 97% and there was no need for further purification as no impurities were detected. However, lower yields most likely indicated that some hydroxyl- groups were not protected. If impurities were still detected after extraction, product required further purification by flash chromatography (Table 10). Pure product was dried by evaporating toluene, followed by filtration in anhydrous acetonitrile (MeCN), using a 0.2 μm PTFE filter. Then MeCN was evaporated and product was left dried for minimum 72 hrs under vacuum.

|  | bis methyl protected 19-22 ethylene glycol |
| --- | --- |
| cartridge | SNAP 100 g KP silica |
| flow | 40 ml/min |
| dry load | 1.5 g product on 8 g silica |
| weak solvent A | DCM |
| strong solvent B | 30% MeOH in DCM |
| equilibration | 3 CV with DCM |
| step 1 | 7 → 7 % B, 2 CV |
| step 2 | 7 → 60 % B, 10 CV |
| step 3 | 60 → 60 % B, 1 CV |

Table 10: Biotage® SP1 purification conditions for bis methyl protected n-ethylene glycols.

### 4.6.5.1. Bis methyl protected 19-ethylene glycol

Bis methyl protected 19-ethylene glycol (BMP19EO) was synthesised according to procedure 4.6.5. The details are shown in Fig. 59.
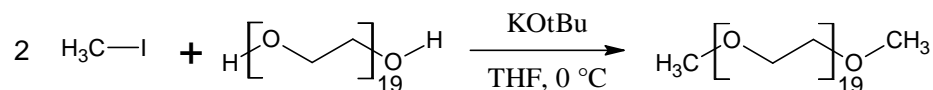


| Compound | purity | n [mol] | m [g] | V [cm³] | d [g/cm³] | M [g/mol] |
|---|---|---|---|---|---|---|
| 19EO | 99.0% | 0.0011 | **0.950** | | | 855.01 |
| THF for 19EO | | | 4.75 | 5.36 | 0.886 | 72.11 |
| CH₃I | 99.5% | 0.0088 | 1.255 | 0.55 | 2.280 | 141.94 |
| THF for CH₃I | | | 2.51 | 2.83 | 0.886 | 72.11 |
| KOtBu | 97.0% | 0.0066 | 0.76 | | | 112.21 |
| THF for KOtBu | | | 13.53 | 15.27 | 0.886 | 72.11 |

Fig. 59 Synthesis of BMP19EO

Pure product (chromatography not required): bis methyl protected 19-ethylene glycol (BMP19EO), white solid, 0.96 g (98.8%). TLC (Silica gel 60): $R_{f\ BMP19EO}$ = 0.30, 9% MeOH in DCM. $^1$H NMR (400 MHz, CDCl$_3$) δ ppm 3.78-3.59 (72 H, m, 36×ethylene glycol CH$_2$), 3.59-3.52 (4 H, m, 2×ethylene glycol CH$_2$), 3.38 (6 H, s, 2×CH$_3$); $^{13}$C NMR (101 MHz, CDCl$_3$) δ ppm 71.95 (CH$_3$OC$\underline{H}_2$...), 70.70-70.50 (multiple CH$_2$), 59.05 (CH$_3$); m/z MALDI-TOF found: 905.50 {[M+Na$^+$], intensity 100%, expected 905.53}, 861.47 {[*target-(1 EO)*+Na$^+$] intensity 1.2%}.

#### 4.6.5.2. Bis methyl protected 20-ethylene glycol

Bis methyl protected 20-ethylene glycol (BMP20EO) was synthesised according to procedure 4.6.5. The details are shown in Fig. 60.
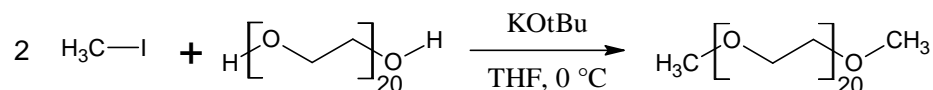


| Compound | purity | n [mol] | m [g] | V [cm$^3$] | d [g/cm$^3$] | M [g/mol] |
|---|---|---|---|---|---|---|
| 20EO | 99.0% | 0.0014 | **1.307** | | | 899.07 |
| THF for 20EO | | | 6.54 | 7.38 | 0.886 | 72.11 |
| CH$_3$I | 99.5% | 0.0115 | 1.642 | 0.72 | 2.280 | 141.94 |
| THF for CH$_3$I | | | 3.28 | 3.71 | 0.886 | 72.11 |
| KOtBu | 97.0% | 0.0086 | 1.00 | | | 112.21 |
| THF for KOtBu | | | 8.85 | 9.99 | 0.886 | 72.11 |

Fig. 60 Synthesis of BMP20EO

Pure product (chromatography not required): bis methyl protected 20-ethylene glycol (BMP20EO), white solid, 1.33 g (99.7%). TLC (Silica gel 60): R$_{f\ BMP20EO}$ = 0.30, 9% MeOH in DCM. $^1$H NMR (400 MHz, CDCl$_3$) δ ppm 3.78-3.59 (76 H, m, 38×ethylene glycol CH$_2$), 3.59-3.52 (4 H, m, 2×ethylene glycol CH$_2$), 3.38 (6 H, s, 2×CH$_3$); $^{13}$C NMR (101 MHz, CDCl$_3$) δ ppm 71.95 (CH$_3$OC̲H$_2$...), 70.70-70.50 (multiple CH$_2$), 59.05 (CH$_3$); m/z MALDI-TOF found: 949.47 {[M+Na$^+$], intensity 100%, expected 949.56}, 905.45 {[*target-(1 EO)*+Na$^+$] intensity 2.3%}.

#### 4.6.5.3. Bis methyl protected 21-ethylene glycol

Bis methyl protected 21-ethylene glycol (BMP21EO) was synthesised according to procedure 4.6.5. The details are shown in Fig. 61.
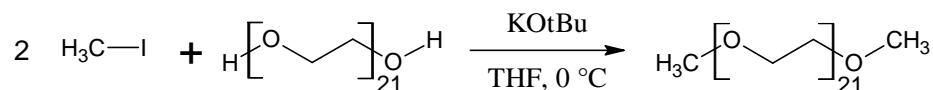


| Compound | purity | n [mol] | m [g] | V [cm$^3$] | d [g/cm$^3$] | M [g/mol] |
|---|---|---|---|---|---|---|
| 21EO | 99.0% | 0.0021 | **2.000** | | | 943.12 |
| THF for 21EO | | | 10.00 | 11.29 | 0.886 | 72.11 |
| CH$_3$I | 99.5% | 0.0168 | 2.384 | 1.05 | 2.280 | 141.94 |
| THF for CH$_3$I | | | 4.77 | 5.38 | 0.886 | 72.11 |
| KOtBu | 97.0% | 0.0126 | 1.41 | _ | _ | 112.21 |
| THF for KOtBu | | | 12.52 | 14.13 | 0.886 | 72.11 |

Fig. 61 Synthesis of BMP21EO

Pure product (chromatography not required): bis methyl protected 21-ethylene glycol (BMP21EO), white solid, 1.99 g (97.7%). TLC (Silica gel 60): R$_{f\ BMP21EO}$ = 0.30, 9% MeOH in DCM. $^1$H NMR (400 MHz, CDCl$_3$) δ ppm 3.78-3.59 (80 H, m, 40×ethylene glycol CH$_2$), 3.59-3.52 (4 H, m, 2×ethylene glycol CH$_2$), 3.38 (6 H, s, 2×CH$_3$); $^{13}$C NMR (101 MHz, CDCl$_3$) δ ppm 71.94 (CH$_3$OCH$_2$...), 70.70-70.50 (multiple CH$_2$), 59.04 (CH$_3$); m/z MALDI-TOF found: 993.55 {[M+Na$^+$], intensity 100%, expected 993.58}, 949.54 {[*target-(1 EO)*+Na$^+$] intensity 3.7%}, 905.50 {[*target-(2 EO)*+Na$^+$] intensity 1.2%}.

#### 4.6.5.4. Bis methyl protected 22-ethylene glycol

Bis methyl protected 22-ethylene glycol (BMP22EO) was synthesised in the course of process optimisation using the *Booth's* method[32]. Iodomethane was added into the slurry of KOH in chlorobenzene at 0°C. Solution of 22EO in chlorobenzene was added last. The details are shown in Fig. 62.
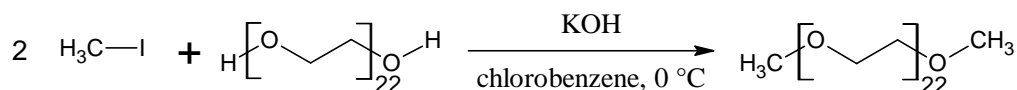


| Compound | purity | n [mol] | m [g] | V [cm$^3$] | d [g/cm$^3$] | M [g/mol] |
|---|---|---|---|---|---|---|
| 22EO | 99.0% | 0.0023 | **2.270** | | | 987.17 |
| Chlorobenzene for 22EO | | 0.2456 | 27.650 | 25.0 | 1.106 | 112.56 |
| CH$_3$I | 99.5% | 0.0182 | 2.598 | 1.1 | 2.280 | 141.94 |
| Chlorobenzene for CH$_3$I | | 0.1965 | 22.120 | 20.0 | 1.106 | 112.56 |
| KOH | | 0.6238 | 35.00 | | | 56.11 |
| Chlorobenzene for KOH | | 0.6878 | 77.420 | 70.0 | 1.106 | 112.56 |

Fig. 62 Synthesis of BMP22EO

Pure product (purified by flash chromatography): bis methyl protected 22-ethylene glycol (BMP22EO), white solid, 1.84 g (79.6%). TLC (Silica gel 60): $R_{f\ BMP22EO}$ = 0.30, 9% MeOH in DCM. $^1$H NMR (400 MHz, CDCl$_3$) δ ppm 3.78-3.59 (84 H, m, 42×ethylene glycol CH$_2$), 3.59-3.52 (4 H, m, 2×ethylene glycol CH$_2$), 3.38 (6 H, s, 2×CH$_3$); $^{13}$C NMR (101 MHz, CDCl$_3$) δ ppm 71.93 (CH$_3$OC̲H$_2$...), 70.70-70.30 (multiple CH$_2$), 59.03 (CH$_3$); m/z MALDI-TOF found: 1037.57 {[M+Na$^+$], intensity 100%, expected 1037.61}, 993.54 {[*target-(1 EO)*+Na$^+$] intensity 2.8%}, 949.52 {[*target-(2 EO)*+Na$^+$] intensity 0.8%}.

### 4.6.6. End-capping with chain elongation

Monomethyl protected di(ethylene glycol) tosylate (MMP2EOTos) was used for end-capping with chain elongation (Fig. 63).
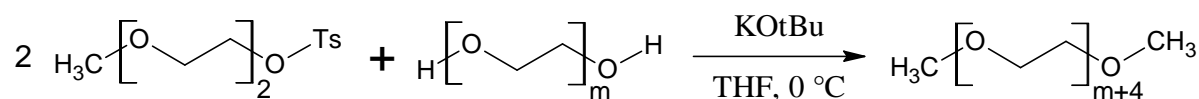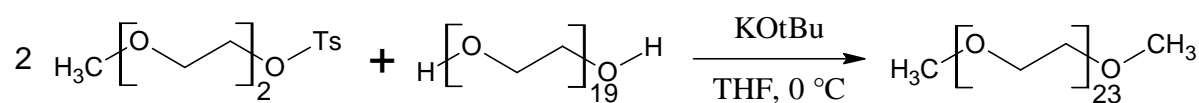


Fig. 63 End-capping with chain elongation using MMP2EOTos

The procedure was a combination of 4.6.3 used for reaction conditions and 4.6.5 used for purification of the crude product.

### 4.6.6.1. Bis methyl protected 23-ethylene glycol

Bis benzyl protected 23-ethylene glycol (BMP23EO) was synthesised according to method described in 4.6.6. The details are shown in Fig. 64.



| Compound | purity | n [mol] | m [g] | V [cm$^3$] | d [g/cm$^3$] | M [g/mol] |
|---|---|---|---|---|---|---|
| 19EO | 99.0% | 0.0010 | **0.855** | | | 855.01 |
| THF for 19EO | | | 5.13 | 5.79 | 0.886 | |
| MMP2EOTos | 99.0% | 0.0030 | 0.82 | | | 274.33 |
| THF for MMP4EOTos | | | 2.47 | 2.79 | 0.886 | |
| KOtBu | 97.0% | 0.0030 | 0.33 | | | 112.21 |
| THF for KOtBu | | | 5.91 | 6.67 | 0.886 | |

Fig. 64 Synthesis of BMP23EO

Pure product (purified by flash chromatography): bis methyl protected 23-ethylene glycol (BMP23EO), white solid, 0.82 g (80.0%). TLC (Silica gel 60): $R_{f\ BMP23EO}$ = 0.30, 9% MeOH in DCM. $^1$H NMR (400 MHz, CDCl$_3$) δ ppm 3.78-3.59 (88 H, m, 44×ethylene glycol CH$_2$), 3.59-3.52 (4 H, m, 2×ethylene glycol CH$_2$), 3.38 (6 H, s, 2×CH$_3$); $^{13}$C NMR (101 MHz,

CDCl$_3$) δ ppm 71.95 (CH$_3$OC$\underline{H}_2$...), 70.65-70.50 (multiple CH$_2$), 59.06 (CH$_3$); m/z MALDI-TOF found: 1081.45 {[M+Na$^+$], intensity 100%, expected 1081.63}, 1037.43 {[*target-(1 EO)*+Na$^+$] intensity 2.5%}, 993.42 {[*target-(2 EO)*+Na$^+$] intensity 1.6%}.

### 4.6.6.2. Bis methyl protected 24-ethylene glycol

Bis benzyl protected 24-ethylene glycol (BMP24EO) was synthesised according to method described in 4.6.6. The details are shown in Fig. 65.
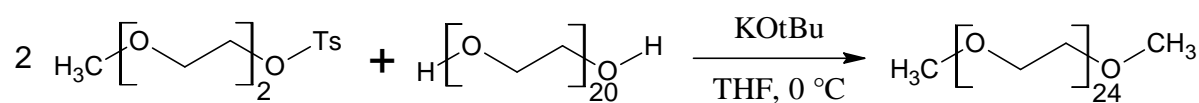


| Compound | purity | n [mol] | m [g] | V [cm$^3$] | d [g/cm$^3$] | M [g/mol] |
|---|---|---|---|---|---|---|
| 20EO | 99.0% | 0.0018 | **_1.618_** | | | 899.07 |
| THF for 20EO | | | 12.94 | _14.6_ | 0.886 | |
| MMP2EOTos | 99.0% | 0.0050 | _1.38_ | | | 274.33 |
| THF for MMP2EOTos | | | 4.15 | _4.7_ | 0.886 | |
| KOtBu | 97.0% | 0.0050 | 0.56 | | | 112.21 |
| THF for KOtBu | | | 4.96 | _5.6_ | 0.886 | |

Fig. 65 Synthesis of BMP24EO

Pure product (purified by flash chromatography): bis methyl protected 24-ethylene glycol (BMP24EO), white solid, 1.66 g (84.4%). TLC (Silica gel 60): R$_{f\ BMP24EO}$ = 0.30, 9% MeOH in DCM. $^1$H NMR (400 MHz, CDCl$_3$) δ ppm 3.78-3.59 (92 H, m, 46×ethylene glycol CH$_2$), 3.59-3.52 (4 H, m, 2×ethylene glycol CH$_2$), 3.38 (6 H, s, 2×CH$_3$); $^{13}$C NMR (101 MHz, CDCl$_3$) δ ppm 71.93 (CH$_3$OC$\underline{H}_2$...), 70.75-70.30 (multiple CH$_2$), 59.04 (CH$_3$); m/z MALDI-TOF found: 1125.62 {[M+Na$^+$], intensity 100%, expected 1125.66}, 1081.59 {[*target-(1 EO)*+Na$^+$] intensity 3.7%}, 1037.57 {[*target-(2 EO)*+Na$^+$] intensity 1.0 %}.

# References

1. N. N. Reed, K. D. Janda, *A one-step synthesis of monoprotected polyethylene glycol ethers.* Journal of Organic Chemistry, 2000, **65**(18): p. 5843-5845.

2. R. Fordyce, E. L. Lovell, H. Hibbert, *Studies on Reactions Relating to Carbohydrates and Polysaccharides. LVI. The Synthesis of the Higher Polyoxyethylene Glycols.* Journal of the American Chemical Society, 1939, **61**(7): p. 1905-1910.

3. F. A. Loiseau, K. K. Hii, A. M. Hill, *Multigram synthesis of well-defined extended bifunctional polyethylene glycol (PEG) chains.* Journal of Organic Chemistry, 2004, **69**(3): p. 639-647.

4. S. A. Ahmed, M. Tanaka, *Synthesis of Oligo(ethylene glycol) toward 44-mer.* Journal of Organic Chemistry, 2006, **71**: p. 9884-9886.

5. A. C. French, A. L. Thompson, B. G. Davis, *High-Purity Discrete PEG-Oligomer Crystals Allow Structural Insight.* Angewandte Chemie-International Edition, 2009, **48**(7): p. 1248-1252.

6. D. Niculescu-Duvaz, J. Getaz, C. J. Springer, *Long functionalized poly(ethylene glycol)s of defined molecular weight: Synthesis and application in solid-phase synthesis of conjugates.* Bioconjugate Chemistry, 2008, **19**(4): p. 973-981.

7. E. M. D. Keegstra, J. W. Zwikker, M. R. Roest, L. W. Jenneskens, *A highly selective synthesis of monodisperse oligo(ethylene glycols).* Journal of Organic Chemistry, 1992, **57**(24): p. 6678-6680.

8. A. J. Brandolini, D. D. Hills, *NMR Spectra of Polymers and Polymer Additives*, Marcel Dekker, New York, **2000**.

9. J. Clayden, *Organic chemistry*, Oxford University Press, Oxford; New York, **2001**.

10. S. T. Balke, *Quantitative column liquid chromatography : a survey of chemometric methods*, Elsevier; Distributors for the U.S. and Canada, Elsevier Science Pub. Co., Amsterdam; New York, NY, **1984**.

11. A. M. Striegel, *Modern size-exclusion liquid chromatography : practice of gel permeation and gel filtration chromatography*, 2nd ed., Wiley, Hoboken, N.J., **2009**.

12. P. G. Bruce, *Solid state electrochemistry*, Cambridge University Press, Cambridge ; New York, NY, USA, **1995**.

13. I. M. Smallwood, *Handbook of organic solvent properties*, Arnold ; Halsted Press, London, New York, **1996**.

14. E. d. Hoffmann, V. Stroobant, *Mass spectrometry : principles and applications*, 3rd ed., J. Wiley, Chichester, West Sussex, England ; Hoboken, NJ, **2007**.

15. D. Yu, N. Vladimirov, J. M. J. Fréchet, *MALDI-TOF in the Characterizations of Dendritic−Linear Block Copolymers and Stars.* Macromolecules, 1999, **32**(16): p. 5186-5192.

16. G. Montaudo, F. Samperi, M. S. Montaudo, *Characterization of synthetic polymers by MALDI-MS.* Progress in Polymer Science, 2006, **31**(3): p. 277-357.

17. K. Shimada, R. Nagahata, S. Kawabata, S. Matsuyama, T. Saito, S. Kinugasa, *Evaluation of the quantitativeness of matrix-assisted laser desorption/ionization time-of-flight mass spectrometry using an equimolar mixture of uniform poly(ethylene glycol) oligomers.* Journal of Mass Spectrometry, 2003, **38**(9): p. 948-954.

18. S. Varray, J. L. Aubagnac, E. Lamaty, R. Lazaro, J. Martinez, C. Enjalbal, *Poly(ethyleneglycol) in electrospray ionization (ESI) mass spectrometry.* Analusis, 2000, **28**(4): p. 263-268.

19. W. Yan, D. M. Ammon, Jr., J. A. Gardella, Jr., E. P. Maziarz, III, A. M. Hawkridge, G. L. Grobe, III, T. D. Wood, *Quantitative mass spectrometry of technical polymers: A comparison of several ionization methods.* European Mass Spectrometry, 1999, **4**(6): p. 467-474.

20. G. Montaudo, M. S. Montaudo, C. Puglisi, F. Samperi, *Characterization of polymers by matrix-assisted laser-desorption ionization-time of flight mass-spectrometry - end group determination and molecular-weight estimates in poly(ethylene glycols).* Macromolecules, 1995, **28**(13): p. 4562-4569.

21. R. M. Whittal, L. Li, S. Lee, M. A. Winnik, *Characterization of pyrene end-labeled poly(ethylene glycol) by high resolution MALDI time-of-flight mass spectrometry.* Macromolecular Rapid Communications, 1996, **17**(1): p. 59-64.

22. A. Marie, F. Fournier, J. C. Tabet, *Characterization of synthetic polymers by MALDI-TOF/MS: Investigation into new methods of sample target preparation and consequence on mass spectrum finger print.* Analytical Chemistry, 2000, **72**(20): p. 5106-5114.

23. C. Enjalbal, B. Sauvagnat, F. Lamaty, R. Lazaro, J. Martinez, P. Mouchet, F. Roux, J. L. Aubagnac, *Chemical reactivity in matrix-assisted laser desorption/ionization mass spectrometry.* Rapid Communications in Mass Spectrometry, 1999, **13**(18): p. 1775-1781.

24. Sigma-Aldrich, *MALDI-Mass Spectrometry.* AnalytiX Newsletters, 2001, **6**.

25. K. Shimada, S. Matsuyama, T. Saito, S. Kinugasa, R. Nagahata, S. Kawabata, *Conformational effects on cationization of poly(ethylene glycol) by alkali metal ions in matrix-assisted laser desorption/ionization time-of-flight mass spectrometry.* International Journal of Mass Spectrometry, 2005, **247**(1-3): p. 85-92.

26. A. Williamson, *Theory of Aetherification.* Philosophical Magazine, 1850, **37**: p. 350-356.

27. M. Smith, J. March, *March's advanced organic chemistry : reactions, mechanisms, and structure*, 6th ed., Wiley-Interscience, Hoboken, N.J., **2007**.

28. P. G. M. Wuts, T. W. Greene, *Greene's protective groups in organic synthesis*, 4th ed., Wiley-Interscience, Hoboken, N.J., **2007**.

29. A. Bouzide, G. Sauve, *Highly selective silver(I) oxide mediated monoprotection of symmetrical diols.* Tetrahedron Letters, 1997, **38**(34): p. 5945-5948.

30. N. Boden, R. J. Bushby, S. Clarkson, S. D. Evans, P. F. Knowles, A. Marsh, *The design and synthesis of simple molecular tethers for binding biomembranes to a gold surface.* Tetrahedron, 1997, **53**(31): p. 10939-10952.

31. J. McMurry, *Organic chemistry*, 7e. ed., Thomson Brooks/Cole, Belmont, CA, **2008**.

32. D. R. Cooper, C. Booth, *Mixing of ethylene-oxide and propylene-oxide oligomers .1. Enthalpy and volume changes.* Polymer, 1977, **18**(2): p. 164-170.

33. N. Kulevsky, C. T. Wang, V. I. Stenberg, *Photochemical oxidations. II. Rate and product formation studies on the photochemical oxidation of ethers.* The Journal of Organic Chemistry, 1969, **34**(5): p. 1345-1348.

34. R. G. Farquharson, M. H. Hall, W. T. Fullerton, *Poor obstetric outcome in 3 quality-control laboratory workers.* Lancet, 1983, **1**(8331): p. 983-984.

35. S. Han, C. Kim, D. Kwon, *Thermal/oxidative degradation and stabilization of polyethylene glycol.* Polymer, 1997, **38**(2): p. 317-323.

36. S. Han, C. Kim, D. Kwon, *Thermal degradation of poly(ethylene glycol).* Polymer Degradation and Stability, 1995, **47**(2): p. 203-208.

37. L. Boughen, J. Liggat, G. Ellis, *Thermal degradation of polyethylene glycol 6000 and its effect on the assay of macroprolactin.* Clinical Biochemistry, 2010, **43**(9): p. 750-753.
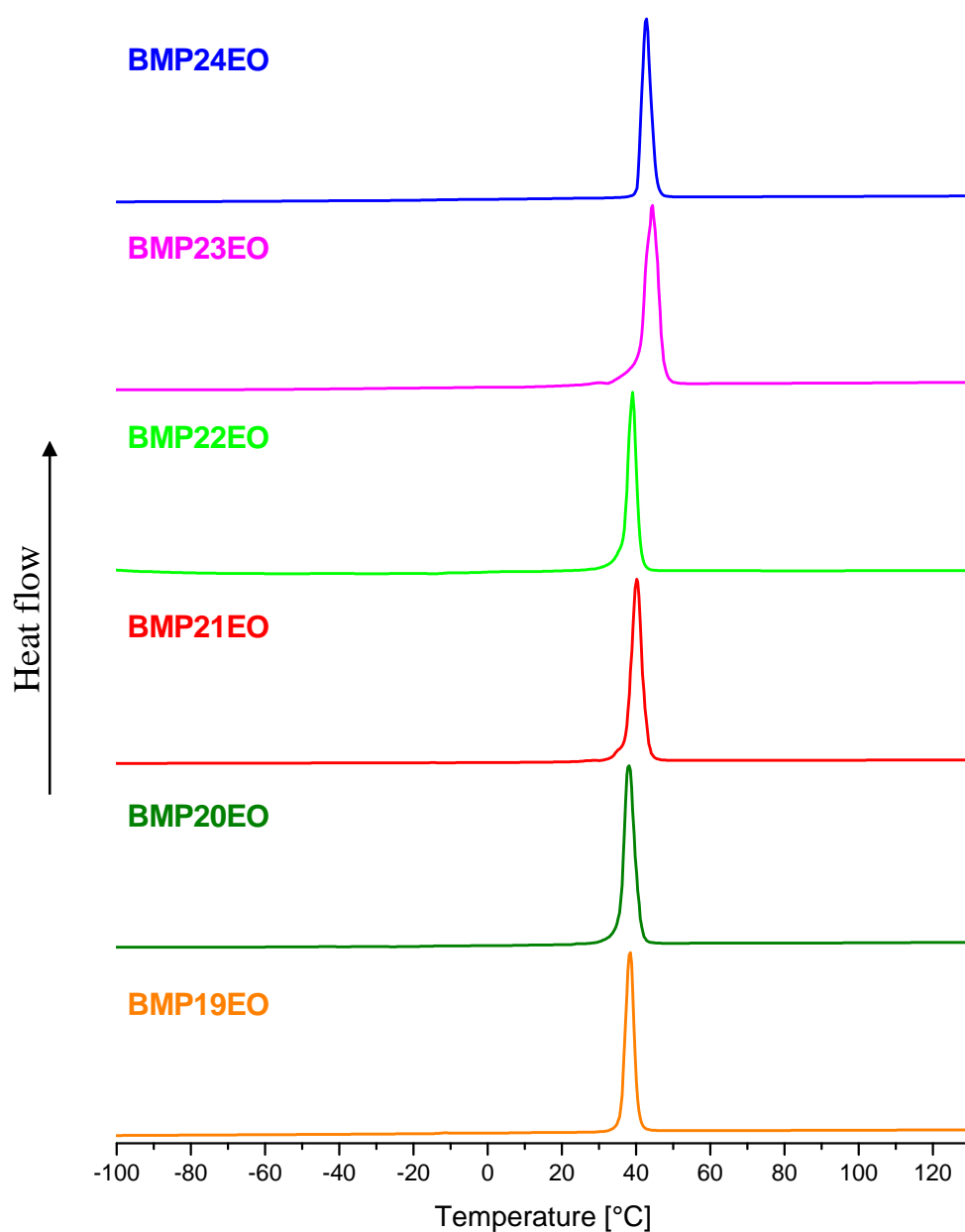
# 5.  ELECTROLYTES WITH MONODISPERSED PEOs

Formation of the desired phase and the absence of unreacted starting chemicals were verified by PXRD and DSC measurements, using diffraction and thermal signatures of the polymer, the salt and the $\alpha$ phase.

## 5.1. Properties of the polymers and the salt used for complexes

High molecular weight polyethylene glycols are predominantly crystalline. The polydispersed PEO ($5 \times 10^6$ Da) is reported to contain 70-85% of crystalline phase which melts at around 65-66°C.[1,2] At the same time, the reported glass transition temperature of the amorphous fraction appears to depend on the Mw, with the maximum value of $T_g$ = -17°C (<Mw> = 6000 Da) while for high molecular weight PEOs (<Mw> $\geq$ 225,000 Da) the value of $T_g$ is in the range -53 to -63°C.[1-6]

As mentioned in the introductory chapter, poly(ethylene glycol) dimethyl ether of Mw = 1000 Da (Fluka, cat. no. 81312, *m.p.* = 36-40°C) has been selected to study crystalline complexes. The melting point of lower Mw PEOs depends not only on the molecular weight but on the type of the end groups. For example, the melting point of 20 EO is reduced from 47°C to 38°C on replacing -OH end groups by -OCH$_3$. No glass transition has been observed in the DSC trace of the 1000 Da PEO, suggesting a high degree of crystallinity. Monodispersed PEOs synthesised in this work are also highly crystalline, as confirmed by the absence of a $T_g$ in the DSC data, Fig. 66. LiPF$_6$ is a crystalline salt with the melting point of 194°C[7]. The $\alpha$ phase of the complex is crystalline and melts at 70-90°C depending on the Mw of the polymer.

Fig. 66 DSC and molecular purity (uniformity of the chain length determined by MALDI) of monodispersed PEOs.

| Monodispersed polymer | Number of ether oxygens $N_O$ | molecular purity (MALDI-TOF) | m.p. [°C] |
|---|---|---|---|
| BMP24EO | 25 | 95.7% | 42.8 |
| BMP23EO | 24 | 96.1% | 44.4 |
| BMP22EO | 23 | 96.6 % | 39.1 |
| BMP21EO | 22 | 95.5% | 40.1 |
| BMP20EO | 21 | 97.7% | 38.1 |
| BMP19EO | 20 | 98.8% | 38.5 |

The absence of a pure salt and polymer in the complex has been further verified by PXRD. Powder diffraction patterns of LiPF$_6$, PEO and the α phase are shown in Fig. 67. It is evident from the figure that several intense peaks from each of the aforementioned phases do not overlap with each other, permitting identification of non-reacted starting materials.
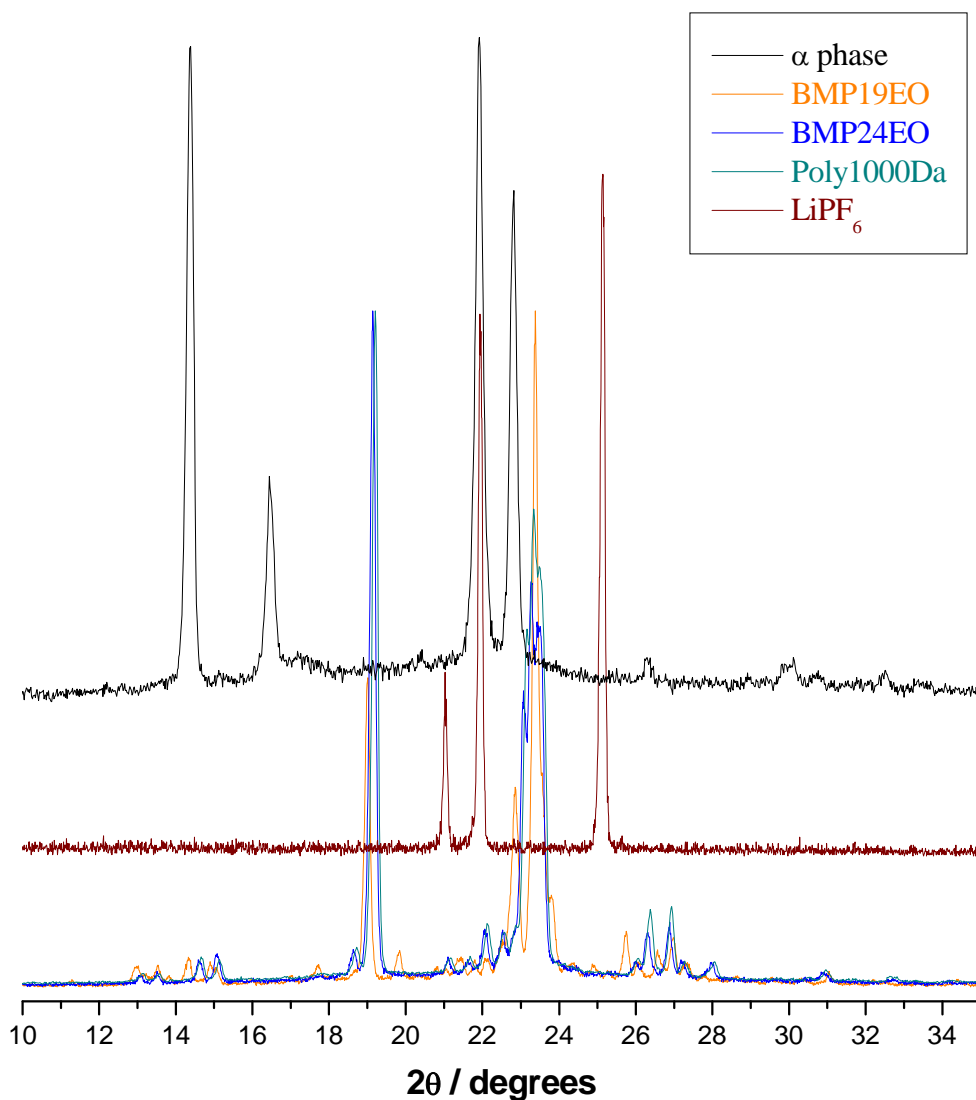


Fig. 67 PXRD data of α phase (black); LiPF$_6$ (wine); dimethoxy PEO <Mw> = 1000 Da (dark cyan); and 2 examples of monodispersed dimethoxy PEO: 19 EO (orange) and 24 EO (blue).

The subtle differences in the PXRD patterns amongst the different grades of PEOs (see Fig. 67) are not surprising. Analysis of the previously reported and our, monodispersed PEO, confirms that the structures are similar but not identical. Modelling study of poly(ethylene oxide) reported in 1964 suggested that each individual chain is a (7/2) helix

with symmetry isomorphous to the point group $D_7$ (Fig. 68a).[8] The study relied on a combination of the infrared absorption and X-ray diffraction methods. The crystal structure could not be established in detail at the time and only a later study, from 1973, revealed the coordinates of atoms in Polyox WSR-301, <Mw> = 4,000,000 Da PEO (Fig. 68b).[9] As clearly seen from the top views in Fig. 68a, b, the 1973 model is less "ideal" and markedly different from the first reported model[9].
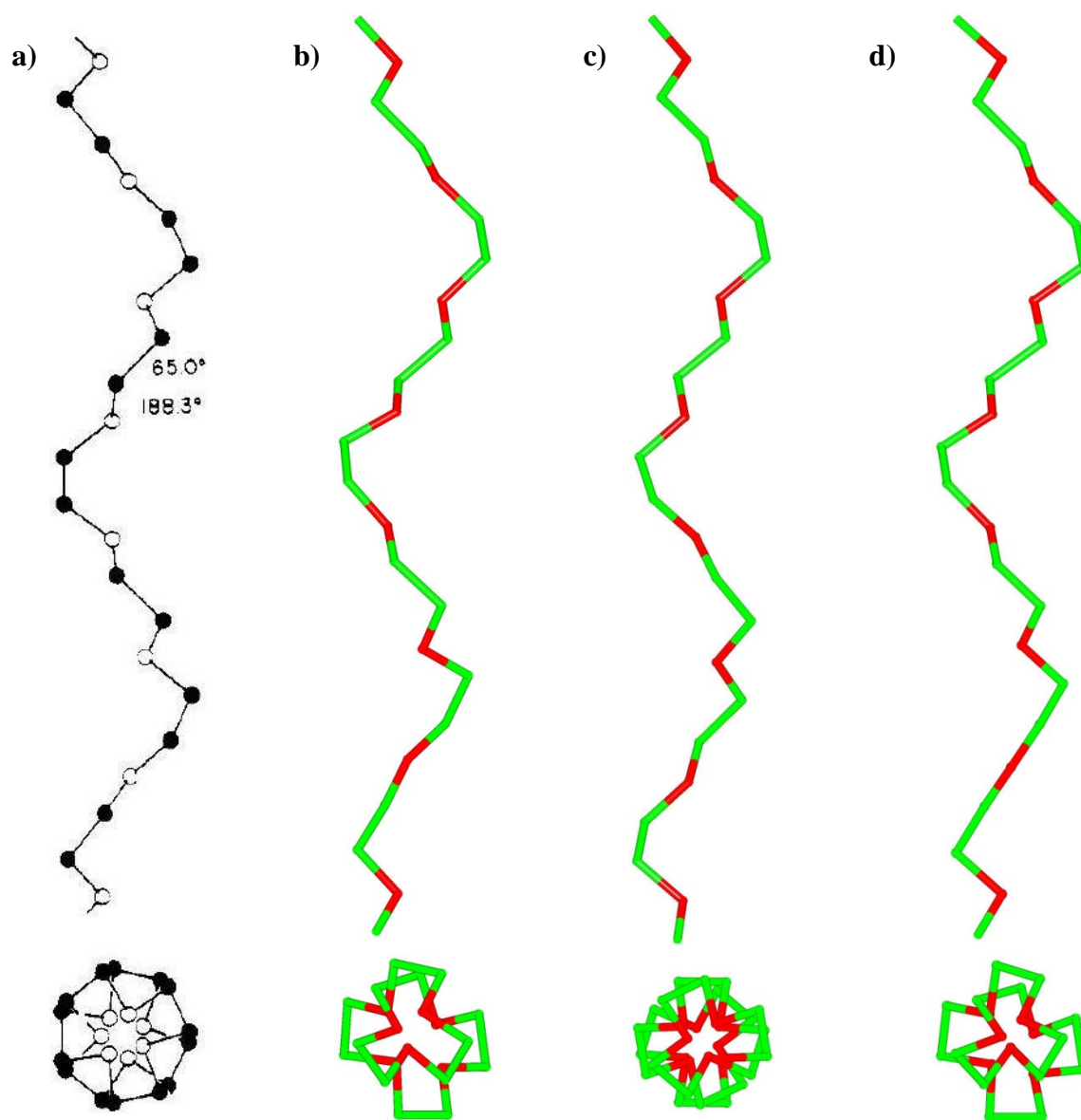


Fig. 68 Conformation of individual PEO chains (top – side view; bottom – top view): (a) IR-XRD model (7/2) helix;[8] (b) molecular structure of Polyox WSR-301, <Mw> = 4,000,000 Da;[9] (c) monodispersed 16EO monomethyl ether (PEG$_{16}$), Mw = 736.88 Da;[10] (d) monodispersed 19EO dimethyl ether (BMP19EO), Mw = 883.07 Da.[This study]

| atom sequence | torsion angles | | |
|---|---|---|---|
| | Polyox WSR-301, **b)** | PEG$_{16}$, **c)** | BMP19EO, **d)** |
| C14-O1-C1-C2 | 179.689 | -176.813 | -174.443 |
| O1-C1-C2-O2 | 60.019 | 74.523 | 71.950 |
| C1-C2-O2-C3 | -177.920 | -175.780 | 178.249 |
| C2-O2-C3-C4 | -169.312 | -179.628 | -174.750 |
| O2-C3-C4-O3 | 79.484 | 75.379 | 72.651 |
| C3-C4-O3-C5 | 178.368 | 179.866 | 174.432 |
| C4-O3-C5-C6 | 177.557 | 179.866 | -176.311 |
| O3-C5-C6-O4 | 57.100 | 75.379 | 70.565 |
| C5-C6-O4-C7 | -166.194 | -179.628 | -172.839 |
| C6-O4-C7-C8 | -171.289 | -175.780 | -175.700 |
| O4-C7-C8-O5 | 67.406 | 74.523 | 66.959 |
| C7-C8-O5-C9 | -176.870 | -176.813 | -179.812 |
| C8-O5-C9-C10 | 174.429 | -168.735 | 179.935 |
| O5-C9-C10-O6 | 73.823 | 81.924 | 70.053 |
| C9-C10-O6-C11 | -154.968 | -168.735 | -174.859 |
| C10-O6-C11-C12 | -177.375 | -176.813 | -175.770 |
| O6 -C11-C12-O7 | 48.365 | 74.523 | 79.795 |
| C11-C12-O7-C13 | 179.967 | -175.780 | -176.500 |
| C12-O7-C13-C14' | -165.859 | -179.628 | -177.608 |
| O7-C13-C14'-O1' | 92.642 | 75.379 | 78.728 |
| C13-C14'-O1'-C1' | -173.989 | 179.866 | -172.655 |

Table 11 Torsion angles of structures b, c and d from Fig. 68.

In a 2009 publication entitled "*High-Purity Discrete PEG-Oligomer Crystals Allow Structural Insight.*" *Davis et al* stated: "*exquisite purities allowed the first crystallizations of PEGs, which in turn allowed the formation of diffracting single crystals. Single-crystal X-ray diffraction experiments on these gave the first indication of the 3D structure and also a unique insight into an extended helical secondary structure of PEGs*".[10] The authors reported the structure of a monodispersed 16EO monomethyl ether, Mw = 737 Da, (Fig. 68c). 19, 21 and 24 EO dimethyl ethers, synthesised in the course of this work, also formed sizeable single crystals, whose structures were determined using laboratory single crystal diffraction. All three structures are practically identical to each other, thus a detailed description is provided only for the 19EO dimethyl ether (BMP19EO) (Fig. 68d). As evident from both Fig. 68 and the list of torsion angles  (Table 11), the established chain conformation is similar to that in the originally reported structure (Fig. 68b) but very different from the one reported by *Davis et al* (Fig. 68c). Differences in Mw and/or in the end groups could be a possible explanation.

### 5.2. Preparation procedure

All polymer electrolyte materials were prepared in a MBraun argon filled glove box, due to the air/moisture sensitive nature of the starting materials and the final product. $LiPF_6$, Stella SC Chemifa, 99.99%, used as received and a dimethoxy endcapped poly(ethylene oxide) was dried at temperature close to the melting point under dynamic vacuum for 3 days. Appropriate for the formation of a 6:1 complex (ether oxygen to salt ratio) amounts of the salt and polymer were dissolved separately in either dry acetonitrile (Sigma-Aldrich, 99.8%, anhydrous, stored over 4Å molecular sieves) or dry methanol (Sigma-Aldrich, 99.8%, anhydrous, stored over 4Å molecular sieves) and, following complete dissolution, mixed together. The solvent was then evaporated slowly. The resulting white powders were dried overnight under dynamic vacuum at room temperature. FTIR spectroscopy and $^1$H NMR confirmed the absence of $H_2O$, MeCN and MeOH in the resulting powders. The target phase composition was confirmed by PXRD and DSC.

### 5.3. α phase with monodispersed PEO

The above procedure for preparation of complexes was applied to obtain the α phase of the PEO:salt complexes. All but 1 of the monodispersed polymers studied in this work, formed pure α phase. Trace amount of an unknown crystalline phase was found in the complex made with BMP19EO, twenty ether oxygens ($N_O = 20$).

#### 5.3.1.  PXRD of monodispersed complexes

PXRD patterns of the complexes are shown in Fig. 69. Following the models discussed in chapter 1.4.2, they can be divided into 3 different groups depending on the number of ether oxygens, $N_O$, in the polymeric chains, i.e. *(3n-1)*, *3n*, *(3n+1)*, where *n* is an integer. The complex made with BMP19EO ($N_O = 20$), Fig. 69 (orange), shows additional peaks which do not belong to the α phase (e.g. at 13.480° or 15.395°, *2θ*). Those peaks do not belong to pure polymer or salt either, suggesting another crystalline phase, different from α.
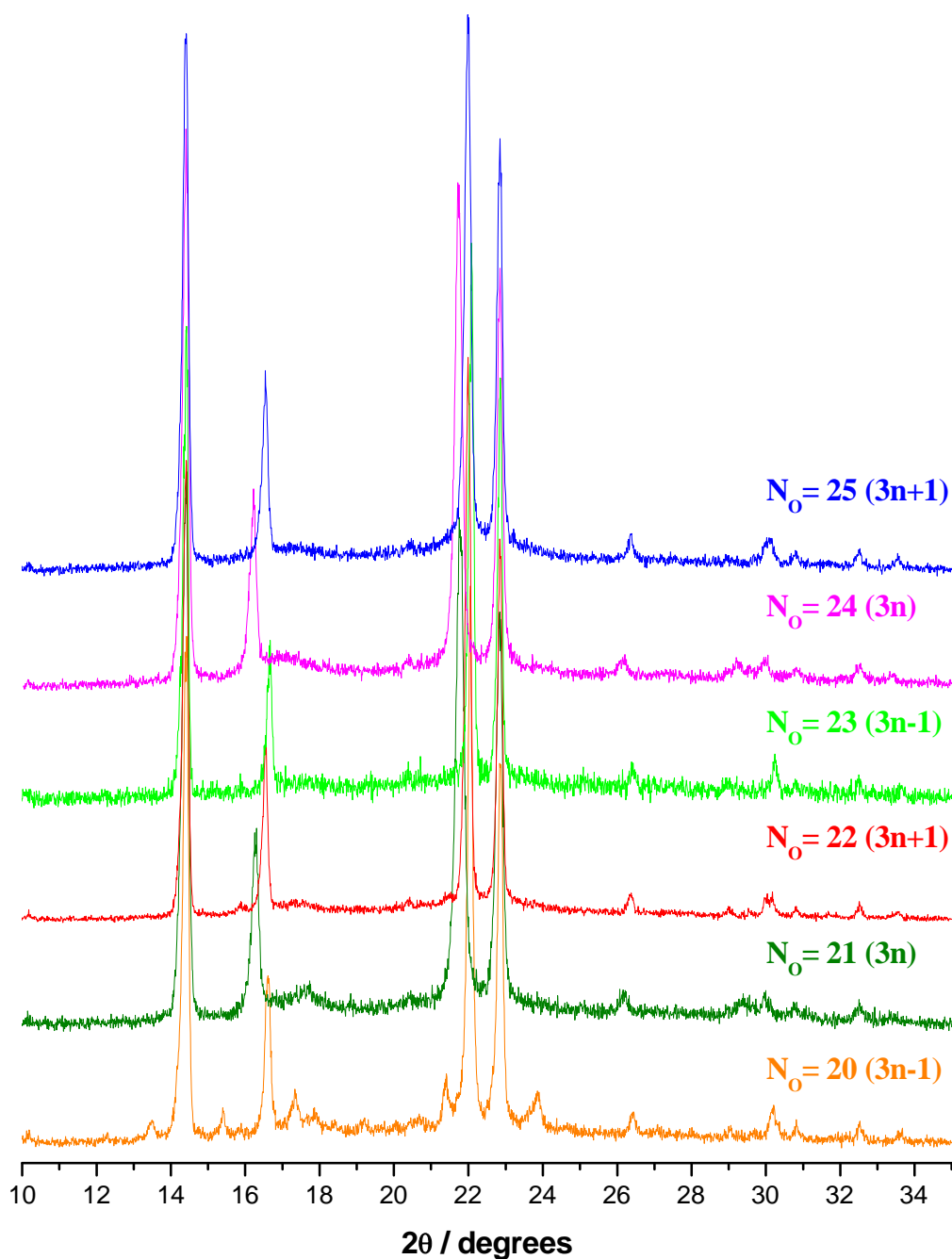
Fig. 69 PXRD patterns 6:1 complexes prepared with monodispersed PEOs.

In 2007 *Bruce et al* reported a single example of the α phase polymer electrolyte, prepared with a monodispersed PEO containing 22 EO units ($N_O = 23$) and $LiPF_6$.[11] Corresponding PXRD pattern revealed peak shifts, when compared to the pattern of the complex prepared with polydispersed PEO of the same average Mw. Shifts of the same diffraction peaks have been observed in all monodispersed complexes studied in this work.

103

When $N_O = 3n+1$ or $3n-1$ the shifts are positive (higher $2\theta$), in agreement with the original report[11]. However, in complexes with $N_O = 3n$ the same peaks are clearly shifted to lower $2\theta$ angles.
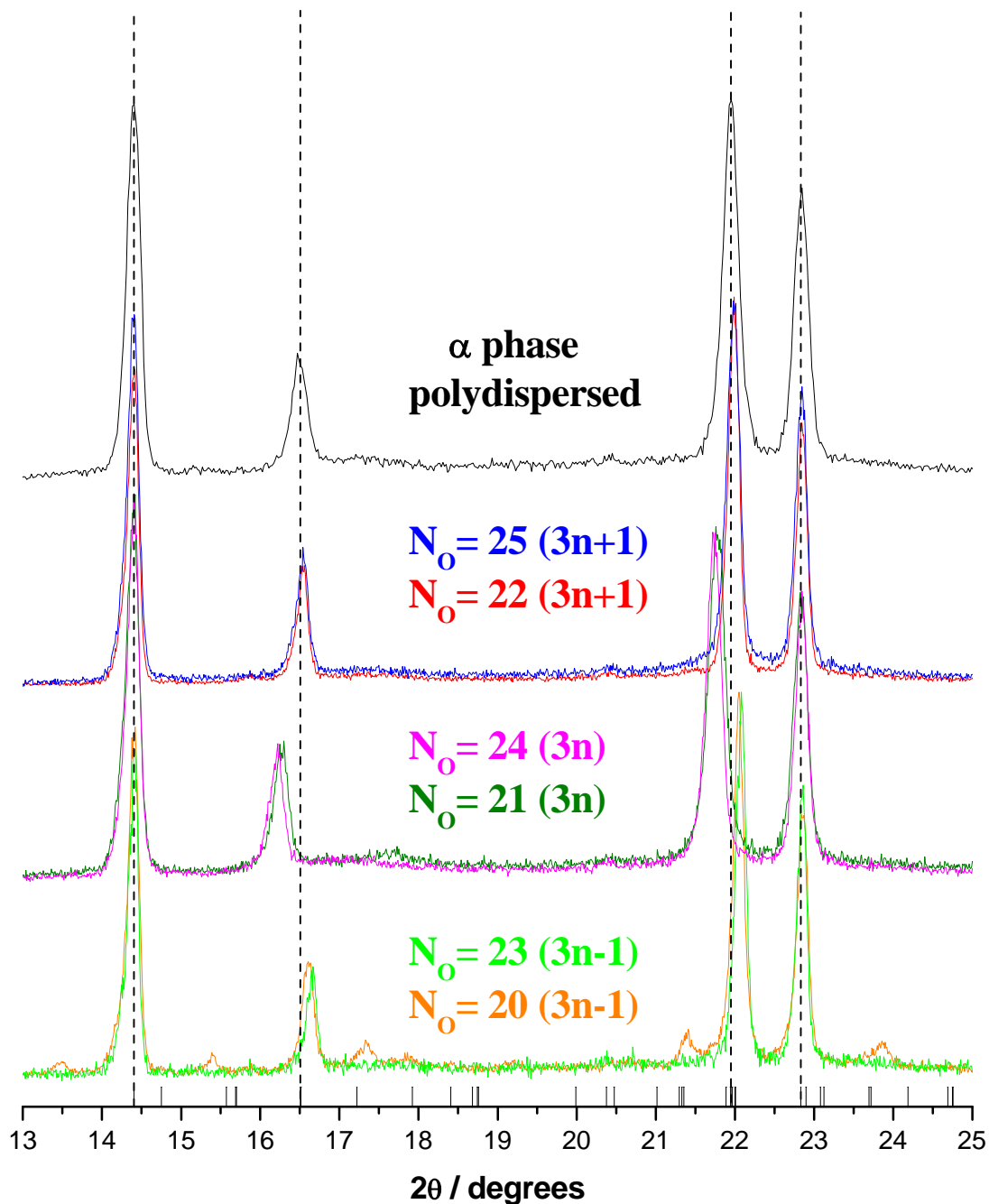


Fig. 70 PXRD patterns 6:1 complexes prepared with mono- and polydispersed PEO. See text for further details.

The shifts are caused by changes in the lattice parameters. Analysis of Miller indices reveals that shifts to the higher $2\theta$ angles are caused by contraction of the $a$ lattice parameter and expansion of $b$. The $a$ lattice parameter lies along the axis of the polymer tunnels.[11] Thus the tunnels in complexes made with PEOs of $N_O = 3n$ are expanded in length, while in both $N_O = 3n+1$ and $N_O = 3n-1$ the tunnels are contracted ($3n-1$ shows the most significant contraction), compared to the polydispersed material. Since the number of chain ends is very close in the 1000 Da poly- and monodispersed materials, such changes must reflect differences in the distribution of the polymer chain ends. Irregular arrangement of the chain ends along PEO tunnels (each of which is formed by 2 PEO chains as described in chapter 1.4.2) does not explain the change in the dimensions of a tunnel, but coincidence of the chain ends along both strands of the tunnels could. The widths of the peaks in all the PXRD patterns shown in Fig. 70 are practically the same, indicating no reduction in the crystallite size in complexes prepared with monodispersed polymers. This rules out coincidence of the chain ends in neighbouring tunnels, as the canting, and hence reduction in size of coherently scattering regions, does not occur (see chapter 1.4.2, Fig. 10). Thus PXRD suggest an arrangement in which the chain ends are in registry within each individual tunnel but there is no registry between the tunnels.

Let us now discuss possible arrangements of the coincident chain ends in the monodispersed complexes with respect to ions. As discussed in chapter 1.4.2, the "ideal" coordination (no disruption of the polymer chains involved in the 6-fold coordination sphere of a $Li^+$ ion) is possible only when the number of ether oxygen atoms in the polymeric chains is a multiple of 3 ($N_O = 3n$) (Fig. 71a). However, the $N_O = 3n$ complex could also adapt "broken" coordination leading to a "broken" 6-fold coordination spheres of a $Li^+$ ion throughout the structure (Fig. 71b).

The arrangement of chain ends in monodispersed complexes in which $N_O \neq 3n$ differs significantly. No matter what the arrangement is at any end of a tunnel, there will always be exactly the same number of "ideal" and "broken" ends across each crystallite. Moreover, this equally applies to both $N_O = 3n+1$ and $N_O = 3n-1$ complexes (Fig. 71c,d) and is in agreement with the trends in PXRD patterns, since the peaks in both cases are shifted in the same direction by a very similar margin, Fig. 70.

Since the presence of the same number of "broken" and "ideal" coordinations leads to contraction of the direction of a ($3n\pm1$ complexes), the expansion along the tunnel axis in $3n$ complexes can only be explained by an excess of one type of coordination.
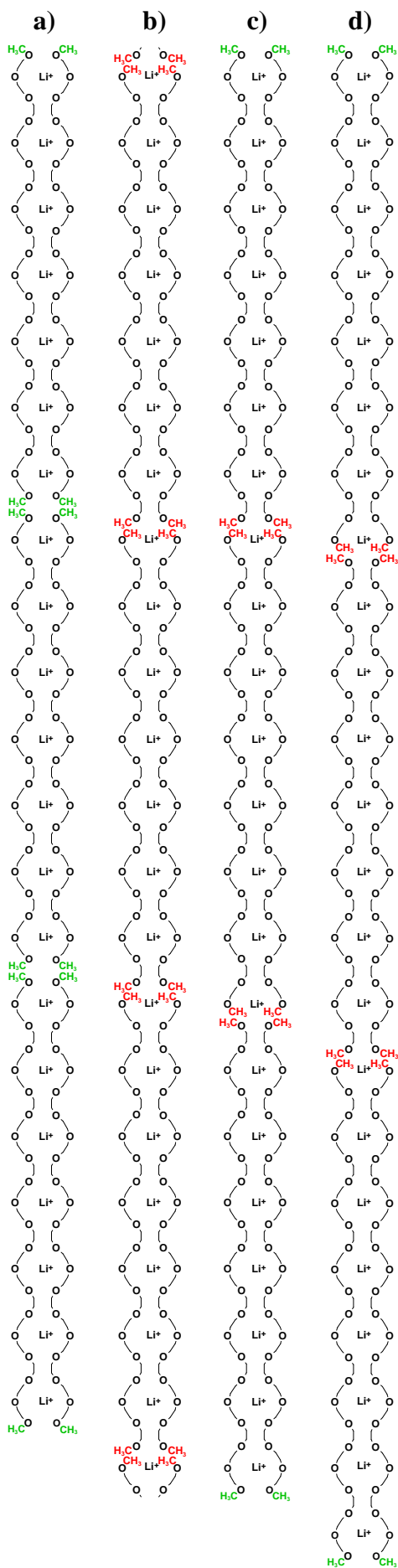
Fig. 71 Possible arrangements of the chain ends in the monodispersed complexes. Every oxygen atom is involved in coordination:

a) "all-ideal" coordination, $N_O = 21$ ($3n$),
b) "all-broken" coordination, $N_O = 21$ ($3n$),
c) 2/3 "broken" and 1/3 "ideal" coordination, $N_O = 22$ ($3n+1$),
d) 2/3 "broken" and 1/3 "ideal" coordination, $N_O = 23$ ($3n-1$),

In accordance with the crystal structure of 6:1 complexes established for infinite chains (the unit cell size is smaller than the size of individual chain), the models presented in Fig. 71 are drawn with every single oxygen atom involved in the formation of 6-fold coordination environment for each $Li^+$ ion. This assumption can be justified by the fact that the complexes are prepared in exactly 6:1 ratio and no free salt or polymer are detected by means of PXRD or DSC. However, one could envisage a situation in which every tunnel starts from "ideal" coordination (Fig. 72). This would imply that at the chain ends $Li^+$ ions are coordinated by either 4 ether oxygens in the case of $N_O = 3n\text{-}1$ complexes or 2 ether oxygens in the case of $N_O = 3n\text{+}1$. As a result, anions will have to be involved in coordination as well (Fig. 72b,c), because otherwise if there is a $Li^+$ vacancy, ~5% of the mass of the complex will be in a salt phase, which falls within the detection limits of both DSC and PXRD. In the majority of crystalline PEO/salt structures anions are involved in $Li^+$ coordination.[12,13] However, here such arrangement at the chain ends is very unlikely, because for the polymers from the studied series e.g. $N_O = 23$ or $N_O = 22$, 4 % or 8 % of the polymer respectively would have to be non-coordinating. That gives 2.6 % and 5.3 % of the mass of respective complexes which, most likely, would be detected by the DSC, and possibly by PXRD – which is not the case. Furthermore, anions involvement in coordination at the chain ends may well introduce a superstructural ordering. Let us also not forget that the polymer/salt ratio was maintained at 6:1 during syntheses of the complexes. Thus the models with even more free polymer should not be considered.
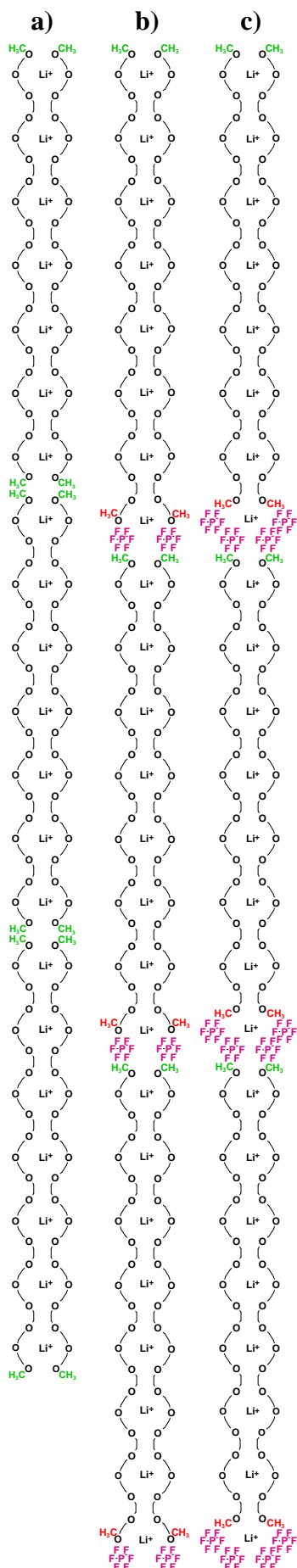
Fig. 72 Possible arrangements of the chain ends in the monodispersed complexes. Every tunnel starts from "ideal" coordination:

a) "all-ideal" coordination, $N_O = 21$ ($3n$),
b) $N_O = 22$ ($3n+1$), 2 anions involved in coordination at the every chain end resulting in 2.6 % of free polymer left in the material,
c) $N_O = 23$ ($3n-1$), 4 anions involved in coordination at the every chain end resulting in 5.3 % of free polymer left in the material.

### 5.3.2. Thermal properties of monodispersed complexes

The formation of pure α phase in all complexes has been confirmed by DSC measurements. DSC traces for all the complexes are shown in Fig. 73. A single endotherm corresponding to melting of the α phase is observed at 87.1°C for the complex produced with the polydispersed PEO Mw = 1000 Da. Single endothermic peaks are also present in the DSC traces of the complexes made with PEO of $N_O = 21$ (*m.p.* = 80.7°C) and $N_O = 24$ (*m.p.* = 83.1°C). For all other $N_O$ values two prominent endotherms are observed. Since PXRD data collected at room temperature indicates the presence of α phase only, for $N_O = 22$, $N_O = 23$ and $N_O = 25$ the lowest temperature endotherm in Fig. 73 is associated with the transition of the α phase into another crystalline phase.

A mixture of 2 phases (α and unknown) was observed in room-temperature PXRD pattern for the complex made with BMP19EO, $N_O = 20$, suggesting that either of the observed endotherms (71.1°C and 79.6°C) can be associated with melting or transition of the α phase.
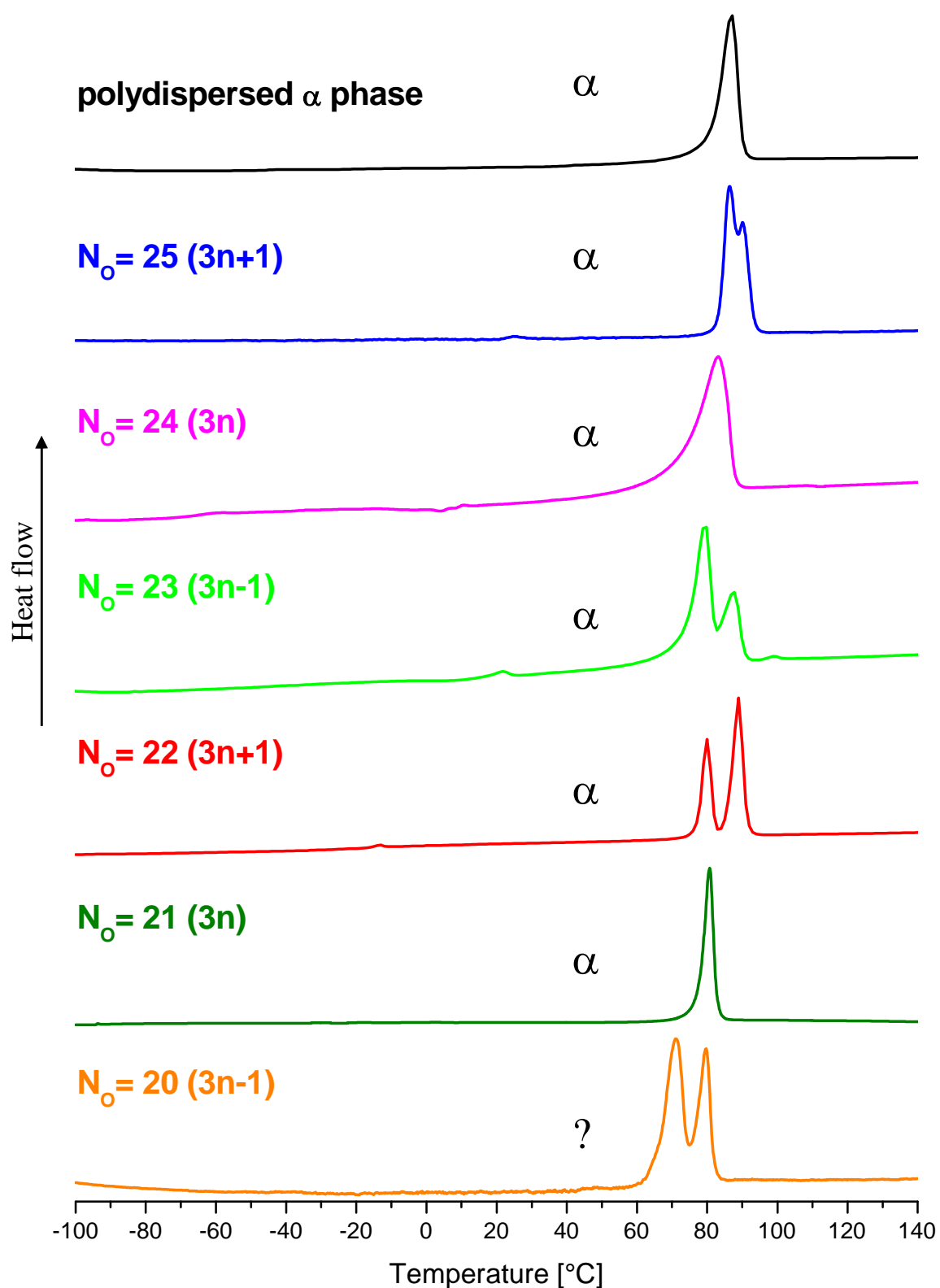
Fig. 73 DSC heating curves of the set of poly- and monodispersed complexes. The endotherms associated with the $\alpha$ phase melting or transition to other, unknown phases.

### 5.3.3. Conductivity of monodispersed complexes

Temperature dependent AC impedance measurements were carried out for all the monodispersed complexes, with the exception of the mixed-phase BMP19EO ($N_O = 20$) complex. The upper temperature limit for the measurements was selected at the onset of the melting or phase-transition temperature for each complex. No reliable data could be collected for the two most resistive complexes ($N_O = 21$ and $N_O = 25$). The conductivity data as a function of temperature along with the respective activation energies are shown in Fig. 74.
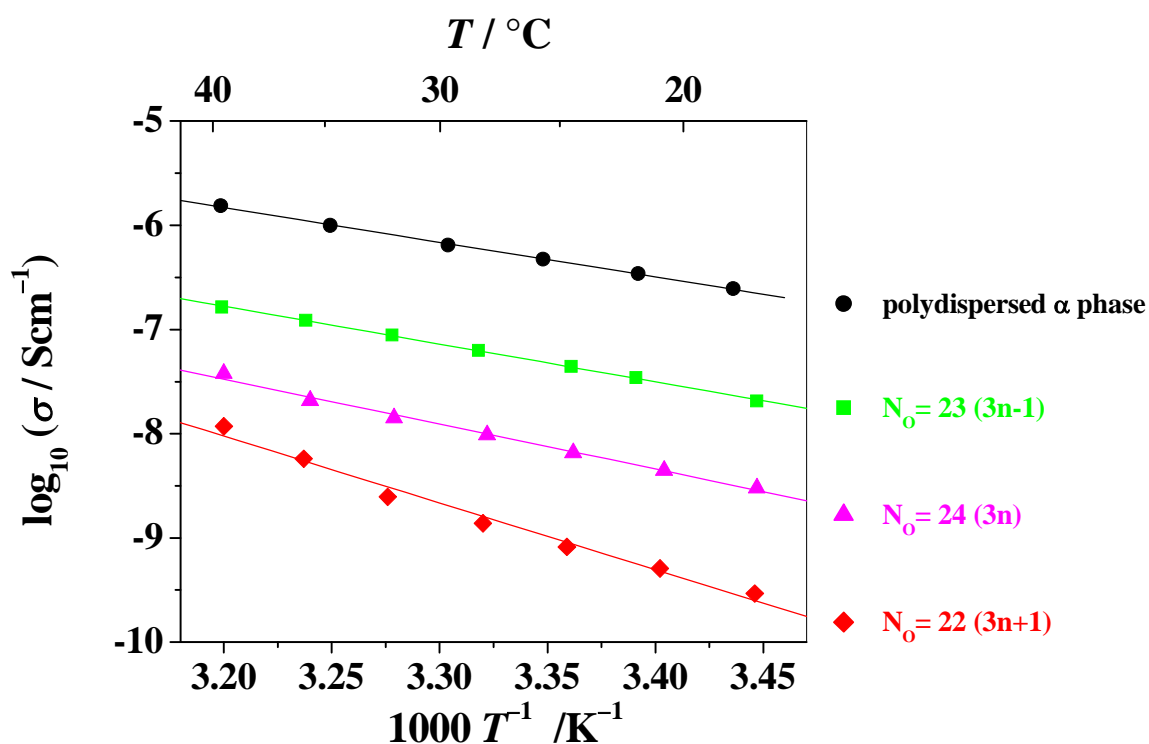


| Number of ether oxygens $N_O$ | Activation energy $E_a$ [eV] |
|---|---|
| polydispersed | 0.66 |
| 22 | 1.28 |
| 23 | 0.72 |
| 24 | 0.86 |

Fig. 74 Conductivity data of poly- and monodispersed 6:1 complexes. Activation energy of each complex is shown in the table.

The ionic conductivity of all monodispersed complexes studied in this work is significantly lower than that of the polydispersed material, which is in agreement with the suggested in ref. 11 dependence of conductivity on the density of the chain-ends. Also the activation energies follow the trend in conductivity, i.e. the higher is the conductivity the lower is the activation energy.

However, further investigation is required in order to explain the dependence of conductivity on the number of ether oxygens ($N_O$) in the monodispersed complexes. It is unclear why the conductivities of the $N_O = 3n-1$ and $N_O = 3n+1$ complexes differ by $1 - 2$ orders of magnitude when, the seemingly plausible, models of the chain-end arrangement appear to be identical. Perhaps other analytical techniques, solid state nuclear magnetic resonance (SSNMR) in particular, will provide more detailed information on mobility of particular species in the complexes and interactions between them, which, in its turn, will explain the trend in conductivity.

Only very high purity (as claimed by suppliers and/or verified by our synthetic and purification methods) starting materials were used in an inert environment (Ar atmosphere) to synthesise the complexes in this study. However, the purity of $LiPF_6$ is notoriously difficult to control because of the inherent instability of the salt, leading to evolution of HF, especially at elevated temperatures[7] and in the presence of even trace amounts of water[14]. Considering the generally low conductivity of the monodispersed complexes, even minimal decomposition of $LiPF_6$ could affect the results. SSNMR should still be able to selectively probe the mobility of the moieties, and is likely to provide information about the diffusion of $Li^+$ and $PF_6^-$ ions. Such decoupling from the possible influence of HF may well alter the trends revealed by the AC impedance measurements and aid our understanding of the mechanism of conductivity in the crystalline PEO/salt complexes.

# References

1. J. R. MacCallum, C. A. Vincent, *Polymer electrolyte reviews vol. 1*, Elsevier, London, **1987**.

2. A. Johansson, J. Tegenfeldt, *NMR Study of Crystalline and Amorphous Poly(ethylene oxide).* Macromolecules, 1992, **25**(18): p. 4712-4715.

3. J. E. Mark, *Polymer data handbook*, Oxford University Press, New York, **1999**.

4. J. A. Faucher, J. V. Koleske, J. E. R. Santee, J. J. Stratta, C. W. Wilson Iii, *Glass Transitions of Ethylene Oxide Polymers.* Journal of Applied Physics, 1966, **37**(11): p. 3962-3964.

5. V. P. Privalko, A. P. Lobodina, *Glass transition in the lower homologues of polyethyleneoxide.* European Polymer Journal, 1974, **10**(11): p. 1033-1038.

6. P. Törmälä, *Determination of glass transition temperature of poly(ethylene glycol) by spin probe technique.* European Polymer Journal, 1974, **10**(6): p. 519-521.

7. E. Zinigrad, L. Larush-Asraf, J. S. Gnanaraj, M. Sprecher, D. Aurbach, *On the thermal stability of LiPF6.* Thermochimica Acta, 2005, **438**(1–2): p. 184-191.

8. H. Tadokoro, Y. Chatani, T. Yoshihara, S. Tahara, S. Murahashi, *Structural studies on polyethers, [-(CH2)m-O-]n. II. Molecular structure of polyethylene oxide.* Die Makromolekulare Chemie, 1964, **73**(1): p. 109-127.

9. Y. Takahashi, H. Tadokoro, *Structural Studies of Polyethers, (-(CH2)m-O-)n. X. Crystal Structure of Poly(ethylene oxide).* Macromolecules, 1973, **6**(5): p. 672-675.

10. A. C. French, A. L. Thompson, B. G. Davis, *High-Purity Discrete PEG-Oligomer Crystals Allow Structural Insight.* Angewandte Chemie-International Edition, 2009, **48**(7): p. 1248-1252.

11. E. Staunton, Y. G. Andreev, P. G. Bruce, *Factors influencing the conductivity of crystalline polymer electrolytes.* Faraday Discussions, 2007, **134**: p. 143-156.

12. P. Lightfoot, M. A. Mehta, P. G. Bruce, *Crystal Structure of the Polymer Electrolyte Poly(ethylene oxide)3:LiCF3SO3.* Science, 1993, **262**(5135): p. 883-885.

13. C. Zhang, D. Ainsworth, Y. G. Andreev, P. G. Bruce, *Ionic conductivity in the solid glyme complexes CH3O(CH2CH2O)(n)CH3 : LiAsF6 (n=3,4).* Journal of the American Chemical Society, 2007, **129**(28): p. 8700-+.

14. A. M. Andersson, K. Edstrom, *Chemical composition and morphology of the elevated temperature SEI on graphite.* Journal of the Electrochemical Society, 2001, **148**(10): p. A1100-A1109.

## 6. CONCLUSIONS

- Development and optimisation of the synthesis conditions yielded monodispersed PEOs with the highest ever purity of chain lengths (>95%). A combination of several characterisation methodologies (NMR, MALDI, GPC, etc.) used in this work, provides correct assessment of purity.

- All 6 complexes ($N_O$ = 20, 21, 22, 23, 24, 25) formed with monodispersed PEOs and $LiPF_6$ in 6:1 ratio of ether oxygens to lithium in each case are purely crystalline. All but 1 of these complexes crystallise in the desired α phase, as proven by both PXRD and DSC.

- The number of ether oxygens in individual PEO chains ($N_O$) has a pronounced effect on the unit cell sizes which, together with the crystallite sizes, support the previously suggested coincidence of the chain ends within the polymer tunnels, but not between the tunnels.

- Several possible arrangements of the chain ends in monodispersed complexes of different $N_O$ have been discussed and in the most likely model all oxygen atoms are involved in creation of coordination environment, while anions remain outside the tunnels and ion-pairing is unlikely. The complexes containing $N_O = 3n$, can either adapt "all-ideal" or "all-broken" coordination at the chain ends, while both $N_O = 3n\text{-}1$ and $N_O = 3n\text{+}1$ complexes always have both "ideal" and "broken" environments at exact ratio 1:2.

- All 5 α-phase monodispersed complexes are ionically conducting, however $N_O = 21$ and $N_O = 25$ are highly resistive. The temperature dependent conductivity supports the ion hopping mechanism and there is a clear dependence between the conductivity and activation energy – the higher the conductivity, the lower the activation energy.

- All monodispersed complexes conduct significantly worse than the complex made with polydispersed PEO of the same average molecular weight which is likely to be due to fewer chain-end occurrences. More investigation is required for the dependence of conductivity on the number of ether oxygens in the PEO chains or modelled arrangements of the chain ends. Solid state NMR could provide deeper insight into the motions of species and thereby the mechanism of conductivity. It is known that $LiPF_6$ salt may be unstable, creating impurities (mainly HF) which could affect intrinsically low conductivities of the monodispersed complexes. SSNMR

would be helpful again because it can selectively monitor the mobility of different species.

- The complexes prepared with monodispersed PEO are the most promising candidate test samples for establishing the detailed mechanism of ionic conductivity in crystalline polymer electrolytes.

**Symbols and abbreviations used**

| | |
|---|---|
| $A$ | - cross section area of electrolyte |
| AC | - alternating current |
| BBP$x$EO | - bisbenzyl protected $x$-(ethylene glycol) |
| BMP$x$EO | - bismethyl protected $x$-(ethylene glycol) |
| Bn- | - benzyl- group |
| BnBr | - benzyl bromide |
| CHNX | - elemental analysis (carbon, hydrogen, nitrogen, unknown element) |
| $C$ | - specific heat capacity |
| $C_p$ | - heat capacity |
| CV | - column volume |
| DC | - direct current |
| DI water | - deionised water |
| DCM | - dichloromethane |
| DMF | - dimethylformamide |
| DSC | - differential scanning calorimetry |
| EC | - ethylene carbonate |
| EDX | - energy-dispersive X-ray spectroscopy |
| EG | - ethylene glycol |
| $EO$ | - repeat unit of PEO |
| ESI | - electrospray ionization |
| EtOAc | - ethyl acetate |
| EtOH | - ethanol |
| FTIR | - Fourier transform infrared spectroscopy |
| $\Delta G$ | - Gibbs free energy change |
| G4 | - tetraglyme, tetra(ethylene glycol) dimethyl ether |

| | |
|---|---|
| GPC | - gel permeation chromatography |
| $\Delta H$ | - enthalpy change |
| HSAB | - hard soft acid base |
| $I$ | - current |
| imp1 | - impurity 1 |
| imp2 | - impurity 2 |
| IR-XRD | - combination of infrared spectroscopy and X-ray diffraction |
| KOtBu | - potassium tert-butoxide |
| $l$ | - distance between electrodes |
| LiTFSI | - lithium bis-trifluoromethanesulfonimide |
| MALDI | - matrix-assisted laser desorption/ionization |
| MBP$x$EO | - monobenzyl protected $x$-(ethylene glycol) |
| MBP$x$EOTos | - monobenzyl-protected $x$-(ethylene glycol) tosylate |
| MeCN | - acetonitrile |
| MeOH | - methanol |
| MMP$x$EO | - monomethyl protected $x$-(ethylene glycol) |
| MS | - mass spectrometry |
| Ms | - mesyl- group |
| Mw | - molecular weight |
| <Mw> | - average molecular weight |
| NMR | - nuclear magnetic resonance |
| PDI | - polydispersity index |
| PEG or PEO | - poly(ethylene glycol) or poly(ethylene oxide) |
| PEI | - poly(ethylene imine) |
| $Ph_3C$ | - monotrityl- group |
| $PhCH_2Cl$ | - benzyl chloride |
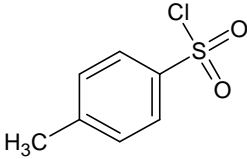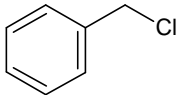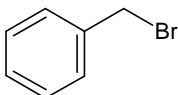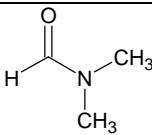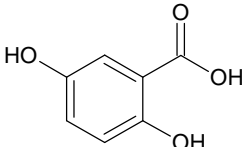
117

| | |
|---|---|
| PVIC | - poly(vinylene carbonate) |
| PVICOX | - poly((1,3-dioxolan-2-one-4,5-diyl oxalate) |
| PSD | - position sensitive detector |
| PTFE | - polytetrafluoroethylene |
| PXRD | - powder X-ray diffraction |
| $Q$ | - heat |
| $R_b$ | - resistance of electrolyte |
| $R_f$ | - retention factor |
| r.t. | - room temperature |
| $\Delta S$ | - entropy change |
| SEC | - size exclusion chromatography |
| SEM | - scanning electron microscope |
| $t$-Bu | - $tert$-butyl group |
| TFSI | - bis(trifluoromethane)sulfonimide, $[(CF_3SO_2)_2N]^-$ |
| $T$ | - temperature |
| $t$ | - time |
| $t_+$ | - cation transport number |
| $T_g$ | - glass transition temperature |
| THF | - tetrahydrofuran |
| THP | - monotetrahydropyranyl- group |
| TLC | - thin layer chromatography |
| TMS | - tetramethylsilane |
| TOF | - time of flight |
| Ts | - tosyl- group |
| TsCl | - tosyl chloride |
| $V$ | - potential |

| | |
|---|---|
| VTF | - Vogel-Tamman-Fulchar |
| $x$EO | - $x$-ethylene glycol |
| $x$ | - number of repeating units |
| $Y$ | - admittance |
| $Z$ | - impedance |
| $\sigma$ | - specific conductivity |
| $\varepsilon$ | - relative dielectric constant |
| $\varepsilon_0$ | - vacuum permittivity |

## Supplementary information

Reagents used during the syntheses of polymers:

| Name grade | structure/formula | Supplier | Product code | Purity/ concentration |
|---|---|---|---|---|
| **Triethylene glycol** puriss., anhydrous | $H(OCH_2CH_2)_3OH$ | Fluka | 90390 | ≥99.0% (GC) |
| **Tetraethylene glycol** | $H(OCH_2CH_2)_4OH$ | Acros Organics | 14959-0010 | 99.5% |
| **Pentaethylene glycol** | $H(OCH_2CH_2)_5OH$ | Aldrich | 335754 | 98% |
| **Hexaethylene glycol** | $H(OCH_2CH_2)_6OH$ | Aldrich | 259268 | 97% |
| **Diethylene glycol methyl ether** | $CH_3(OCH_2CH_2)_2OH$ | Sigma-Aldrich | 579548 | ≥99.0% |
| **p-Toluenesulfonyl chloride (p-TsCl)** ReagentPlus, |  | Sigma-Aldrich | 240877 | ≥99% |
| **Benzyl chloride** puriss., |  | Fluka | 13270 | ≥99.5% |
| **Benzyl bromide** reagent grade, |  | Sigma-Aldrich | B17905 | 98% |
| **Tetrahydrofuran** unstabilised |  | Fisher Scientific | T/0706/PB17 | 99.8+% (GLC) |
| **Chloroform** CHROMASOLV Plus, for HPLC, contains 0.5-1.0% ethanol as stabilizer | $CHCl_3$ | Sigma-Aldrich | 650471 | ≥99.9% |
| **Methanol** CertiFied AR | $CH_3OH$ | Fisher Scientific | M/4000/17 | 99.9+% (GLC) |
| **Ethanol** absolute AnalaR NORMAPUR | $C_2H_5OH$ | VWR | 20821.330 | 99.8% |
| **N,N-Dimethylformamide (DMF)** CHROMASOLV Plus, for HPLC |  | Aldrich | 270547 | ≥99.9% |
| **Dichloromethane (DCM)** puriss. | $CH_2Cl_2$ | Sigma-Aldrich | 24233 | ≥99% (GC) |
| **Iodomethane** purum | $CH_3I$ | Sigma-Aldrich | 67692 | ≥99.0% (GC) |
| **Acetone** CertiFied AR | $CH_3COCH_3$ | Fisher Scientific | A/0600/17 | 99.8+% (GLC) |
| **Chloroform-d** | $CDCl_3$ | Aldrich | 151823 | 99.8 atom % D |
| **2,5-Dihydroxybenzoic acid (DHBA** or **DHB)** |  | Aldrich | 149357 | 98% |
| **Potassium tert-butoxide (KOtBu)** | $(CH_3)_3COK$ | Aldrich | 60098 | ≥97.0% (T) |

| Palladium on carbon extent of labelling: 5 wt. % loading (dry basis), matrix activated carbon support | Pd/C | Aldrich | 205680 | 5% |
|---|---|---|---|---|
| **Palladium on carbon** extent of labelling: 10 wt. % loading (dry basis), matrix activated carbon support | Pd/C | Aldrich | 205699 | 10% |
| **Hydrochloric acid** CertiFied AR | HCl | Fisher Scientific | H/1200/PB17 | 35.5-37.5% |
| **High Purity Hydrogen** | $H_2$ | BOC | | 99.995+% |
| **Silica gel** Geduran Si 60 | $SiO_2$ | VWR | 1.11567.9025 | |
| **Sodium hydride** dry | NaH | Aldrich | 223441 | 95% |
| **Sodium carbonate** anhydrous (dried) | $Na_2CO_3$ | Fisher Scientific | S/2880/53 | 99.5+% |
| **Sodium chloride** (dried) | NaCl | Fisher Scientific | S/3120/60 | 99.5+% |
| **Sodium hydroxide** CertiFied AR | NaOH | Fisher Scientific | S/4920/53 | 98+% |
| **Sodium sulfate** anhydrous | $Na_2SO_4$ | Fisher Scientific | S/6600/60 | 99+% |
| **Silver (I) nitrate** CertiFied AR | $AgNO_3$ | Fisher Scientific | S/1280/46 | 99.9+% |
| **Potassium iodide** CertiFied AR (dried) | KI | Fisher Scientific | P/5880/50 | 99.9+% |

Reagents used during the syntheses of complexes:

| Name grade | structure/formula | Supplier | Product code | Purity/ concentration |
|---|---|---|---|---|
| **Lithium hexafluorophosphate** battery grade | $LiPF_6$ | Stella Chemifa Corp. | | ≥99.99% trace metals basis |
| **Acetonitrile** anhydrous | $CH_3CN$ | Sigma-Aldrich | 271004 | 99.8% |
| **Methanol** anhydrous | $CH_3OH$ | Sigma-Aldrich | 322415 | 99.8% |